# GEO-3900

MASTER'S THESIS IN GEOLOGY

Seismic evidence for fluid migration and gas accumulation in sediment formation beneath the giant Storegga slide complex (Grip high 3D cube)

Krishna Kumar Shrestha

June 2012

FACULTY OF SCIENCE AND TECHNOLOGY
Department of Geology

University of Tromsø

GEO-3900

MASTER'S THESIS IN GEOLOGY

Seismic evidence for fluid migration and gas accumulation in sediment formation beneath the giant Storegga slide complex (Grip high 3D cube)

Krishna Kumar Shrestha

June 2012

Acknowledgement

Abstract

The study area covers the northern sidewall of the Storegga slide located at the southern limit of the Vøring Plateau. The water depth at mid-Norwegian margin varies approximately between 500 and 1500m. The mid-Norwegian margin area has been known to be prone for submarine sliding and is therefore a key location for studying morphological features to improve our understanding of slide mechanisms. The master thesis aims to investigate fluid migration into the Naust formation from deeper reservoirs and its potential role in slope failure. The 3-D seismic dataset GH01 allowed mapping and visualizing of three slides at the northern sidewall of the Storegga slide. Fluid migration from deeper sources through polygonal and extensional faults and acoustic pipes, gives rise to fluid accumulations under impermeable glacigenic debris flow deposits within Naust formations. The role of fluid flow for slope failures is difficult to decipher. Acoustic pipes north of northern sidewall of the Storegga slide indicate focused fluid flow and a possible active fluid migration system. The layer-bound polygonal faults within Brygge and Kai formations and their extension to the lower Naust formation may be caused by rapid loading adding to the fluid migration pathways to the Naust formation. Thus migrated fluids have been documented to accumulate within the slide prone Naust formations. The three slides identified at the northern flank of the Storegga slide have their basal surface on the marine clays indicating the slope failure on marine deposits. Fluid flow is not considered solely responsible for slope failures but the presence of faults down to the headwall of each slide does support an important buildup of zones of weakness for fluid migration contributing to slope failure.

Contents

1.   INTRODUCTION

1.1 Objectives

The main objectives of this thesis are to map out submarine slides and their morphology along with the fluid migration and gas accumulation within the giant Storegga slide complex. This master thesis presents the result of my interpretation of a 3D seismic cube (GH01), which covers a portion of northern escarpment of the Storegga slide focusing on the southern part of Helland Hansen Arch (HHA) (Fig. 1).

1.2 Motivation

Submarine slides have been discovered in both active and passive continental margins (e.g. Mienert et al., 2005b) around the world oceans. Sliding of the material downslope continental margins takes place when the shear stress within sediments exceeds the shear strength of the material thereby causing failure which initiates the movement of materials downwards. Sliding materials include rock, soil mud and mixtures of all these three (Locat and Lee, 2002). The Storegga slide (mid Norwegian margin) is one of the largest known submarine slides in the eastern Atlantic (Fig. 2). Its headwall lies only approx.120 km offshore the western coast of mid Norway (Bugge, 1983) (Figs.1 and 3).

There is an increasing need for a better understanding of submarine mass wasting process because of the ongoing development activities towards deep-water hydrocarbon exploration, coastal zone development and underwater communication cable routes. Some reasons for the increased research on sub marine mass movements includes; a) hydrocarbon exploration in offshore regions where slides are common, b) global climate change impacts on gas hydrate and upper margin stability c) earthquakes triggering downslope movement of sediments and tsunamis, and d) large amount of sand transport across shelf regions. Sub marine slides are a potentially dangerous marine geohazard. Therefore, a detailed investigation has been carried out by many scientists in Orman Lange gas field area, the second largest gas field on the mid Norwegian margin, located within the slide scar of the Storegga slide.

The advent of new technology has made a better understanding of submarine slides, their deposits and the processes involved possible. The use of 3D seismic data acquisition and seismic processing technology has led to the discovery of many previously unknown features on the seafloor and beneath it. As a result of many possibilities inherent to new technology, different group of scientists have focused their study on different aspects of submarine slides and their processes. This master thesis concentrates on the distribution of fluid flow and gas accumulation in today's Storegga slide scar. Some projects that have been carried out to investigate the Storegga slide are; STRATAFORM (1995-2001) and COSTA (Continental Slope Stability, 2000-2004).

Figure 1. Locations of different submarine slides in the Atlantic investigate by the COSTA project (Mienert, 2004) The Gebra slide is located off the northern tip of the Antarctic Peninsula (from Canals et al., 2004)

1.3 Study area

The Storegga slide is a large submarine slide on the Norwegian continental margin about 120 km off the western coast of Norway (Bugge, 1983) (Fig.2).This slide took place 8200 years

before and has removed around 3500km^3 of sediments from the slide scar areas (Haflidson et al., 2005).
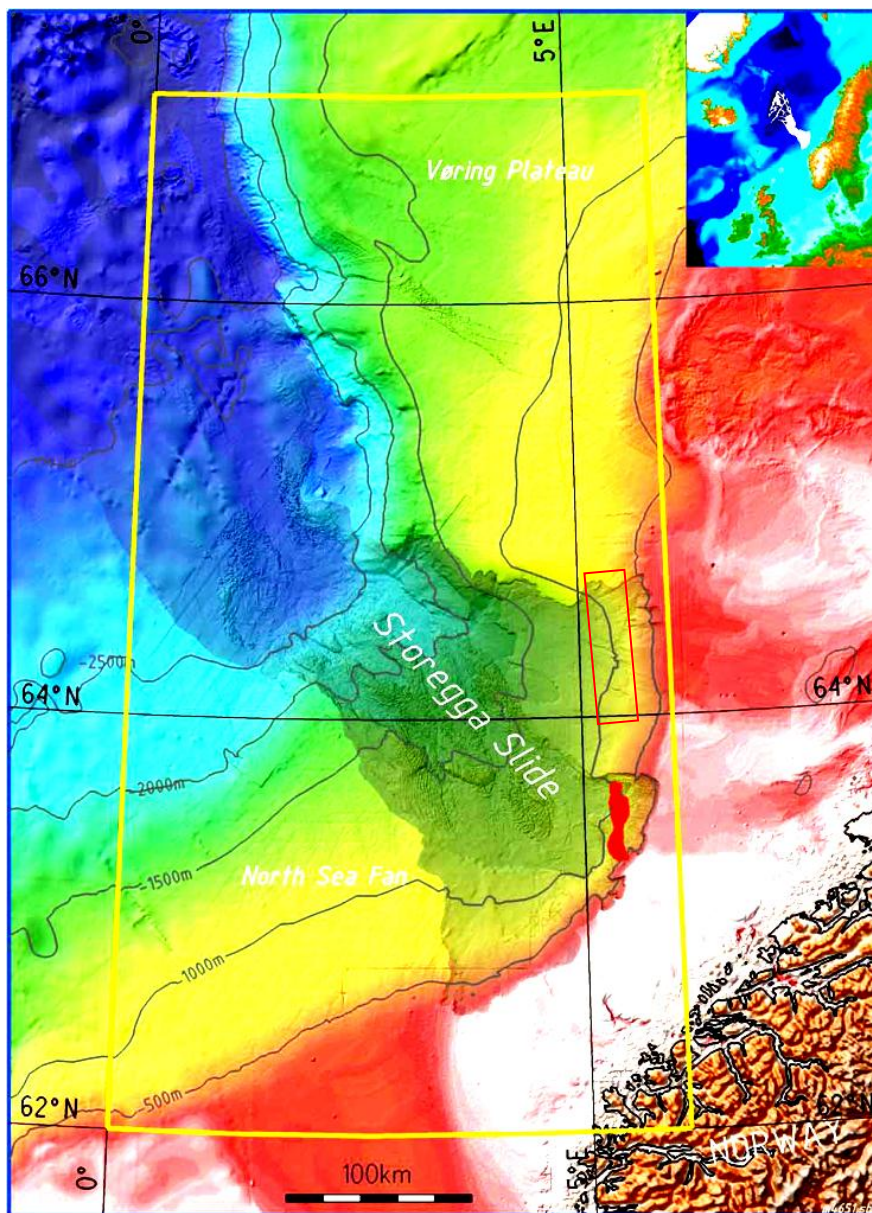
Figure 2. Colored relief map from part of the mid-Norwegian continental margin. The study area is outlined in the red square on the northern slide scar of the Storegga Slide. The yellow frame marks the area investigated by Solheim et al. (2004). The Storegga Slide is outlined in darker colors. The total outline of the slide, including distal turbidites, is marked in white in the inlet map in the upper right corner. The Ormen Lange gas field is marked in red and lies inside the Storegga Slide scar. Figure from Solheim et al. (2005).

This slide has generated a strong tsunami that hit the west coast of Norway, Scotland, Shetland and Faroes (Bondevik et al., 2003). Sediments deposited by tsunami have revealed that waves reached elevation to at least 20m above the contemporary sea level (Bondevik et

al., 2003). The main concern about the Storergga slide is about its long history of slope instability related to cyclic sediment deposition by interchanging glacial and interglacial climatic oscillations (Solheim et al., 2005). Proximal glacial till (on the shelf), glacial debris flow (on continental slope), glacigenic debris flow deposits deposited during the peak of glaciations time period is interlayered with hemipelagic, contouritic and glacial marine sediments deposited during interglacial time period (Berg et al., 2005). Excess pore pressure due to rapid deposition of the glacial deposits reduced the effective shear strength in the underlying clays and preconditioned this region to fail during interglacial periods in the last 0.5Ma (Bryn et al., 2003; Berg et al., 2005). Bungum et al., 2005 have also provided the increased seismicity resulted from post glacial isostatic rebound as a possible trigger mechanism for the submarine slope failure.

1.3.1 Tectonic Setting of the Study Area

The Study area is located on the southern edge of the Vøring Plateau partly covering the undeformed seabed north of northern sidewall of the Storegga slide and extending 95 km southward. The tectonic build up of this area is best described by the tectonic setting of the basins on the mid-Norwegian continental margin.

The Møre and Vøring basins (Fig 2) are the two prominent basins in the mid-Norwegian margin formed as a result of several rifting episodes until late paleoccene/ early Eocene continental break up (crustal thinning) and subsequent thermal subsidence (Skogseid and Eldholm, 1989; Brekke, 2000). The north-south oriented dome structures were developed from the moderate compression that took place between the Eocene and middle Miocene times (Bunz et al., 2004).

The present structural make up of the Norwegian Continental margin can be traced back to Permo-carboniferous tectonic time periods (Bukovics and Ziegler, 1985). The tectonic activities at different geological time units can be discerned into three phases as; **Carboniferous to Permian**, **Late mid-Jurassic to Early Cretaceous** and **Late Cretaceous to Early Eocene** (Brekke, 2000). In general, these phases of tectonic development comprise a long period of extension and rifting from Late Paleozoic to Early cretaceous which is then followed by continental separation at Early Eocene.

Carboniferous to Early Cretaceous time period is identified as the extension phase related to continental rifting. These extensional tectonics were related to with-in plate continental rifting. The tertiary extensional phase were more directly influenced by the relative movements along plate boundaries just before and during the continental break up and onset of seafloor spreading in the North Atlantic (Brekke, 2000).
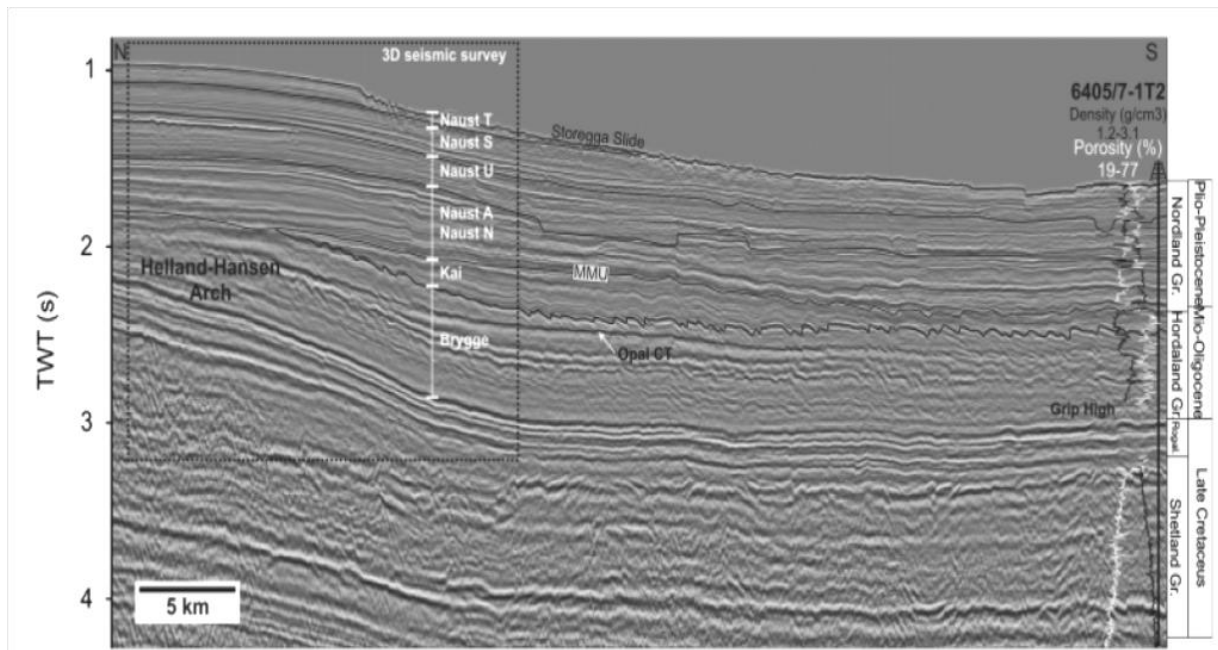
Figure 3. Regional two-dimensional (2D) seismic profile (KWF98-206) showing the stratigraphy of the study area. The density and neutron porosity logs illustrate the variations in sediment properties of the Plio-Pleistocene Naust formation. From Hustoft et al., 2010.
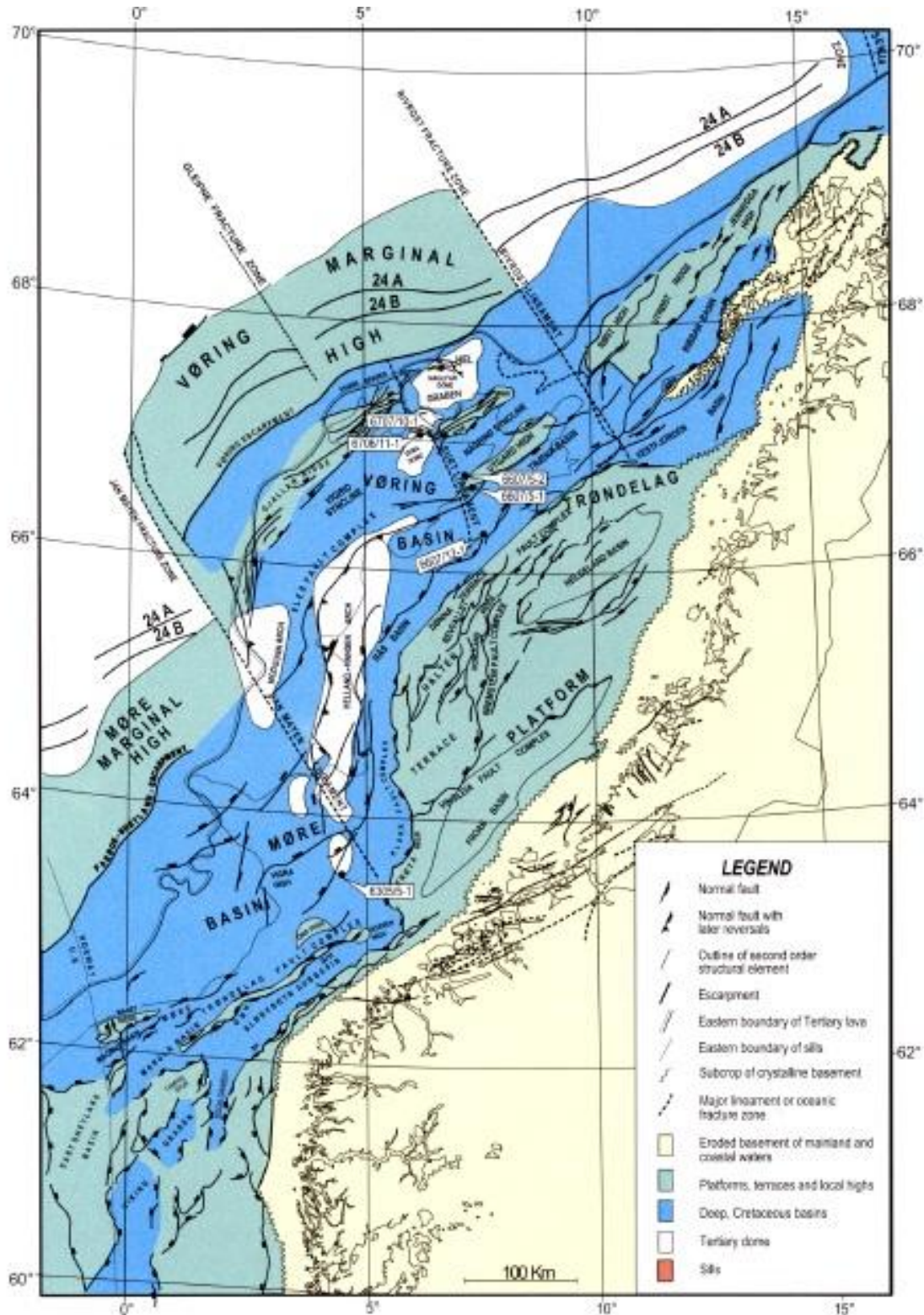
Figure 4. Structural map of Norwegian Sea Continental margin. GIH, Giske High, GNH, Gnausen High;SH, Selje High. From Brekke, 2000.

During the Late Palaeozoic to Mid-Jurassic a broad zone was affected by tensional faulting. During the Late Jurassic and Cretaceous the Trondelag Platform was little affected by faulting whilst major rift systems in the Møre and Vøring Basins subsided rapidly and their

shoulders became concomitantly upwarped. During the latest Cretaceous and Early Palaeogene terminal rifting phase only the western Møre and Vøring Basins were affected by intrusive and extrusive igneous activity. Following the Early Eocene crustal separation and the onset of sea floor spreading in the Norwegian-Greenland Sea, the Vøring segment of the Mid-Norway marginal basin subsided less rapidly than the Møre segment. During the Early and Mid Tertiary, minor compressional deformations affected the Vøring Basin and to a lesser degree the Møre Basin. Tensional forces dominated the Late Palaeozoic to Early Cenozoic evolution of the Mid-Norway Basin and effected strain mainly in the area where the crust was weakened by the previous lateral displacements. The lithosphere thinned progressively and the effects of the passively upwelling hot asthenospheric material became more pronounced. Massive dyke invasion of the thinned crust preceded its rupture (Bukovics and Ziegler, 1985).

Several episodes of crustal movements on the Mid-Norwegian margin throughout the Cenozoic have led to the development of regional highs that have later been covered by the Cenozoic sediments over these regional highs. Helland Hansen Arch(70km north), Orman Lange dome (40km south) are such regional highs nearby the Grip high which are the result of seafloor spreading in the North Atlantic. Basically, there are two schools of thoughts about the formation of such highs in the mid Norwegian margin. One believes that the plates on each side of the spreading ridge were pushed apart and folded against areas of bedrock during the seafloor spreading thereby forming regional highs. Another believes that these were formed due to Jurassic movements at deeper crust affecting the younger layer on their tops as well. These highs seem to be elevated in different episodes in between 70 to 100 Ma with respect to their size and age. These differences in size in terms of time of formation show the different geological process for their evolution.

1.3.2 Stratigraphy and Sedimentation:

The two major regional basins of the Norwegian Continental margin are Møre and Vøring basins which are the result of crustal thinning and subsequent thermal subsidence along the main axis of rift movements. The main Campanian-Palaeocene rifting and seafloor spreading took place to the west of these basins (Brekke et al., 2000). These two deep basins are characterized by thick Cretaceous sedimentary succession of 6-9 km thick and Cenozoic

sedimentary succession of 2-3 km (Bukovics and Ziegler, 1985). This thick succession of Cretaceous basin fill is because of high degree of subsidence in the Cretaceous following the Mid-Jurrassic-Early Cretaceous extensional phase (Brekke, 2000).

Since there is no well drilled through the whole **Cretaceous succession**, the lower Cretaceous stratigraphy of the deep basin is not well known so far but sand-rich deltaic and fluvial deposits occur along the basin margins. Drilled wells on the Vøring margin have shown that the sediments contain clay and silt with some proportion of sand (Hjelstuen et al., 1999). The provenance for the Early Cretaceous sediments is East Greenland which infilled the Norwegian Sea Basin notably the outer Vøring Basin. Most of the Møre and Southernmost part of the Vøring Basins consist of thick units of Late Cretaceous marine mud (Fjellanger et al., 2004; Lien, 2005). The Møre Basin consists of bio-turbated mudstone along with some sandy turbidites (Swiecicki et al, 1998).

During **Paleocene**, the main depocenters were located to the central and western part of the Vøring Basin with the main source from the Vøring high (located to the westernmost part of Vøring Basin) and fault blocks. The thickness of these depocenters goes on decreasing eastwards and sometimes absent over some regional highs (Hjelstuen et al., 1999).

Eocene and Oligocene mega sequence comprising the Brygge formation lies over the Cretaceous and Paleocene deposits. After regional uplift during the Palaeocene with shallow marine conditions and subaerial exposure of large areas, the entire margin subsided and the sea transgressed the margin and part of the mainland. The Brygge Formation was deposited in this period and is clay-dominated on the present day shelf and ooze-dominated in the distal, deeper marine Møre and Vøring basins. Deposition was concentrated in the Møre Basin and the outer part of the Vøring Basin, with thicknesses of 600-1000 m and 500-700 m, respectively (Norwegian Deepwater Programme 2004). The Eocene sediments over some highs are sometimes absent as these have been eroded to a large extent and did act as the source area for nearby depositional systems. Oligocene deposits mostly occur south of the Helland-Hansen Arch which is not present over the topographic high as that of Eocene deposits (Hjelstuen et al., 1999).

The Neogene succession of the mid Norwegian continental margin can be studied under two divisions; **Miocene to Lower Pliocene** as Kai Formation and **Late Pliocene to recent** as Naust Formation (Dalland et al., 1988). After the Mid Miocene uplift, sedimentation resumed on the outer and middle part of the margin. Clay-dominated sediments belong to this Kai Formation (Eidvin et al., 2007). This clayey ooze deposits are rich in siliceous and calcareous microfossils with glacial flour and fine grained minerals as a consequence of physical erosion (Forsberg and Locat, 2005). The change in sedimentation of Naust formation after Late Pliocene are attributed to glacially derived material transported from the Norwegian mainland areas and inner shelf and deposited in the form of prograding sediment wedges (Rise et al., 2005).

This overlying Naust formation inferred to be after 2.7 Ma and afterwards, encompasses sediments of the Pliocene-Pleistocene glacial-interglacial cycles that significantly changed the sedimentation pattern, yielding a thick wedge of clastic sediments on the shelf (Stuevold and Eldholm, 1996; Hjelstuen et al., 1999). Within this formation, current-controlled drift-sediments (contourites) deposited along slope during deglaciation and interglaciations commonly interlayer the glaciogenic downslope-transported debris flows (Rokoengen et al., 1995; Laberg et al., 2001; Evans et al., 2003; Vorren et al., 1998).

The deposits of Naust Formation are overlying the thick siliceous oozes of the Kai and Brygge formations. During the periods from the 54 to 2.5 Ma fine-grained oozes and shales of the Brygge and Kai Formations dominated the sedimentation. In most of the Storegga and North Sea Fan regions, Brygge formation has thickness of 600-1000m. Within Kai formation, the main depocenter is about 1000m of contourite deposit on the northern flank of the Storegga slide. In the central parts of the Storegga area and at dome structures the sediments of Kai formation are very thin or absent (Bryn et al., 2005). This multiphase submarine slides remobilized the sediments of Naust Formation, partly removing up to 450m of sedimentary strata. The eastern headwall runs north to south and reaches a height of up to 300m. The northern sidewall is up to 100m high and runs roughly east to west along the border between Vøring and Møre basins.

According to Bryn et al., 2005, the Naust Formation comprises five main seismic units separated by an equal number of high amplitude and laterally continuous reflectors. These five sequences (Naust W, U, S, R and O) with their boundaries can be traced throughout the Mid-Norwegian Margin. Each sequence may contain more than one shelf glaciations. Naust S, R and O units have been subdivided into 16 sub-units in the Ormen Lange area, based on seismic data, and supported by geological and geotechnical analyses of the sediment samples and from the results of borehole geophysics.

The nomenclature of Naust formation has been followed after Rise et al., 2006 (Fig. 4) throughout this dissertation works hereafter. On the basis of this recent nomenclature, the Naust formation has also been divided into five main sequences as Naust N (Oldest), A, U, S and T. Though most of the sediments for Naust formation are of glacigenic origin, glaciomarine, contouritic and hemipelagic sediments occur intermittently. The rate of sediment deposition after 2.8 Ma was significant (Rise et al., 2005).

The mid Norwegian margin received large quantities of sediments from the Norwegian mainland and inner shelf areas, which prograded into a basin with water depths inferred to be in the order of 500–1000 m. This increase in sediments is resulted from the mainland upliftment and glaciations of Scandinavia in combination. Seismic sections have proved that the crest of Helland-Hansen Arch reduced the dispersal of sediments towards the Vøring Basin thereby forming a barrier in the sediment distribution westwards. As a result, the continental shelf prograded upto 200km westwards,, leaving behind a thick sediment package of 1-1.5 km on the outer shelf and upper slope (Rise et al., 2006). Deeply weathered crystalline bedrock and/or unconsolidated Tertiary sediments were easily eroded in early Naust time. Additionally, the inner part of the shelf was uplifted,and the pronounced truncation of westerly dipping sedimentary rocks indicates that much material was removed and transported farther west (Rokoengen et al., 1995; Riis, 1996; Stuevold and Eldholm, 1996; Henriksen and Vorren, 1996; Rise et al., 2005).
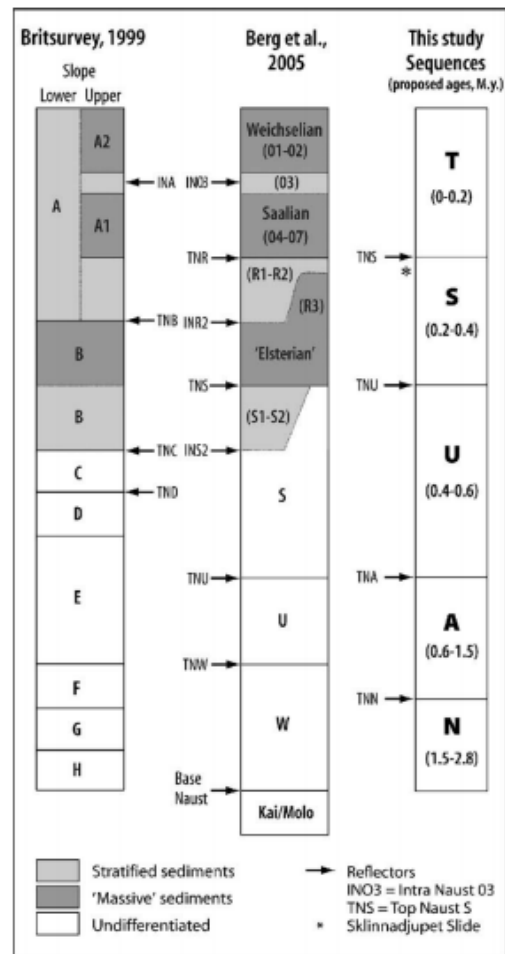
Figure 5. Diagram showing the Naust stratigraphic scheme (NDP, unpublished data, 2004a). Correlation with previous terminologies and subdivisions in and north of the Storegga Slide is shown (NDP, unpublished data, 1999; Berg et al., 2005). The proposed ages for the Naust N, A and U sequences are uncertain. From Rise et al., 2006.

Large amounts of sediment were deposited along the mid-Norwegian margin during Naust N-time (suggested age 2.8–1.5 Ma BP) because of the glacial erosion and transportation activities on the uplifted mainland that is evident from the iceberg plough marks on seismic data. During Naust A times (suggested age 1.5–0.6 Ma BP), marine ice sheets occasionally reached the palaeo-shelf edge (Rise et al., 2005). During Naust U time (suggested age 0.6–0.4 Ma BP), several cycles of glacigenic debris-flow deposition occurred. The Naust S sediments were probably rapidly deposited during an extensive phase of the Elsterian glaciations (Rise et al., 2006).

In general, the margin has had repeated advances and withdrawals of major ice sheets in the last 500ka with a period of 100ka for each cycle. The thick till deposits at the shelf deposited by fast ice-stream eventually released further down slope in the form of debris flow and turbidites (Solheim et al., 2005). During 'ice-free' periods, hemipelagic and contouritic

sediments were deposited on the slope. These kinds of sediments are most common in the Storegga Slide area, where they hosted glide planes beneath the major slides (Rise et al., 2005). The thickest Naust formation is found at Vøring Plateau and in the North Sea fan where thickness is approximately 1500-1750ms (TWT) (Fig. 5) (Berg et al., 2005).
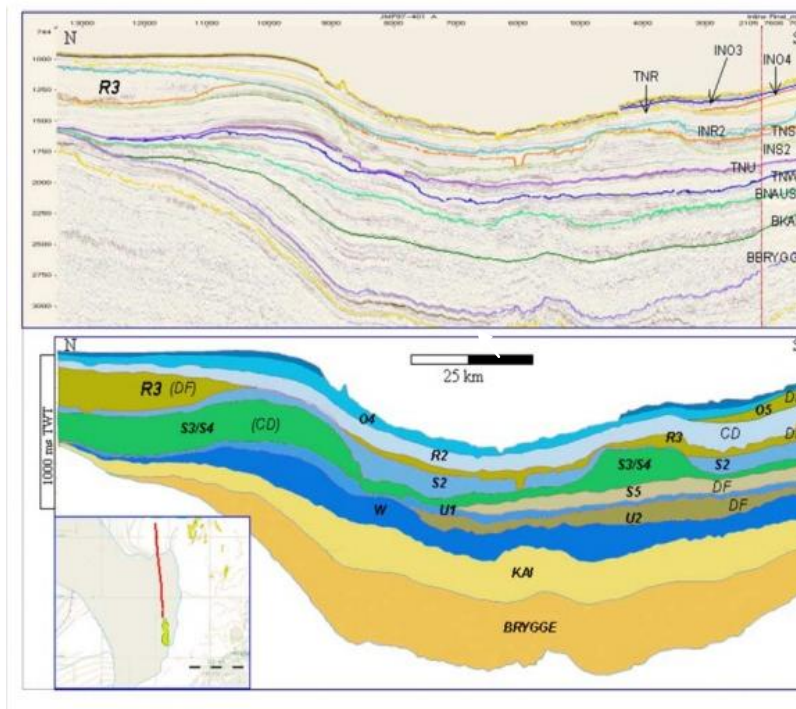
Figure 6. Seismic stratigraphy of the Ormen Lange area, and a north-south running regional seismic section through the northern part of the Storegga Slide. DF and CD in the interpreted section mark debris flow deposits and contourite deposits, respectively. From Berg et al., 2005.

1.4 Processes influencing submarine land sliding

There are few processes that have direct impact on the shear strength properties of the slope material in combinations. Slope failure takes place when the applied force to the material exceeds the shear strength of the material. The shear strength is directly related to the pore pressure of the material. Whenever pore pressure increases, effective stress on the material decreases. At a critical point of increment of pore pressure, slope failure takes place. Triggering factors are an external stimulus that changes or tends to change any one of the parameters responsible for slope instability (Sultan et al., 2004a).

Mechanisms that increase the pore pressure include sedimentation rates that are high enough to trap fluids, wave loading, earthquake loading and localized transport and

accumulation of gas and fluids (Mienert et al., 2005b). Dissociation of gas hydrate may take place on the continental slope because of the changes in sea level or increase in the bottom water temperature and produce large amount of free gas within the sediment layers (Mienert et al., 1998, Bouriak et al., 2000). Thus produced free gas will eventually decrease the bulk shear strength of the slope material within the sediment column and lead to the slope failure (Paull et al., 1996; Mienert et al., 1998). Likewise, bottom water current may erode the base of the slope as in deltaic environment and increases the slope instability.

Long et al., 2003 from the study of slope failure on Faroe-Shetland Channel has concluded that the dominant contouritic sediments deposited along the slope are more porous than the intervening glacial deposits and possesses lower shear strength. These kinds of sediments are more susceptible to liquefaction under dynamic loading. This may create plane of weakness and increases the pore pressure to the surrounding cohesive sediments and reduces the shear strength of the materials thereby causing the slope failure.

1.5. Features characterizing submarine slides

The characteristic features of a sub marine slide includes headwall and scar as upslope termination of the slope failure, glide plane as a surface along the sliding of a slab takes place and a disrupted or chaotic sediment and morphology with debris flow material down-slope.

The headwall is the most characteristic seabed feature caused by extensional movement that is represented by headwall scarps as extensional failure surfaces. Headwall scarps have been developed in many slides like the Storegga slide as the failure spreads upslope thereby creating several headwall scarps (Gauer et al., 2005). These kinds of failures spread upslope are termed as retrogressive slide (e.g. Mienert, 2008, Storegga slide). The dimension of headwall scarps vary from one slide to another; with headwall scarps ranging from a few meters to more than hundred meters. The Storegga slide shows a headwall scarp that is 250 m high and 300 km long (Bryn et al., 2005b). Crown cracks more often found on headwall scarps, which are linear elongated depressions created in the headwall strata. These cracks have been formed because of the extensional stress applied to the material as a result of downslope movement of materials (e.g. Bull et al., 2009a).

Glide planes are the basal shear surface along which the materials slide downslope. In most of the cases these planes are more or less parallel and continuous to the sedimentary bedding. Glide planes in some cases may make ramps (discordantly cut part across the bedding) and flats (parts parallel to bedding plane) (Solheim et al., 2005a, Bull et al., 2009a) (Fig.7).
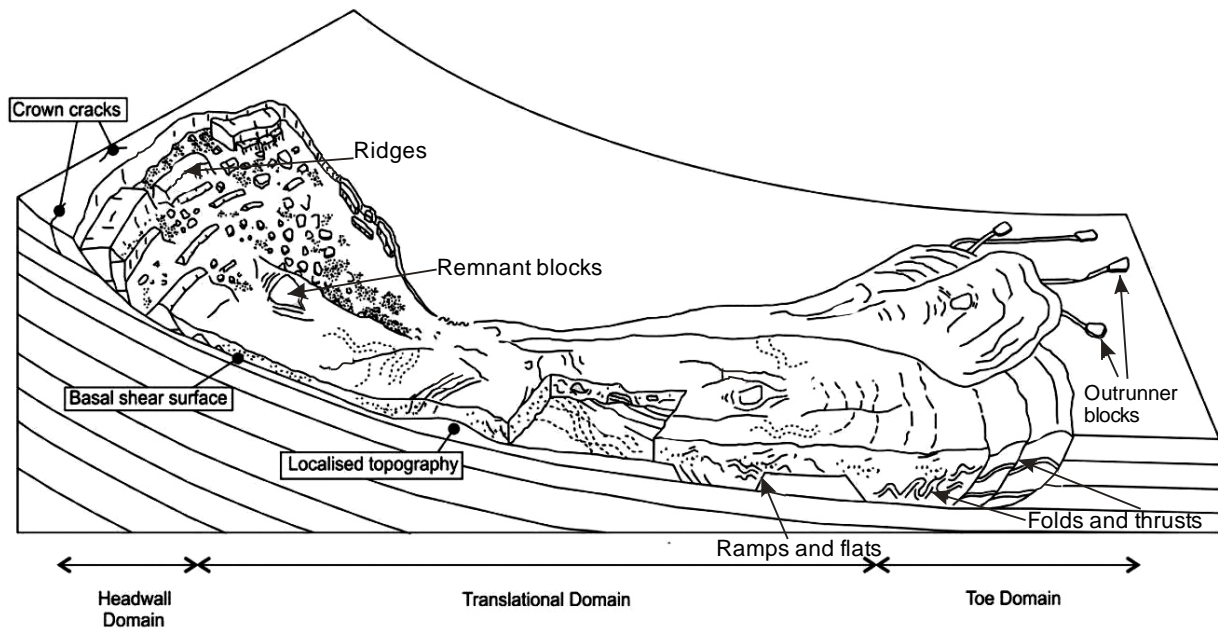
Figure7. A schematic representation of a submarine slide and occurrence of headwall domain, gliding plane (basal shear surface) and failed material. From Bull et al., (2009a).

The displaced materials can be recognized within seismic sections in the form of disrupted and chaotic patterns of reflections. Sometimes, several blocks of coherent sediments have been observed within and in front of slide deposits. These blocks are clearly identifiable because of their concordant and continuous reflection in comparison to surrounding chaotic reflection. The sizes of these blocks vary greatly; from a few meters to a few km wide and a few hundred meters of high (e.g. Vanneste et al., 2006) .
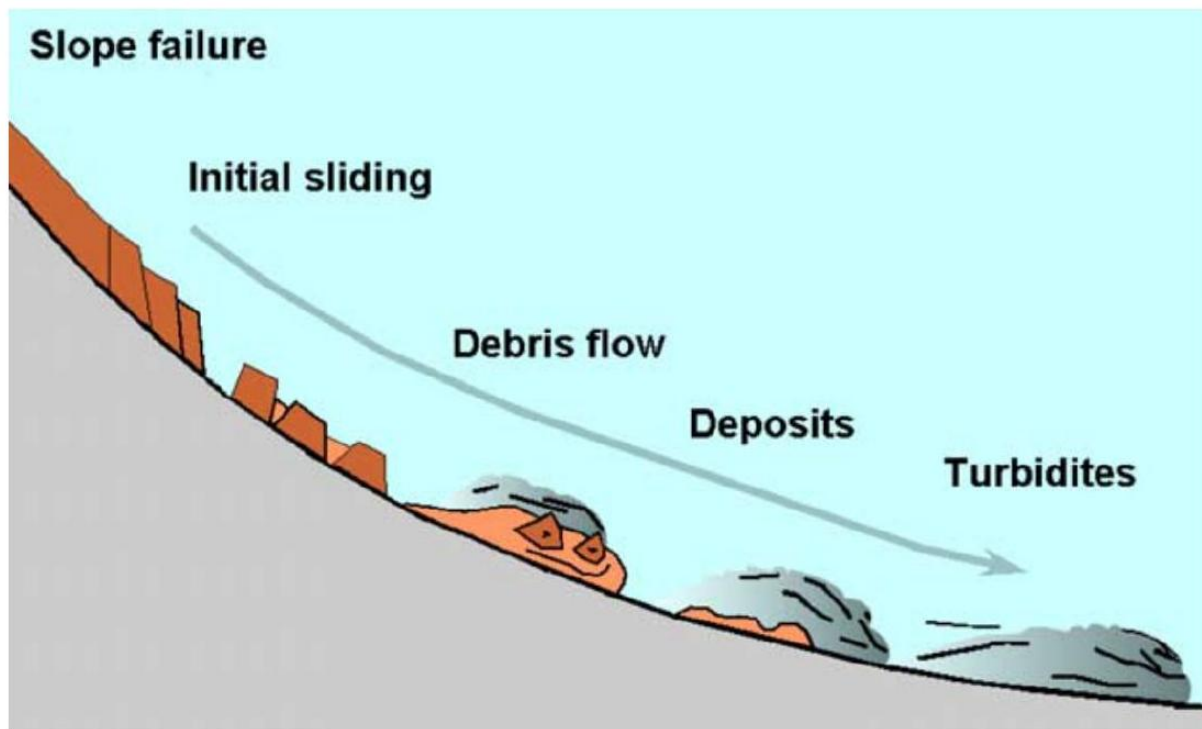
Figure 8. Schematic representations of the different stages of slide development from slope failure to turbidites. From Bryn et al., (2005).

A cohesive force between particles remains to some extent at the initial phase of the block sliding. However, blocks and slabs detach tend to detach from the parent rock. In the course of moving downslope, these blocks further break down into smaller fragments and flow with more fluid content in the form of debris flows (Fig. 8). Debris flows are slurry like flow which contains sediments of varying grain size concentration, velocity and internal dynamics (Leeder, 2006). This matrix of debris flow consists of fine grained sediments to grains of all sizes. The debris flow transform into surge-like turbidity flow along their upper edges by turbulent separation (Hampton, 1972).Turbidity flows basically takes place as a result of changes in densities between local fluid and surrounding fluids (Leeder, 2006). This density difference arises due to the content of the material suspended in the turbidity current (Fig. 8). These turbidity currents carry the suspended material to a large distance downslope into the basin (sometimes hundreds of kilometer) until they lose their energy so that the suspended material can settle down.

Run out distance for a submarine slide is the horizontal distance between the upper edge of the slide headwall and the most distal point of sediment deposition including the turbidity current (Canals et al., 2004). Actually this run out distance depends upon the in-situ stress,

sediment properties and local morphology. The run out distance vary from one slide to another on the basis of its nature of mode of occurrence; for instance, Storegga slide has a run out distance of 770km, Canary slide has 600km, the Traenadjupet slide has 200km (Canals et al., 2004), Arctic Hinlopen slide has ~ 300km (Vanneste et el., 2006).

1.6 Fluid migration and gas accumulation systems

The advent of three dimensional seismic data has significantly improved our estimation of lateral and vertical distribution of fluids. It has also improved the understanding of fluid migration from deep reservoirs to shallow subsurface (Heggland, 1997, 1998; Løseth et al., 2001). The 3D seismic data (GH01) used in this master thesis encompasses the northern escarpment of the Storegga slide in the north to Grip high in the south (Fig. 2). Different sizes of gas accumulation systems and fluid migration pathways will be mapped and interpreted in the proceeding chapters. The introduction of different aspects of the petroleum system and the process involved are described in the following.

1.7 The Petroleum System

A petroleum system is defined as a natural system that encompasses an active source rock and all related hydrocarbon accumulations in the reservoir rock, which all the geologic elements and processes that are essential if a hydrocarbon accumulation is to exist (Magoon, 2003).

Basic elements for the petroleum system are: source rock, reservoir rock, seal rock and overburden rock. The basic processes are trap formation and the migration-accumulation period of hydrocarbon, which basically concerns temperature and pressure evolutions.

Source Rock:
A source rock contains large amount of organic material and can produce hydrocarbons (oil and gas) if it undergoes a maturation at high enough temperature and pressure under the suitable depth. Organic materials are the main constituents, which sink down to the seabed, lake or river together with mineral particles in anoxic water column conditions. Typical environments for these kind of organic materials would be nutrient rich coastal upwelling, swamps, shallow seas and lakes (Gluyas and Swarbrick, 2004). Organic sediments deposited would be preserved only when the water column above is anoxic and prevents the oxidation

of organic materials. Preservation especially takes place at shallow water depths, high sedimentation rates and the absence of benthic organisms and bioturbation.
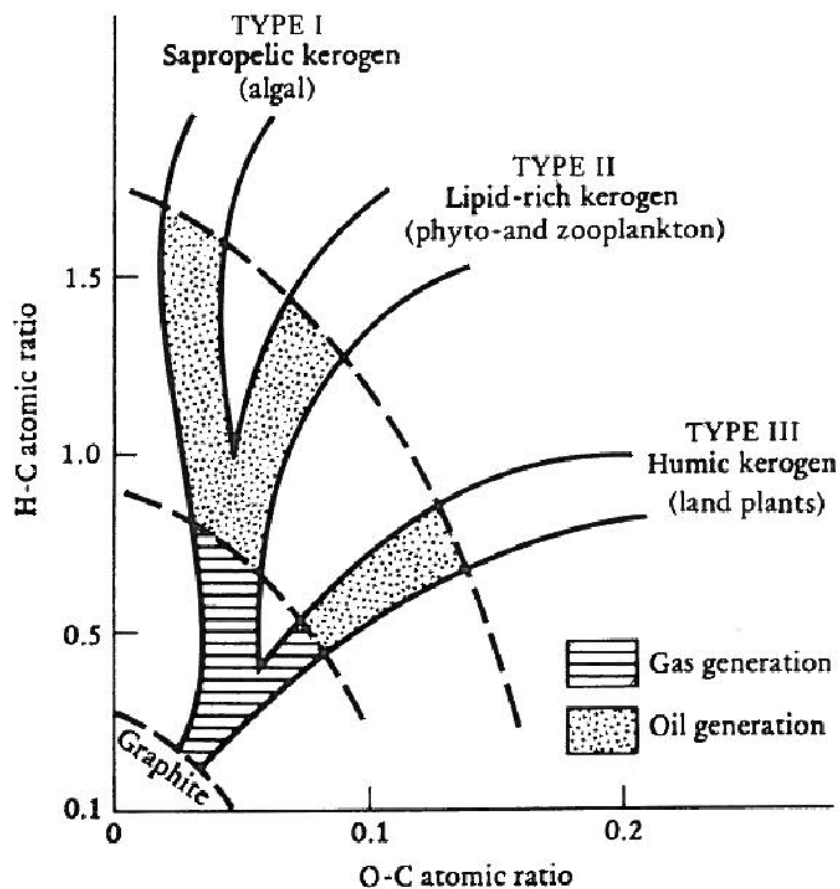
Figure 9. Maturation paths of the three different types of Kerogen with their origin (Selley, 1998).

1-5% of the initial organic compounds (mainly lipids and lignin) undergoes chemical changes and transform into source rock organic matter, which later produces hydrocarbon under thermal maturation. This thermal maturation indicates that the end product (hydrocarbon) of the source rock is mainly dependent on temperature along with other various minor factors. Kerogene which is a complex hydrocarbon is left after the removal of methane, carbondioxide and water from the source rock organic matter (Selley, 1998). With increasing maturity of this Kerogene, *first oil and then gas are expelled* but nothing (neither oil nor gas) is produced when it is over mature (Selley, 1998). Significant amount of oil is generated on lower temperatures (60-120°C) and significant amount of gas in between 120-225°C. Above 225°C, the remaining carbon transforms into Graphite through a metamorphic process (Fig. 9) (Selley, 1998). The hydrocarbon generated depends on the origin of organic material and

can be classified into different types of Kerogen determined on organic source and Hydrogen Index (Fig. 9) (Hunt, 1996).

Reservoir Rock

A reservoir rock is a permeable subsurface rock that contains moveable fluids. Reservoir rocks are dominantly sedimentary (shales, sandstones and carbonates) as they do possesses interconnected pore spaces for the fluid migration within them. A reservoir rock can also be called an aquifer (Fig. 10)

Traps (Seal rock)

A seal rock is in basic a rock that is impermeable. Orton (1889) has defined traps as "stocks of oil and gas that might be trapped in the summits of folds or arches found along their way to higher ground". Traps are the place where oil and gas are barred from further movements laterally and vertically (Levorsen, 1967). Fluids reside into the traps cannot migrate further because of the sealing of impermeable rocks on top. However, traps are limited in extent and may have a spill point. There are several types of traps; stratigraphic traps, structural traps, diapiric traps, hydrodynamic traps and a combination of the two.

1.8. Fluid migration

On the basis of the mode of migration, fluid migration is often separated into three different categories: primary migration, secondary migration and tertiary migration (Gluyas and Swarbrick, 2004; Tissot and Welte, 1984) (Fig. 10).
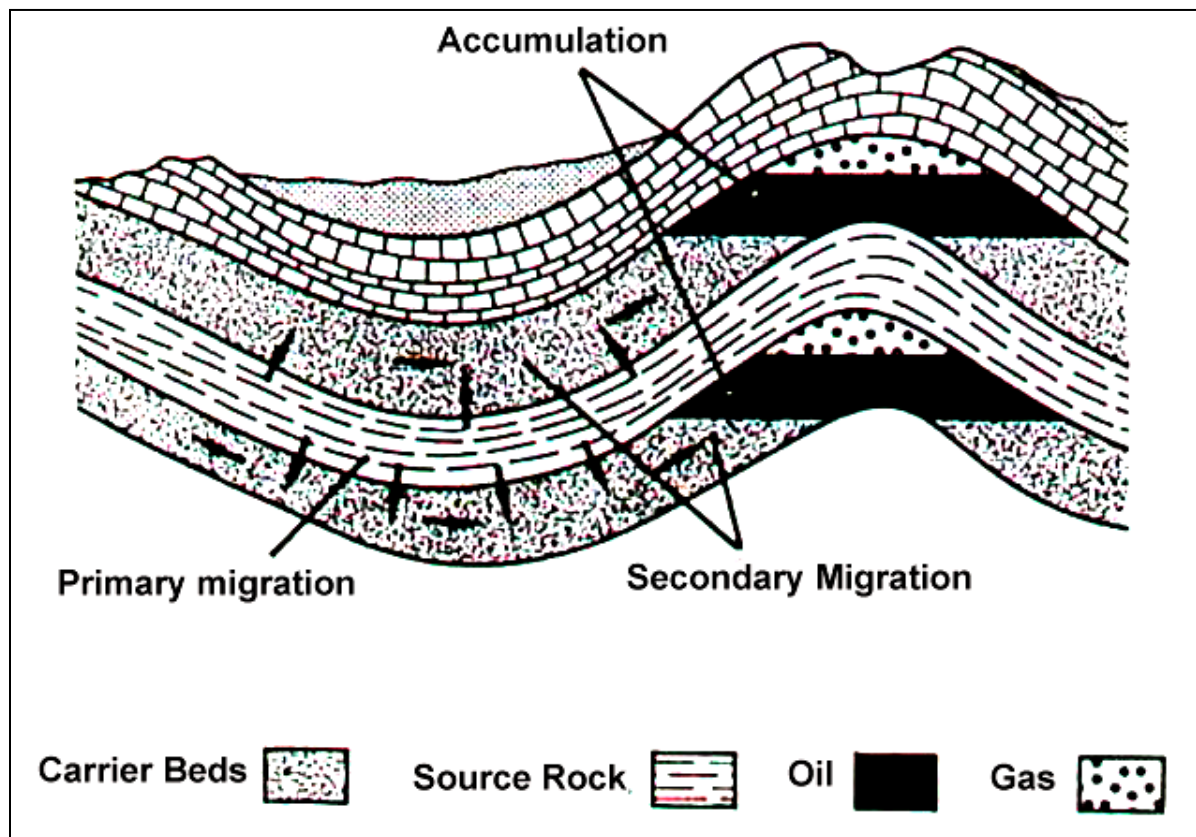
Figure 10. Descriptive sketch of the basics between source- reservoir- cap rock and primary- and secondary migration. (from Tissot and Welt 1984)

Basically, the movement of fluid from source rock to reservoir rock is primary migration. Tissot and Welte (1984) has defined the primary migration as the release of petroleum compounds from kerogen, and their transport within and through the capillaries and narrow pores of a fine-grained source rock (Fig. 10). Primary migration is a complex phenomenon and its mechanism is not fully understood yet.

The subsequent movement of oil and gas within the permeable carrier beds and reservoir is referred to as secondary migration of fluids (Showalter, 1979; England, 1994). This movement of petroleum compounds through rocks with high enough permeability allows free migration of hydrocarbons within the carrier beds and reservoir and its accumulation into a trap. The secondary migration occurs because of buoyancy due to different densities of the respective fluids in water-saturated porous rocks, low capillary pressure which is forced downwards since the pressure is higher in the pore throats than in pore space and hydrodynamic fluid flow (Tissot and Welte, 1984).

Minescu et al., 2010 have defined the fluid movement that takes place after reservoir abandonment as tertiary movement. Tertiary migration is basically defined as leakage, seepage, dissipation and alteration of hydrocarbon as it reaches the Earth's surfaces escaping from an already accumulated reservoir. Typical features of tertiary migration are gas chimneys, gas hydrate layers, pockmarks, mud volcanoes and live "tar oil" and gas seepages at the sediment surface. Tertiary migration is different from the secondary migration because of its rapid supply of hydrocarbon products (Gluyas and Swarbrick, 2004).

1.9. Gas Hydrates

Gas hydrate have been considered as unconventional source of energy, which is an ice-like substance composed of gas molecules (guest compound) caged within a crystal structure composed of water molecules (host compounds) (Sloan, 1998) (Fig. 11). Usually the trapped gas within the water molecule is mainly methane. Thus, gas hydrates naturally occur when methane gas saturates the pore fluid within the marine sediments under specific temperature and pressure conditions, which is typically found in ocean floor sediments at water depths greater than 500 m (Brown et al., 2006). Gas hydrates often behave as cementing material in the pore space of sediments that are found in the form of lamina, vein and nodules of pure hydrates (e.g. Boswell and Collett, 2010; Collett et al., 2011).

Gas hydrates occur worldwide in both active and passive continental margins and in high latitude permafrost regions (Boswell and Collett, 2010; Collett et al., 2011). Kvenvolden (1993) has suggested that gas hydrate deposits contain the largest reservoir of methane on Earth.

Figure 11. Gas hydrate recovered from an embedded hydrate structure of a sediment ridge offshore Oregon, USA. Gas Hydrates are not stable under atmospheric pressure and will release gas and water if not kept under high pressure and low temperature (picture from: http://feww.wordpress.com/category/east-siberian-arctic-shelf/).

Temperature and pressure are the important physical factors for the formation of gas hydrate where abundant methane supply takes place from beneath the base of the gas hydrate stability zone (BGHSZ). Typical conditions for the formation of gas hydrates within the marine sediment down the seabed are when temperatures is less than 300K and pressure more than 0.6 MPa (e.g. Chand and Minshull, 2003). Along with these two parameters; temperature and pressure, the amount of gas (methane) supply and water present within the sediment pore spaces control the mechanism of formation of gas

hydrate. So far, natural gas hydrates have been found to contain both biogenic and thermogenic gas; biogenic gas is produced from the microbial activity through the degradation of organic matter whereas thermogenic gas is produced by chemical reactions that takes place at high temperature and burial depths (e.g. Rice and Claypool, 1981).
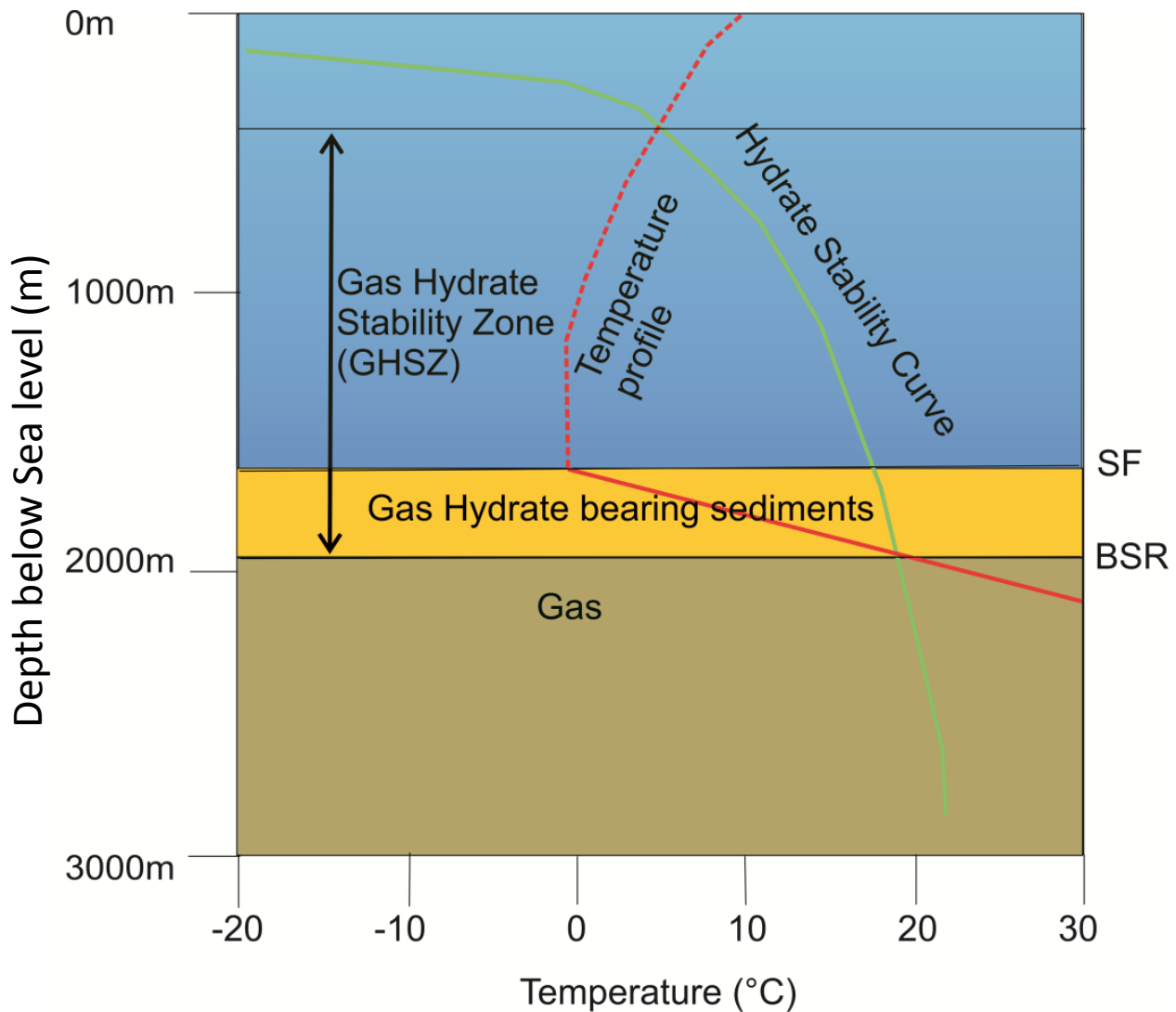
Figure 12. Basic phase diagram indicating the transition state from gas hydrates to free gas. Gas hydrates released to the water column will due to positive buoyancy rise and dissociate before reaching sea level. Gas hydrates created below seafloor will be trapped and can make up a constant layer. Temperature is mainly affected by the geothermal gradient below seafloor. Figure is from Chand and Minshull (2003) and based on polar marine conditions.

Gas Hydrate Stability Zone (GHSZ)

The stability of gas hydrate persists until and unless the physical and chemical criteria do not change significantly.   The zone within gas hydrates are stable is called the gas hydrate stability zone (GHSZ) (Fig. 12). GHSZ is referred as a geological section where gas hydrates exists under in-situ conditions (Ginsburg and Soloviev, 1997). The dissociation of gas hydrate is due to a change in pressure and/or temperature which is greatly affected by the change in both water temperature and sea level (Dickens, 2001). An increase in temperature and decrease in pressure affects the stability and will cause the hydrate to dissociate and release free gas that may escape through sediments to the seabed into the water column.

The GHSZ is limited in particular by the geothermal gradient, pressure, gas composition, pore water salinity, bottom water temperature and the physical properties of the host sediment (Buenz et al., 2003). The thickness of the GHSZ varies according to these parameters. The thickness will increase with increasing water depth due to increasing pressure. The dissolved salt and small pore volumes within the sediments decease the surface energy enough in order restrict the formation of gas hydrates. Higher order gases such as ethane, butane and propane will increase the GHSZ thickness as well. A higher geothermal gradient will cause a decrease of the GHSZ thickness (Sloan, 1998c).

Identification of gas hydrates in reflection seismic sections

The presence of gas hydrates and free gas beneath it is recognized from the presence of a bottom-simulating reflector (BSR) on the seismic section which has a distinct characteristic reflection pattern. These anomalous signatures include high amplitude and reverse polarity if compared to the seafloor (Fig. 32). The BSR runs sub-parallel to the seafloor (Shipley et al., 1979). The base of the gas hydrate bearing sediment follow iso-temperature lines that is why it is sub-parallel to the seafloor. Gas hydrates fill the pore space of the host sediments thereby increasing its bulk and shear modulus, which in turn causes an increase in both P- and S-wave velocities within the hydrate bearing sediments (Chand and Minshull, 2003). The interval P-wave velocities (Vp) for hydrate bearing sediment is ~1700-2400 m/s (Andreassen et al., 1990). The formation of gas hydrate within the pore space of the host sediments

reduces both porosity and permeability and makes the sediments within the gas hydrate stability zone (GHSZ) more or less impermeable. Free gas often accumulates in layers of varying thickness below the BSR. The base of gas hydrate stability zone (BGHZ) may act as a seal for upward moving fluids. The increase in both density and velocity within the BHGZ and the low velocity just below the BHGZ with the free gas zone, which lowers the P-wave velocity within it, creates a distinct change in acoustic impedance and thus a strong reflection coefficient. This distinct impedance contrast at the transitional margin is easily traced on seismic data as a bottom-simulating reflection (BSR) (Buenz and Mienert, 2004) (Fig. 32).

2. BASICS OF REFLECTION SEISMIC

2.1 Basic theory of reflection seismic

Seismic waves transmit through fluids (P-wave), solids (P- and S wave) and porous solids. On the basis of knowledge of mechanical and acoustic properties of rocks, a reflection seismic image of the subsurface can be created and interpreted afterwards.

The seismic source, for example an air gun, produces pulses of seismic energy which propagates down to the subsurface layers and reflects back from the seafloor and subsurface interfaces to hydrophones (streamers) in the water column. When a wavefront explained by a seismic raypath travels through a sedimentary succession it is bent, reflected, refracted, diffracted, scattered and attenuated through different sedimentary features which will decrease the signal amplitude. Spherical divergence or geometric spreading due to an expanding wavefront will cause the amplitude to decrease proportionally with the radius of the propagating wave front sphere (e.g. Andreassen, 2009). The resolution and penetration of the seismic wave is related to its frequency. The higher the frequency the higher the resolution becomes but the lower the penetration and vice versa (e.g. Andreassen, 2009).

Figure 13. Schematic view of polarity convention (Sheriff and Robert, 1995)

Important basic terms in reflection seismic are:

Acoustic impedance (Z) = density x velocity …………………. Equation 1

Reflection coefficient (R) = $(Z_2 - Z_1) / (Z_2 + Z_1)$ …………………….Equation 2

Where the density is defined and calculated by formula:

$\rho = (\rho f)\phi + \rho m (1-\phi)$ ………………………………………….Equation 3

25

The reflection of a seismic wave takes place only when it encounters the interface of two layers with different acoustic impedances. This impedance contrast may bedue to lithological variations, faults or fluid densities of the sediment formation. The reflection coefficient (R) of a layer can be positive or negative depending on the velocity of the wave within this layer and its density (Fig.14). The energy reflected back and the energy transmitted into next layer is determined by Snell's law (Fig.14)

Sin$_\psi$inc /V$_1$ = sin$_\psi$trans/V$_2$ = sin$_\psi$ref/V$_1$..............................Equation 4
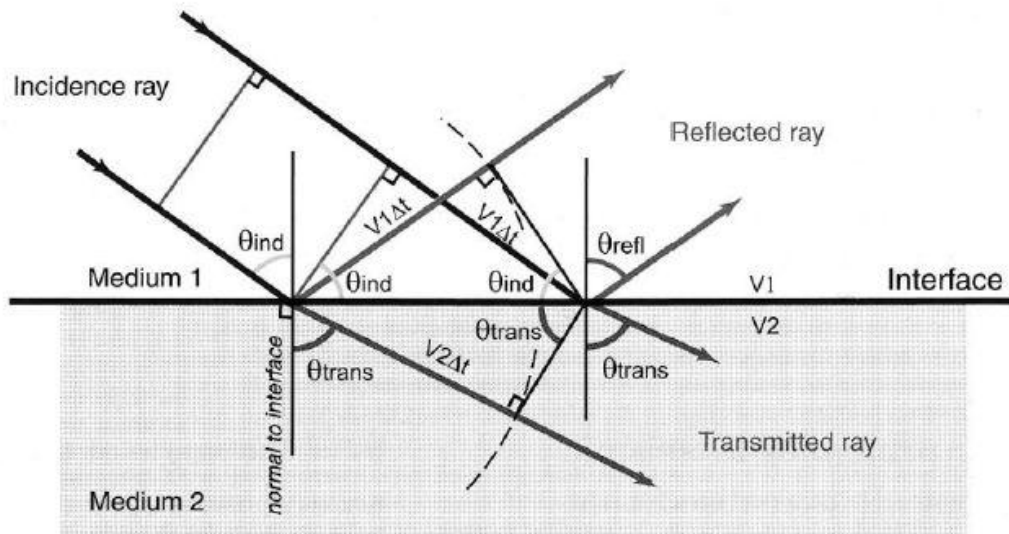
Figure 14. Acoustic sound waves are affected by velocity and density of medium (acoustic impedance which results in the reflection coefficient). P and S-wave generation is ignored for this figure. Figure from Andreassen (2009).

Compressional (P) wave and shear (S) wave propagates differently in the subsurface and have different velocity which can be calculated based on the empirical formulas from Gassman (Gassman, 1951):

$$V_p = (\frac{\rho}{0.32})^4 \qquad\qquad \frac{V_p}{V_s} = 1.8$$

Equation 5   **Equation 6**

2.2. Seismic Resolution

Resolution is defined as the ability to separate two features that are close together or in other words the minimum separation of two boundaries before their individual identities are lost in a cross-section (Sheriff, 2006).

Generally the resolution of a seismic trace decreases in response to its depth as wavelength of seismic wave increases with depth of penetration (Fig.15). There are several reasons for the increase in wavelength while penetrating deeper into the subsurface. Main reasons for the decrease in the amplitude, energy and frequency are: Spherical divergence or geometrical spreading, which causes the seismic energy to decrease proportionally with the increasing radius of the travelling wavefront sphere (Andreassen, 2009).

Vertical resolution:

It concerns the minimum thickness of a bed that can be resolved, which means that a reflection from the top and bottom of the bed is discernible. One can distinguish between a bed of finite thickness from a single reflecting interface. Vertical resolution is determined by ¼ of a wavelength (Badley, 1985; Brown, 1999).

$\lambda = v/f$ ....**Equation 7**

This means that it is possible to distinguish the top and base of the layers that are thicker than ¼ of the wavelength.

Tuning thickness is determined as the lowest possible thickness of a layer to have an effect of the seismic signal. Tuning thickness is generally defined as $1/30\ \lambda$ (Badley, 1985). Tuning thickness or limit of visibility for most cases is not $1/30\ \lambda$ because of background noise, so it is determined from s/n ratio of dataset (Bulat, 2005).
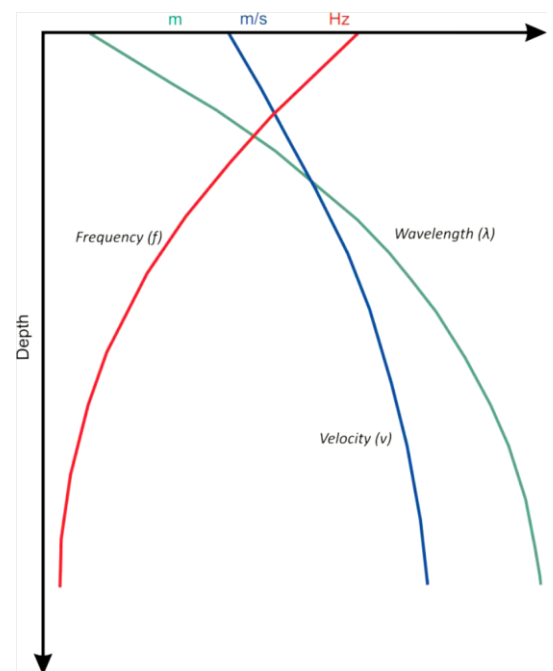

Figure 15. Sketch of the general relation between frequency, velocity and wavelength. Velocity and wavelength increases with depth and frequency decreases. Figure from Brown (1999).

Horizontal resolution:

Horizontal resolution is determined in terms of the Fresnel zone. In order to distinguish lateral features in the seismic data it has to be wider than the Fresnel zone. Two features that lie within the radius of the Fresnel zone are not visible within the seismic data.

The Fresnel zone is a function of depth, velocity and dominant frequency (Eq.8). The horizontal resolution decreases with depth, increased velocity and lower frequency, which justifies that a deeper-lying features need a larger areal extent to produce the same effect as that of a smaller and shallower features (Badley 1985) (Fig.16).

The Fresnel zone of 3D is greatly reduced in comparison to 2D allowing a much higher resolution of objects within 3D seismic data. Migration of 3D seismic data collapses all the diffractions back to their point of origin thereby reducing the radius of the Fresnel zone and increasing the horizontal resolution. The extent of the horizontal resolution will be around ¼ λ in all directions on 3D seismic data (Brown, 1999; Bulat, 2005, Yilmaz, 2001).
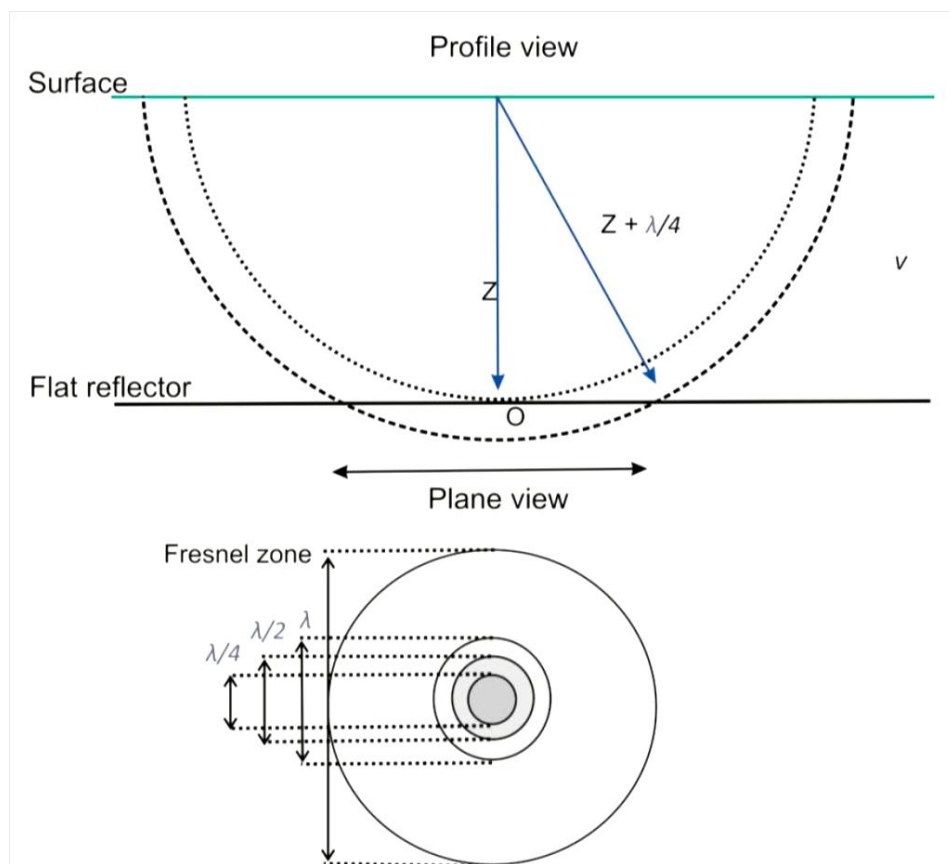
Figure 16. Demonstrating the principle of the Fresnel zone which determines the horizontal resolution of unmigrated seismic data. Figure is from Bulat (2005) and it is based on the principles from Yilmaz (2001).

rf = (v/2) × √(t/𝑓)………………………….**Equation 8**

rf = radius of Fresnel zone

v = velocity

t = TWT of Z (time to reflector)

f = dominant frequency

2.3 Fluid identification

There are several methods to recognize fluid flow pathways and fluid accumulation areas.

Fluid flow features are commonly separated into two categories (Løseth et al., 2009);

1. Fluid flow processes that have permanently changed sediment sequence and caused permanent deformations and / or created a new permanent "syn leakage" feature.

2. Changes in pore fluid densities show changes in the seismic response though sediment bedding remains constant without deformation.

2.3.1 Reflections associated with changes in pore fluid density

Hydrocarbon fluids within the pores of host sediment cause a change in p-wave velocity due to changes in pore fluid density (Fig. 17).

If hydrocarbons substitute water of a highly permeable rock the acoustic wave velocity will be reduced within the rock formation. The effect can be calculated by the Gassman equation (Gassman, 1951) (simplified in equation 5). This equation is based on several empirical approximations. Based on sandstones the bulk modulus and shear modulus are used and one can calculate expected synthetic velocities of both shear (Vs)- and compressional (Vp) wave velocity (Eq.5-6).
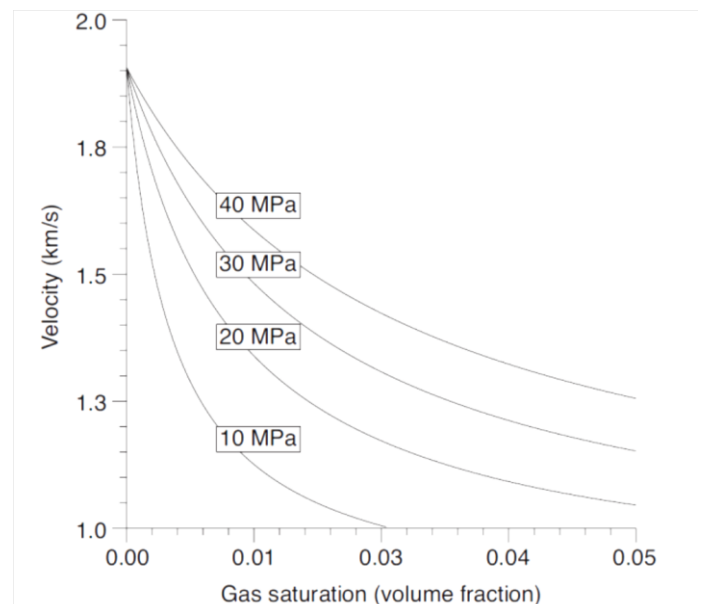
Figure 17. Compressional seismic velocity as a function of gas saturation and pore pressure where temperature is constant at 48°C. Figure from Arntsen et al. (2007).

Accumulation of gas will show the most distinct decrease in seismic velocities (Andreassen, 2009).

Common indicators of gas accumulations are (Andreassen, 2009):

1. Amplitude anomalies (Fig. 18, 19)

i. Bright Spot

ii. Dim Spot

2. Flat spot (Fig 18, 19)

3. Polarity reversal (Fig. 18, 19)

4. Velocity effects (Fig.17)

5. Loss of high frequencies

6. Diffractions

7. Masking and piping

1. Amplitude anomalies show a difference in amplitude along a continuous reflector. An amplitude anomaly can be strong and positive, strong and negative or weak (Figs. 18 and 19). The description of a reflector as positive or negative is done in terms of reflector.
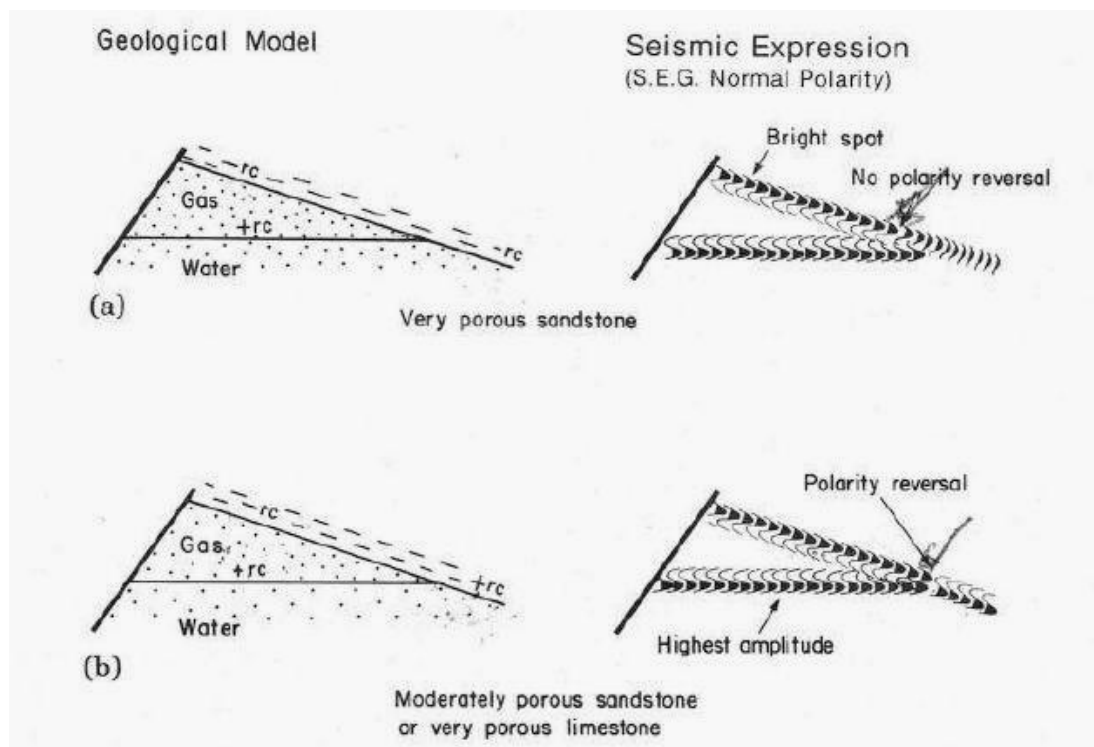
Figure 18. a,b) Illustrating the basic theory behind flat spot, bright spot and dim spot. Notice the polarity convention. Figure from (Andreassen, 2009).

2. A flat spot (Figs. 18 and 19) can be observed in both the gas and oil contact. The difference in pore fluid density is the basic theory behind the occurrence of a flat spot. Sufficient acoustic impedance contrast at the gas-oil or gas-water filled portion of a reservoir causes a flat spot to appear at the base of gas. A flat spot will often overprint the original sedimentary structure and it will always have positive reflection coefficients. Velocity difference effects can cause the reflection not to appear horizontal. Flat spots are usually found shallower than 2.5 km because the effect of gas on velocity below this depth is less marked and doesn't provide a good reflection from a gas contrast (Andreassen, 2009).
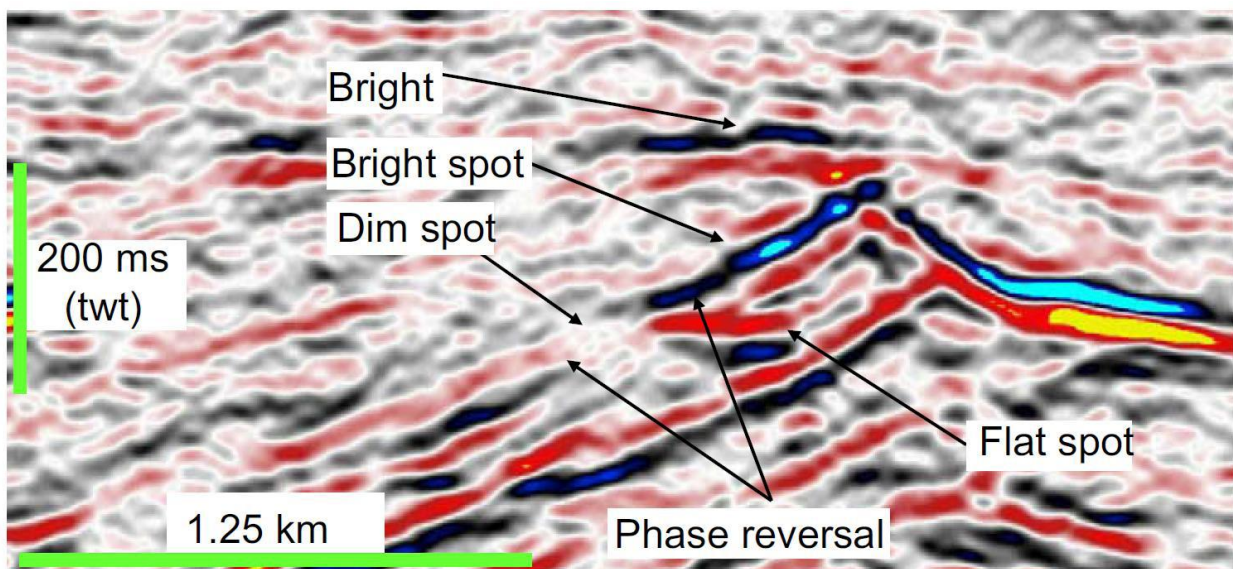
Figure 19. Classical example of bright, dim and flat spots. Phase reversal is also indicated. From (Løseth et al., 2009).

3. Polarity (phase) reversal is due to changes in the reflection coefficient. It occurs when the phase shifts by 180° along a continuous reflector. Figure 18b) illustrates this effect. Figure 19 shows a seismic example.

4. A sufficient thick gas or fluid zone may create a push-down effect on underlying horizons. This effect can be recovered by applying depth conversion mode into the seismic data. One important thing that we have to bear in mind is that the velocity effects (push down) are not solely related to the presence of gas and thus a decrease in p-wave velocity only. It may sometimes arise due to combination of other effects too.

5. When seismic energy travels through gas bearing sediments, absorption of energy within the gas bearing sediment causes the loss of frequencies within it. The absorption depletes the signal of higher frequencies. Loss of these high frequencies can be observed beneath bright spots.

6. Diffractions can be seen on flanks of gas/fluid pockets, which is due to a significant acoustic impedance contrast.

7. Acoustic masking can occur along fault zones and pipes.

2.3.2. Seal bypass system (SBS)

Seal bypass systems (SBS) are geological structures that have infringed sealing sequences of low permeable lithofacies and that acts as a conduit for fluid flow vertically or sub vertically across the sealing rocks (Cartwright et al., 2007). What we should bear in mind is the intrinsic permeability of all types of rocks, even if it is a seal rock. Because of this property seals may also be permeable and petroleum migrates through sealing sequences if one considers only a long enough time period (Cartwright et al., 2007). The rate of leakage is controlled by the relative permeability of the sealing sequences. This leakage takes place through resulting fractures when the pore pressure within the seal rock is sufficiently high enough to cause mechanical failure (Grauls and Cassingnol, 1992; Gaarenstroom et al., 1993).

SBS is classified into three main groups on the basis of seismic interpretation criteria (Cartwright et al., 2007): (i) fault-related, (ii) intrusion related, and (iii) pipe related.
Fault bypass can be subdivided into two families:

i. Trap, where a fault defines and delimits trap within a lateral component of sealing succession (Fig. 20).

ii. Supratrap, where a fault is embedded within the sealing sequence. It causes a constrained flow through the sealing sequence, but does not necessarily imply an empty reservoir. A polygonal fault system is classified as a supratrap. These polygonal

fault planes transmit fluids though they do not posses fault gouge along the fault plane and the static permeabilities of this slip zone at the vicinity are lower than in adjacent wall rocks (Cartwright et al., 2007).
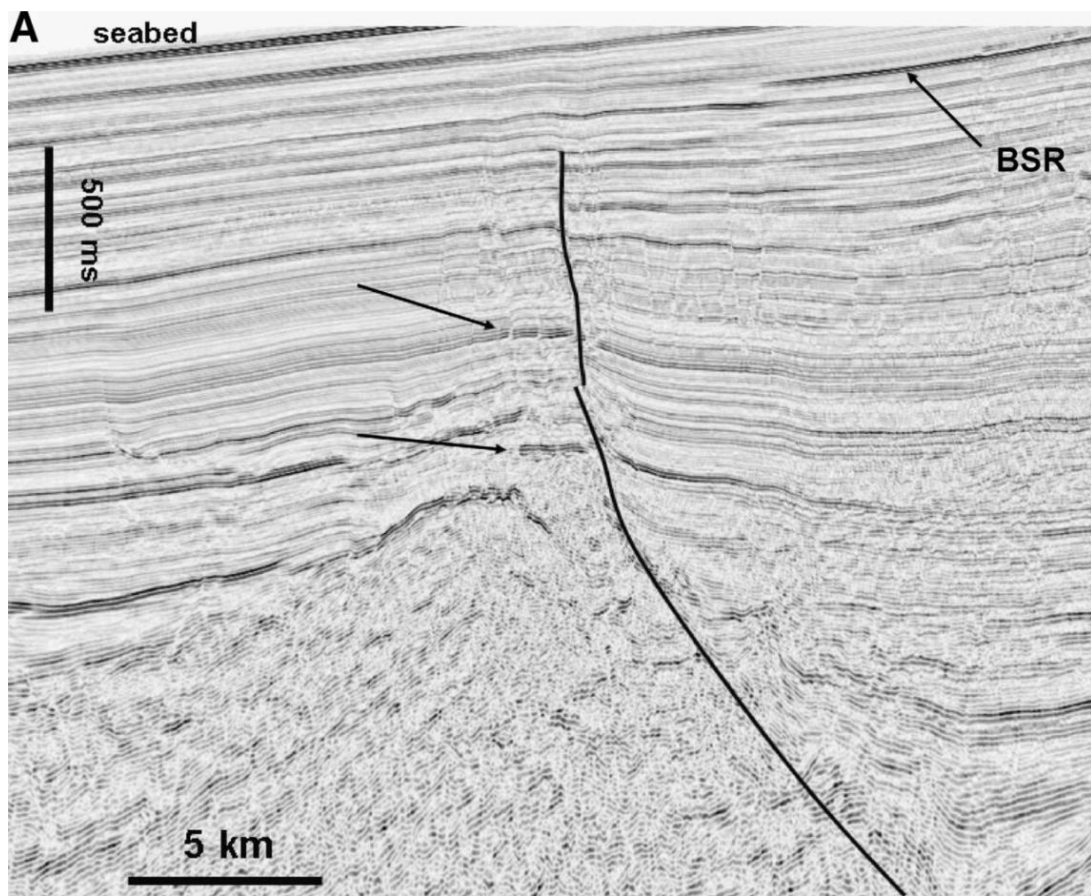
Figure 20. Seismic section of a large tilted fault block where arrow indicates different vertically distributed amplitude anomalies defined as hydrocarbon leakage zone and trap to be a major trap-defining fault. There is also indicated a bottom simulation reflector (BSR) which is relevant to hydrocarbon leakage. Figure modified from (Cartwright et al., 2007)

2.3.3. Intrusive bypass systems (IBS)

Intrusive bypass are intrusive structures breaching the integrity of a sealing sequence. Thus intruded material possesses a markedly higher permeability in comparison to sealing sequence and focused fluid flow takes place through this intrusion. IBS can be classified into four groups:

i. Sandstone Intrusions is a regional scale fluid flow in basin with a significant mode of seal failure in which the flow is not restricted to the period of the intrusion event

33

(could be only a few days). The intruded sandstone may remain as a high permeable conduit for millions of years allowing fluid flow through SBS until the vertical continuity is broken by deformation or the pore space is cemented (Hurst et al., 2003;Husse et al., 2004; Jonk et al., 2005). Typical flow rate is 1-2 cm/s (Shoulder, 2005).

ii. Igneous Intrusions may have lower permeability than the host sealing rocks. Intrusion of hot magma at greater than 1000°C into cold and wet sediments results in a major change in host rock properties for tens of meters around the immediate contact of intrusive body (Einsele et al., 1980). Different fracture sets develop in association to forceful injection of intrusive body, prograded metamorphism, hydrothermally driven fluid loss from surrounding sediments (Einsle et al., 1980) and thermal contraction during cooling of intrusive body. Thus created fractures increases the fracture permeability within and surrounding the intrusive body that actually provides a bypass system in sealing rocks sequence (Cartwright et al., 2007).

iii. Mud diaparism and mud volcanism liquefy parent fine-grained sedimentary unit because of inflation, in-situ overpressuring and external vibrations (like earthquake). Thus liquefied mud then ascends rapidly and comes out to the surface with different rate according to conduit geometry and viscosity of mud itself. Fractures and fault systems are well developed around the mud volcanoes zones because of forceful injection, stopping of mud, caldera style collapse of mud chambers (Kopf, 2002; Morley, 2003; Davies and Stewart, 2005). Thus developed fractures provide additional means for upward fluid flow.

iv. Salt diapirs often occur in hydrocarbon provinces and that involve forced folding and concentric faulting. These folding and faulting mechanisms create complex fracture networks in the immediate contact zone between the salt body and the forcibly intruded host sediments and in the carapace just immediately above the crest of the diapir too (Alsop et al., 2000; Davison et al., 2000). The fault and fracture networks surrounding the salt diaper are permeable for finite time periods. The

alterations brought into the local aquifers and seals by salt diapir may have a potential to change the local hydrogeological settings and finally can lead to seal failure due to excess pressure heads (Evans et al., 1991)

2.3.4 Pipe bypass systems (PBS)

Pipe bypass are defined on reflection seismics in terms of columnar zones of disturbed reflections that could be associated with sub vertically stacked amplitude anomalies (Cartwright et al., 2007). In some cases, these deformed reflections might be related to minor folding and faulting. Even if there is no visible systematic offset of reflections, analogs suggests intense fracturing within the pipe structures (Løseth et al., 2001, 2003). The fracturing is responsible for augmenting the permeability and loss of seal integrity (Bryner, 1961). Cartwright et al. (2007) have subdivided pipe bypass into four families; dissolution pipes, hydrothermal pipes, blowout pipes and seepage pipes.

    i. Dissolution of rock minerals at depth causes the overburden to collapse as it forms subsurface cavities (Stanton, 1966; Cooper, 1986) and is likely to occur in areas where evaporites and karst exist (Cartwright et al., 2007). The collapse of overburden creates tall cylindrical zones of sagging, intense faulting and fracturing through which vertical migration of fluids takes place (Bertoni and Cartwright, 2005). The dimension of dissolution pipes are governed by the dimensions of solution cavity, overburden strength and heterogeneity of materials (Branney, 1995).

    ii. Hydrothermal pipes are formed by the release of high influx of hydrothermal fluid (Svensen et al., 2004) derived from magma that is related to igneous intrusions. These pipes are characterized as columnar or steep-sided, downward-tapering conical zones of distributed or collapsed stratigraphic reflections. They may be formed in direct connection with an igneous sill layer too (Cartwright et al., 2007).

    iii. Blowout pipes are columnar zones of disturbed reflections or vertically stacked localized amplitude anomalies. They are distinguished on the basis of their association with surface or paleopockmarks (Løseth et al., 2001). The driving processes involved in the development of blowout pipes are extremely energetic and

the fracturing of the conduit takes place by the expansion of gas before migrating the fluids.

iv. Seepage pipes may form under the same conditions as blowout pipes, but they lack blowout craters (pockmarks) at the upper pie termination. This type of pipe is mainly seem to occur in sand or silt-dominated sequences. The higher bulk permeability of this sequence allows fluid seepage through pore networks thereby reduces the overpressure buildup. This reduction in overpressure terminates the pipe within the subsurface before reaching to host-rock fracture gradient (Cartwright et al., 2007).

3. DATA AND SEISMIC INTERPRETATION TOOLS

3.1 Data

The 3D dataset (GH01) used in my master thesis is an already processed 3D seismic cube, and the interpretation is based on seismic reflection and imaging techniques to identify gas accumulation and fluid migration pathways along and across different strata.

The 3D seismic dataset GH01 covers a part of northern escarpment of the Storegga slide extending south to Grip High (Fig. 2). This 3D dataset covers an area of 98.6×24.9 km^2 which falls within the slide area of the giant Storegga slide and has a recording length of 4 s. The dataset consists of 998 inlines and 3946 crosslines. The bin spacing is 25 m and thus gives a very good spatial resolution.

The Processing software "Promax" provided by Landmark was used for frequency analysis. Inline 2536 was exported as a 2D line (SEGY format) and imported into Promax for performing a spectral analysis to determine the dominant frequency. This analysis shows a dominant frequency of 27 Hz while frequencies ranging from 24-35 Hz are also dominant.
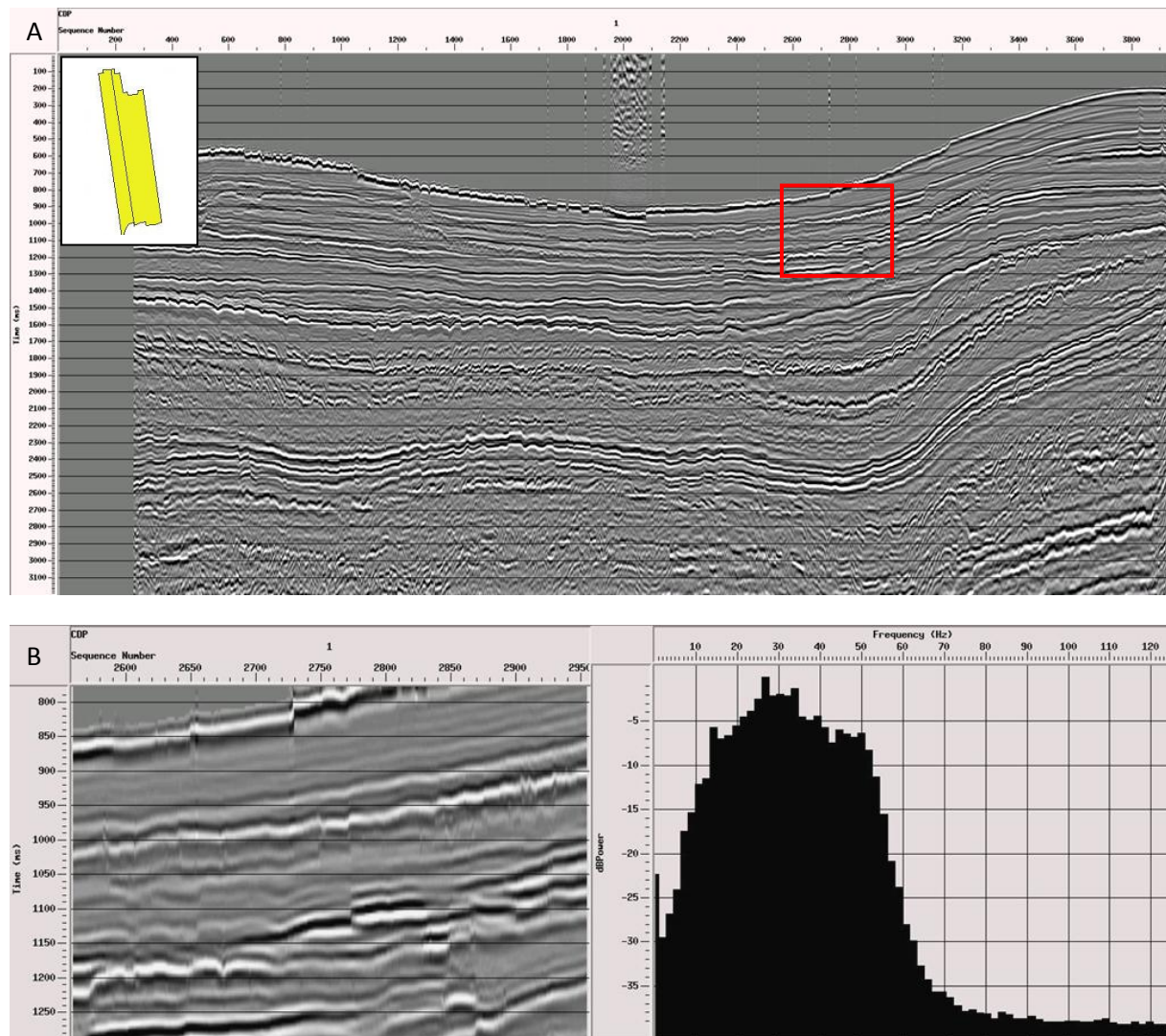
Figure 21. A) Display of seismic inline 2536 in Promax seismic processing program where red rectangle is the area selected for a spectral analysis. B) Display of spectral analysis of area marked in A. The dominant frequency is found to be 27 Hz.

3.2 Seismic interpretation tools (Petrel)

The analysis for the 3D data set GH01 for the purpose of acquiring the set objective for this thesis was carried out using Petrel® 2011 software at the University of Tromsø (UiT). Petrel® 2011, Schlumberger, is seismic to simulation software which helps to develop multi-disciplinary integrated workflows for streamline processes (Schlumberger, 2011).

3.2.1 Interpretation of 3D data

Seismic interpretation is used for interpreting seismic horizons. The first step for seismic interpretation is to create a seismic horizon and then to set the parameters for further interpretation from these horizons. In creating horizons, autotracking allows one to interpret

a continuous reflector. But before applying this tool, it is necessary to determine which part of the signal is to be interpreted, the trough or the peak, upper or lower zero crossings (Fig. 22). In petrel, there are two options; manual and automatic for interpreting the horizons. In manual, one can choose freely where to interpret while in automatic interpretations parameters can be set. There are three options for automatic interpretation of horizons; guided autotracking, seeded 2D autotracking and seeded 3D autotracking. The tool is based on values of amplitudes in a seismic trace and will follow the given reflector determined by the continuity and signal strength. There are several parameters where the interpreter can chose different constrains of the seismic signal to be followed. For a good continuous reflector like seafloor, one can set loose constraints whereas for a chaotic event as in slide deposits, a more strict constraint is suggested.
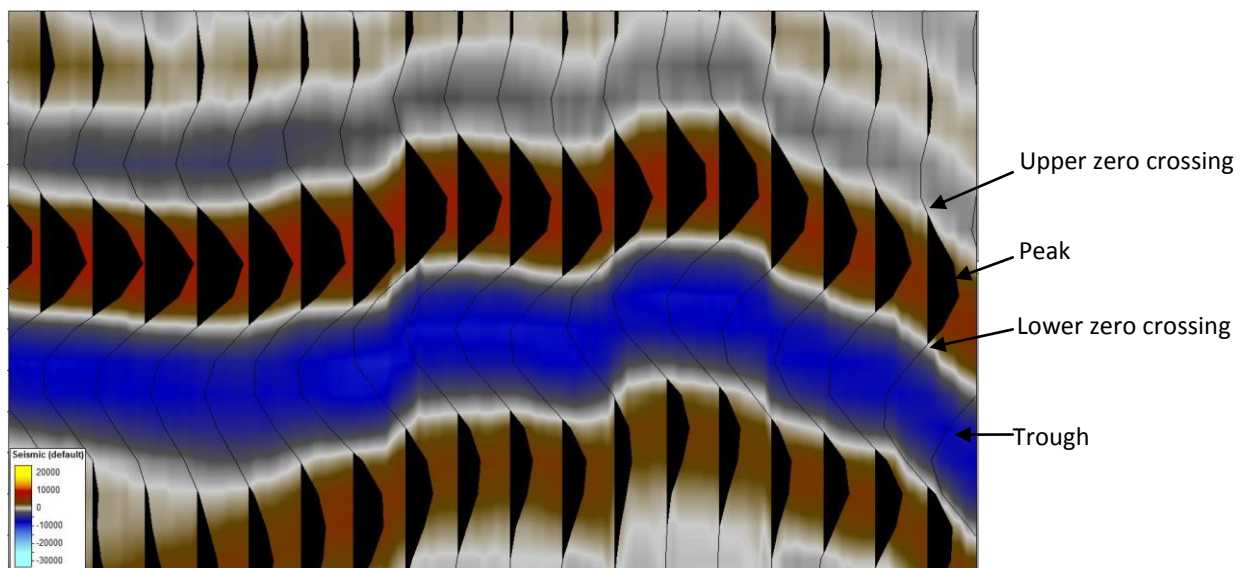
Figure 22. The peak, trough, upper-and lower-zero crossings of a seismic signal. The peak is displayed in red, the trough in blur and the zero crossings in white.

3.2.2 Seismic Attributes

Seismic attributes give more details and specific knowledge about the research interests. Chopra, 2005 has defined a seismic attribute as a quantitative measure of a seismic characteristic of interest. The advanced computer technology has aided the attribute analysis more easy and successful. The attribute analysis carried out in this thesis has been grouped under two divisions: volume based attributes and surface based attributes.

The color scale has been adjusted to each seismic section in order to define the anomalous area distinctly.

3.2.3 Volume Based Attributes

Volume attributes are extracted data from a specific seismic volume where different physical properties of the seismic traces with different values are calculated and displayed in a volume window. There are a number of volume attributes available in Petrel that can be applied to a specific seismic volume but few attributes that are useful for this present thesis are described here underneath.

3.2.4 Structural smoothing

Structural smoothing for a given volume locally smoothens the input data thereby increasing the continuity of seismic reflections (Schlumberger, 2011). It also helps to identify flat spots for a given seismic volume.

3.2.5 RMS

RMS amplitude is the square root of the sum of the squared amplitudes within a desired volume interval divided by the number of live samples in interval. RMS amplitudes are only positive and shows the strength of amplitude over a given volume interval. Changes in amplitude pattern vertically and horizontally are apparent in RMS amplitude map.

RMS amplitude = $\sqrt{\dfrac{(\Sigma_i^n amp^2)}{k}}$ where k is the number of live samples.

The color scale for the RMS amplitude map has been adjusted to each RMS amplitude map in order to define the anomalous area distinctly.

3.2.6 Chaos

The chaos attribute demonstrate the "chaoticness or the lack of organization" of the seismic data within a given volume. The chaos attributes picks the regions of low consistency seismic traces and that can be correlated to geological features like faults or discontinuities, gas migration pathways, salt body intrusions, reef textures, channel infill etc. which have lack of organization in dip and azimuth.

3.2.7. Variance

Variance is similar to Chaos attribute which displays the variance in the seismic signal. It indicates the lateral continuity of a seismic reflector. It is used for imaging discontinuities based on the difference in where fault planes are laterally separating data which can be auto-tracked using voxel-picking algorithms. Lack of continuity indicates the presence structures like faults or slide deposits. Both chaos and variance attribute cubes are based on the edge detection method.

3.2.8. Surface Based Attributes

Surface attributes can be generated at different intervals relating to a single surface, between two surfaces or in a constant time window. RMS surface attribute visualizes the RMS volume along a certain surface of interest. Lateral changes in seismic amplitudes are apparent in this method and helps to identify the area of interest easily and accurately.

4. RESULTS

The study mainly focus on the potential impact of fluid flow on the Storegga slide with special focus on the northern escarpment along with the high amplitude anomalies (possible gas accumulations) within different units of Brygge, Kai and Naust formations. For this purpose, fluid migration pathways, high amplitude anomalies (possible gas accumulations) and sildes near the northern sidewall of the Storegga slide have been mapped and evaluated.

4.1 Potential fluid migration pathways and accumulation areas

Polygonal faults along with some major faults in the form of polygonal fault extension are the major pathways for the fluid migration within the study area.

4.1.1 Polygonal faults

3D seismic profiles and time slices have been analyzed to get an overview of polygonal faults within the study area. The polygonal faults are found to be widely distributed within Brygge, Kai and lower sequence of the Naust formation. Within the study area, they have variable extensions showing that upper and lower terminations of adjacent faults do not occur at the same stratigraphic level. So many small offset faults have been confined within the bound layer while some of the major faults have extended to the lower sequence of Naust formation (Fig. 23a).
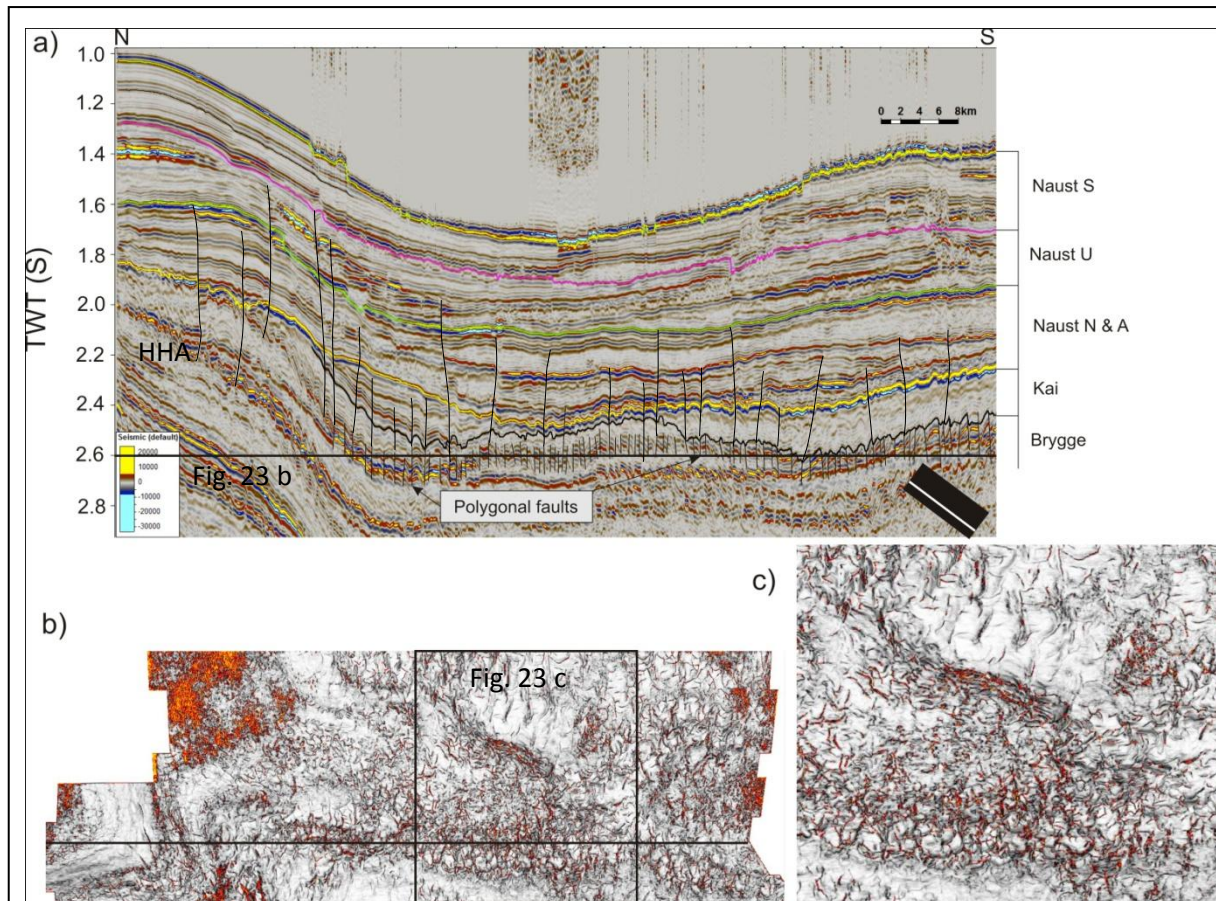
Figure 23. a) Seismic section of inline 2496 of 3D seismic survey GH01 showing polygonal faults within Brygge formation. b) Time slice variance map at 2600 ms as indicated by a black straight line in (a) passing throughout the Brygge formation showing polygonal faults within the Brygge formation. c) Enlarged view of polygonal faults in a plan view within a rectangle in Fig. 23b.

At the top of the Brygge formation within 2400-2900ms TWT, layer bound polygonal faults are characterized by small displacement of around 20ms, steep slopes of 50-85° with average spacing of 1km (Fig 24a). In a time slice, they appear in the form of polygon with curvilinear outlines (Fig. 24b and c). The polygonal faults have greater vertical extent towards south of the study area where thick succession of Kai formation exists but towards north they have less vertical extent due to the thinning out of the Kai formation (Fig. 23a). In NW part of the study area where Kai formation has pinched out over the HHA, some of the faults have reached close to the seafloor (Fig. 23a).
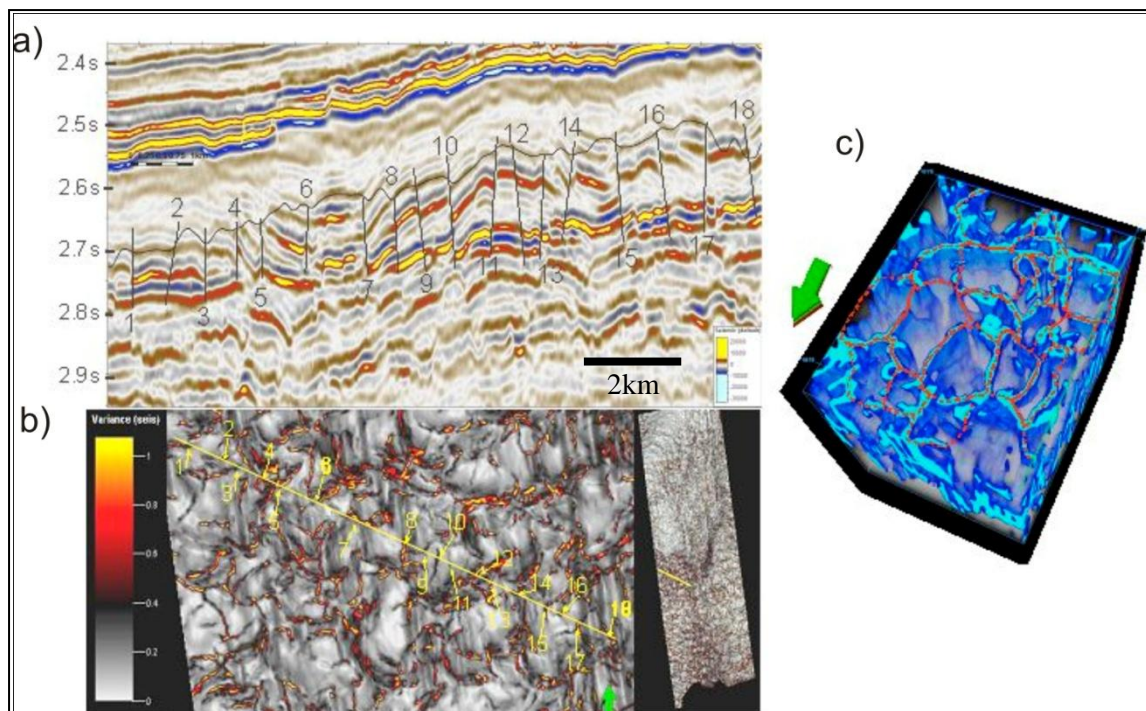
Figure 24. a) Interpreted seismic section showing the distribution of polygonal faults within the Brygge formation. b) Variance map showing corresponding polygonal faults in comparison to seismic section (see a). c) Polygonal fault in 3D showing their shape and vertical extent. Location of figures a and b is shown in inset Fig. b.

4.1.2 Acoustic Pipes

Laterally narrow (20-200m wide), elliptical to circular zones (Fig. 25b, 25c) of up bending, low amplitude reflectors termed as acoustic pipes of various sizes are observed to the north of the northern escarpment of the Storegga slide (Fig. 25). Two prominent pipes (Fig. 25a) on the northernmost part of the inline 2596 show the upward bending reflectors because of their blowout nature. Both pipes show approx. 25 ms upward bending reflector. Most of the pipes show their root between 1600-1700ms TWT (Fig. 25a). They have originated at the top the southern flank of the Helland Hansen Arch (HHA) (Fig. 25a). The upper termination of these pipes is at different stratigraphic levels within the Naust formation or at the seabed resulting pockmarks (e.g. Berndt et al., 2003) (inset figure of 25a). Some pipes show down bending reflectors, which are interpreted to be the result of velocity pull down possibly indicating active fluid expulsion (Berndt et al., 2003, Plaza Faverola et al., 2012). These seismic indicators fluid flow pipes are common near the northern headwall of the Storegga slide and are not found downwards within the study area.
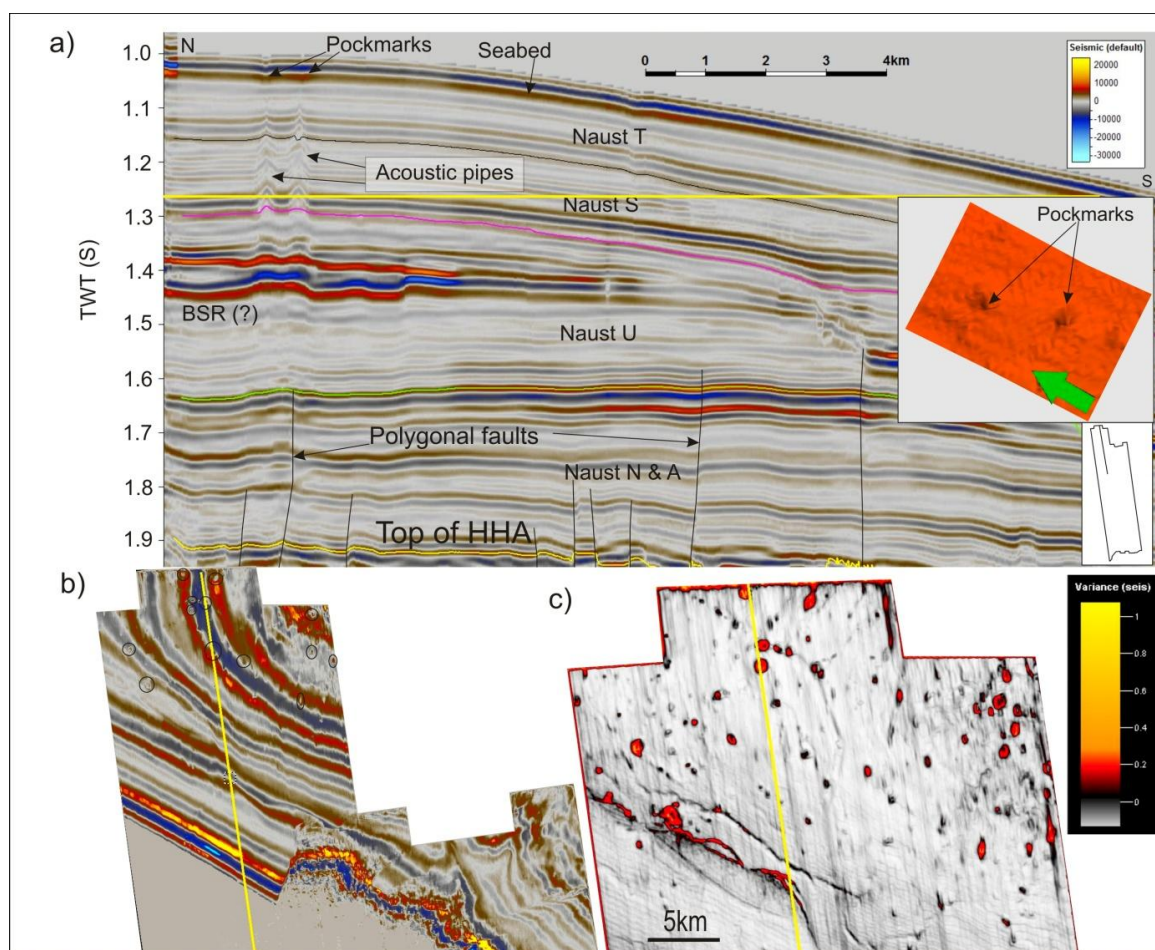
Figure 25. a) Interpreted seismic section of inline 2596 showing two prominent pipes at the northernmost part of the survey. b) Time slice at 1268ms passing through the two pipes showing circular and elliptical pipes. Most of these pipes concentrate at the north of northern escarpment of the Storegga slide. Inset figure in (a) shows pockmarks on the seabed. c) Time slice of variance map at 1296ms showing the sub seabed distribution of pipes.

4.2 Amplitude anomalies

Seismic profiles within GH01 3D survey reveal high amplitude anomalies within Brygge, Kai and sub-units of Naust formations (Fig. 26). The amplitude anomalies have reverse polarity if compared to seafloor (Fig. 26 and Fig. 27) indicating acoustic impedance contrast with the sediments in which they are embedded. The high amplitude anomalies on certain layers seem to be continuous and extend for several kilometers (Fig. 28a, 30a, 30d) and are as thick as 24-80m (assuming sound velocity ~2000m/s). Majority of high amplitude anomalies are discontinuous (Fig. 26, Fig. 27, Fig. 34) and these single features are about 0.2-1.8km wide (Fig. 28a). High lateral resolution of the 3D survey with advance 3-D interpretation techniques help to map out the distribution of these high amplitude seismic anomalies. RMS

amplitude map for certain volume window have been applied for imaging and mapping out them in different sedimentary units. Lateral distribution of high amplitude anomalies within each sedimentary unit of the study area have been described underneath.
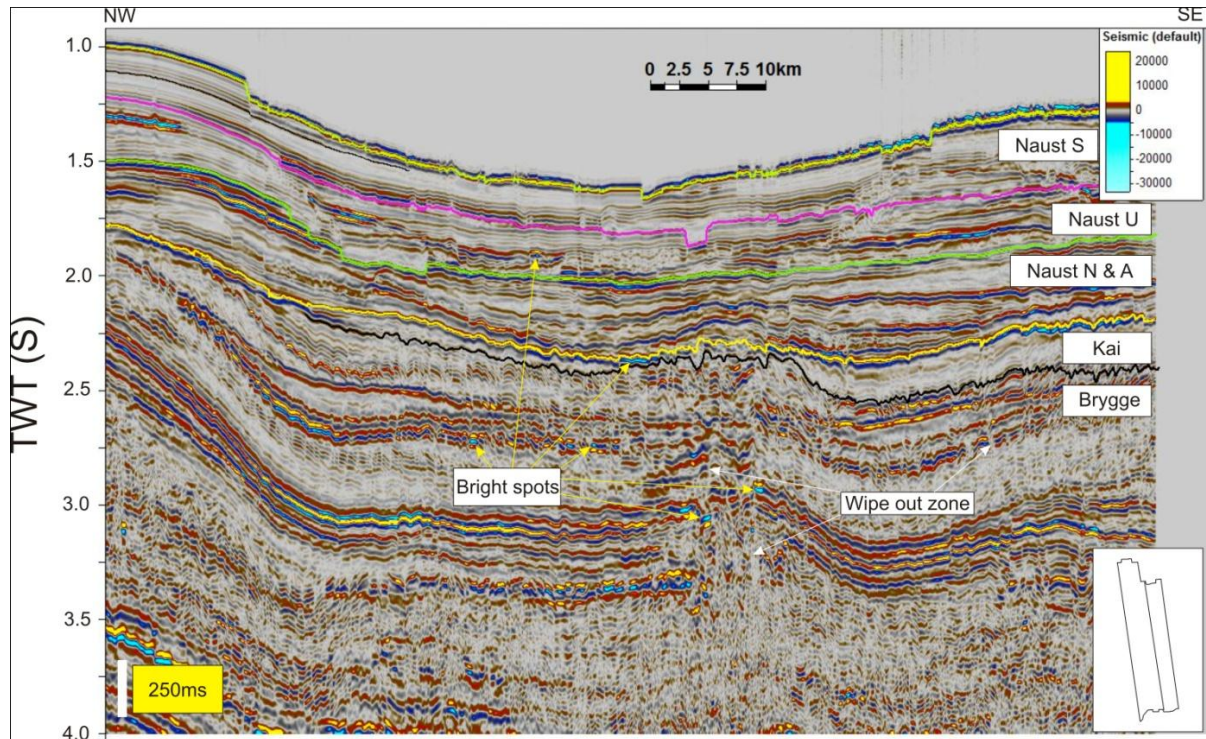
Figure 26. Interpreted seismic section of inline 3350 showing bright spots and wipeout zone. These bright spots may be the zones of gas accumulations. The bright spots have been recognized within Brygge, Kai, Naust N & A and Naust U units.
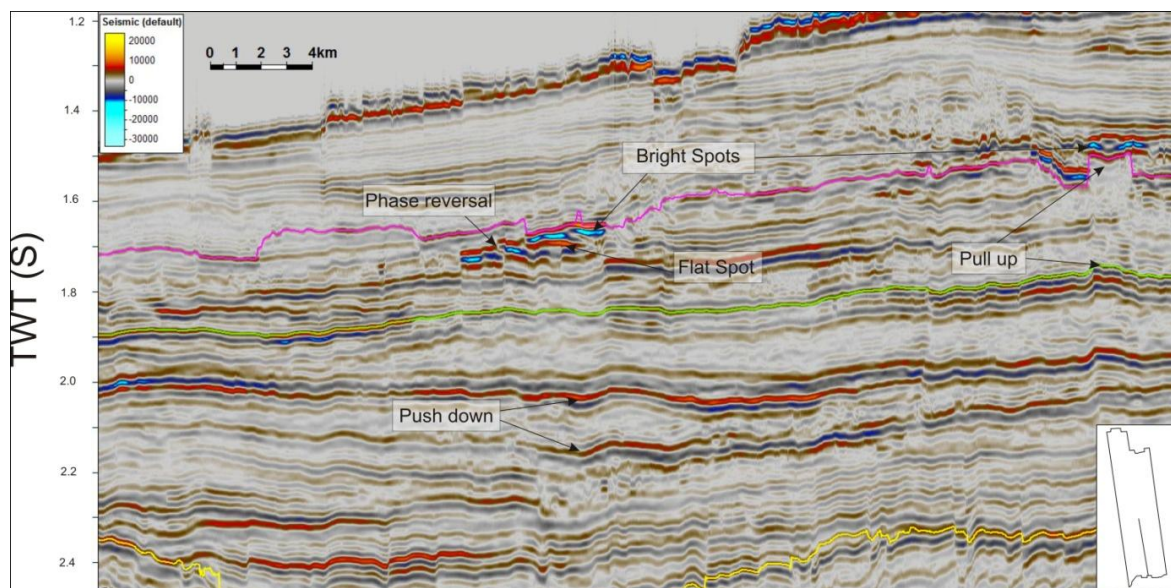

Figure 27. Interpreted southern part of seismic section of inline 2900 showing bright spots, flat spots, phase reversal and push down and pull up effects.

4.2.1 Acoustic anomalies within Brygge Formation:

Brygge formation occurs within the whole study area (Fig. 36). The RMS amplitude map for a window of 50ms below the top of Brygge formation south of HHA shows the distribution of high acoustic anomalies in the form of bow-tie shape (Fig. 28b). These amplitude anomalies seem to be continuous in a seismic profile but are separated into small patches by polygonal faults crossing them. They are confined within 2600-2750ms TWT (Fig. 28a). Towards west of the study area, each anomaly have lateral extension 250-1040m and towards east it is 220-1860m.

High amplitude anomalies on the southern limb of HHA within the study area lies within 150-200ms TWT down the top of Brygge formation. RMS amplitude map for a window of 50ms (150-200ms down the Brygge top) shows the distribution of acoustic anomalies towards west which is ~ 20km long and ~12 km wide (Fig. 29a, 29b).

4.2.2 Acoustic anomalies within Kai Formation:

The Kai formation is thinning towards west to HHA. In a N-S oriented seismic profile (Fig 30a), high amplitude anomalies seem to be continuous reflector at the top of the Kai formation that lies within 2250-2450ms TWT down. This reflector is also cut by polygonal faults into many smaller single features. The offset of these single features have been reported 10-30ms. The whole Kai formation looks transparent in comparison to its surroundings. RMS map calculated for 30 ms window below the top of the Kai fm (Fig. 30a) indicates the distribution of acoustic anomalies on the southwestern part of the study area (Fig. 30c). The total length for this anomaly is ~30km and is ~10 km wide. This amplitude anomaly might have further extended westwards out of the study area.
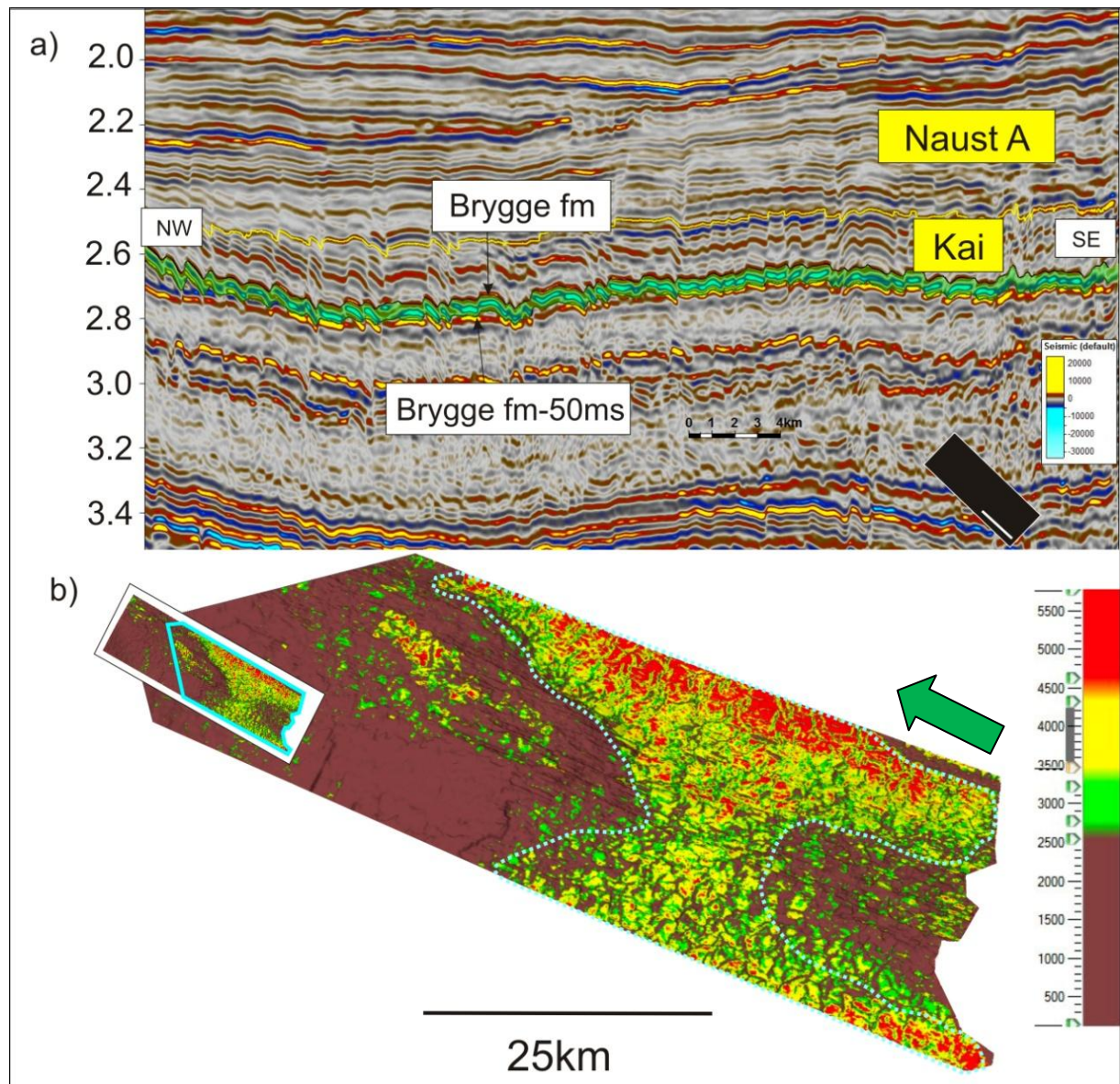
Figure 28. a) Seismic section of inline 2300 south of HHA showing high amplitude with negative anomalies at the top of the Brygge formation for a 50 ms window. The window is shaded with light blue. b) RMS amplitude map of 50ms window below top of Brygge formation (light blue shaded in a). Sky blue dotted line in b shows the inferred high amplitude anomalies at southern limit of the study area.
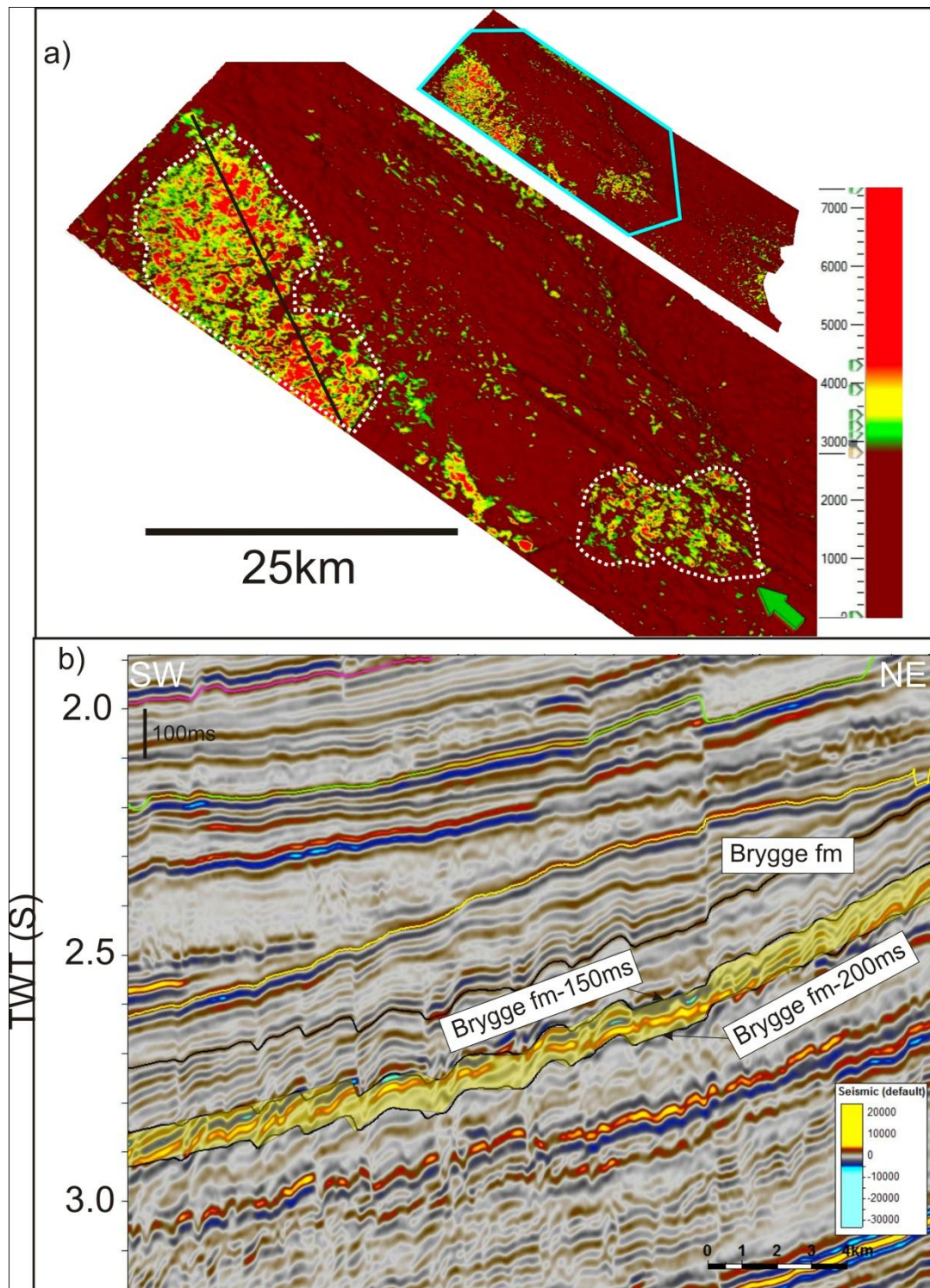
Figure 29. a) RMS amplitude map for 50ms window (Top Brygge to 150-200ms TWT) showing high amplitude with polarity reversal on the southern flank of HHA and on the middle part of the survey that are outlined by a white dotted line. b) The interpreted seismic section corresponding to a black line in (a) shows a high amplitude reflector with reversed polarity within 50ms shaded window.
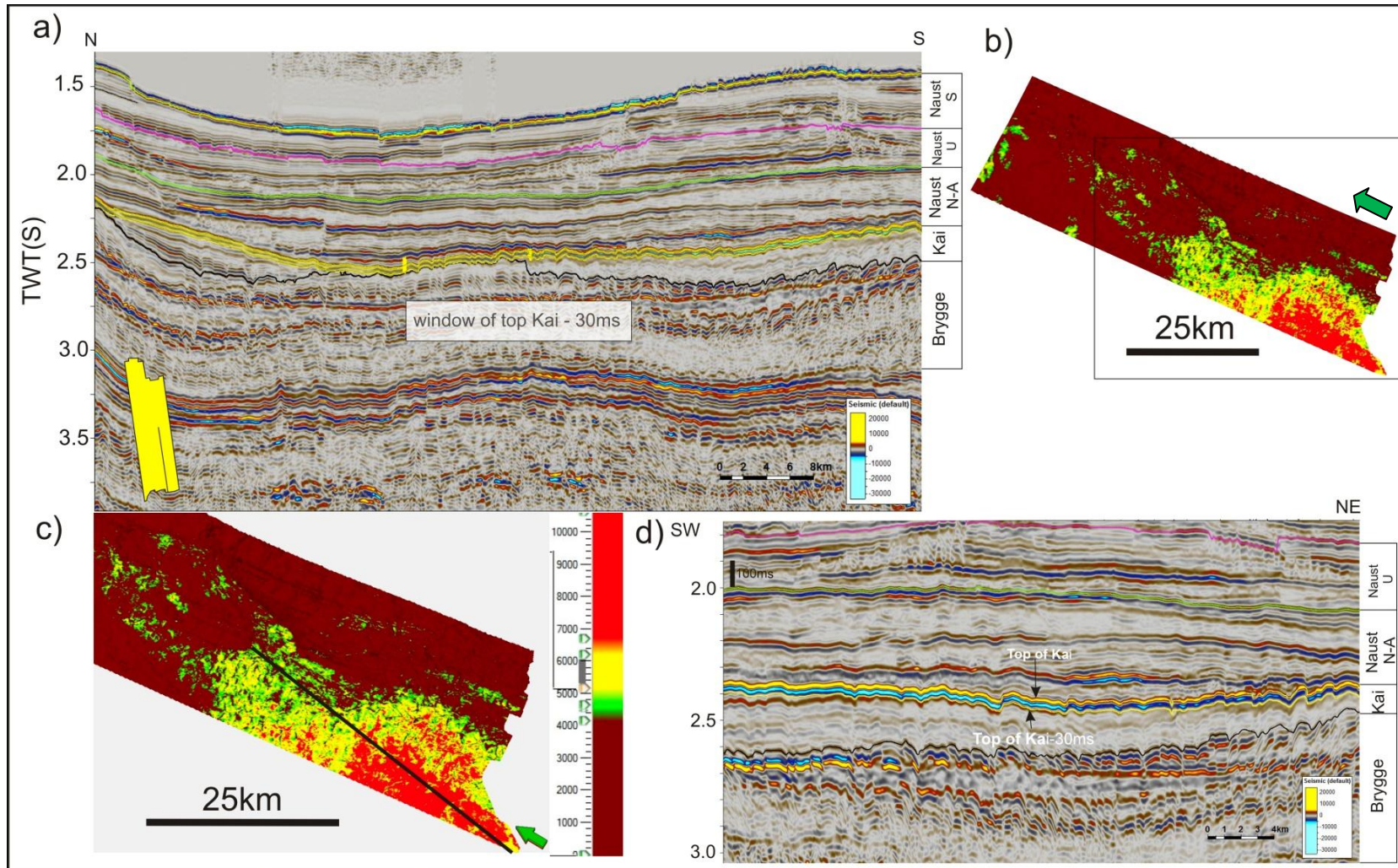
Figure 30. a) Seismic inline 2900 shows the stratigraphic units. Pale yellow shaded region represents the 30ms window from the top of the Kai formation. b) RMS amplitude map of Kai-30 ms (shaded portion in a) shows high amplitudes at southeastern part of the survey area. c) The enlarged portion of RMS map at b shows the survey with corresponding seismic line in d. d) Seismic line indicated by a black line in c shows high amplitude negative reflector within 30ms of window.

4.2.3 Acoustic anomalies within Naust N and A units:

The two units have a more or less uniform thickness throughout the study area (Fig. 36). The prominent reflector lies at the top of Naust A unit that lies within 20ms window from the top of Naust A unit. RMS amplitude map for a window of 20ms down the top of Naust A unit shows the distribution of acoustic anomalies on northeast, central east and southwest of the study area (Fig. 31 a-e). This reflector is more or less continuous within the seismic profile and is found to be embedded in marine sediments.

4.2.4 Acoustic anomalies within Naust U unit.

Naust U unit in a seismic profile contains both chaotic and continuous reflector. The most prominent high amplitude reflector lies in a 80ms window (30-110 ms down the top of Naust U unit) (Fig. 33). A seismic reflector at the upper part of this unit on the northern undisturbed part is parallel to the seafloor and is interpreted as bottom simulating reflector (BSR).

BSR and Gas hydrate

At 200ms TWT below the seafloor, a high amplitude reflection parallel to seafloor and characterized by a reverse polarity if compared to seafloor reflection (Fig. 32) is interpreted as a Bottomm simulating Reflector (BSR). It can be observed only on the north of northern flank of the Storegga slide within the study area which is extended further northwards. Within the study area, BSR on the western part is found at greater depth than at the eastern part. In the westernmost part of the study area, it is documented at 1400ms TWT but towards east part it is documented at 1280ms TWT. The most extension of the BSR is found at the northwestt part of the study area which extends about 10km within the seismic profile (Fig. 32). It is not observed after inline 3000 where the survey doesn't cover the undisturbed part towards east. BSR is found at the upper part of the Naust U unit within the contouritic drift deposits (Fig. 32). It indicates the base of the gas hydrate stability zone (BGHS) (Bouriak et al., 2000). Gas hydrate is found within the sediment just above it while the transparent zone just beneath it represents the free gas. The present BSR on the northern flank of the Storegga slide is located under the water column of 700m.

RMS amplitude map for a window of 80ms (30-110ms down the top of Naust U unit) shows the distribution of high amplitude anomalies on the northernmost undisturbed part of the study area and under the slide mass on the central east region of the study area (Fig. 33b). The high amplitude reflector on the northern part lies within a continuous reflector while on other parts they are associated to some chaotic reflection (Fig 33a). The zone just below this high amplitude reflector on the northern part within this unit is transparent thereby indicating the absorption of seismic energy.

4.2.5 Acoustic anomalies within Naust S:

There are no remarkable amplitude anomalies within this unit except at the southeastern base within 1350-1450ms (Fig 34). These amplitude anomalies occur on both flanks and top of a velocity pull up zone. RMS amplitude map for 80ms at the bottom of this unit shows the distribution of acoustic anomaly at the southeastern limit of the study area (Fig 34 a-d).
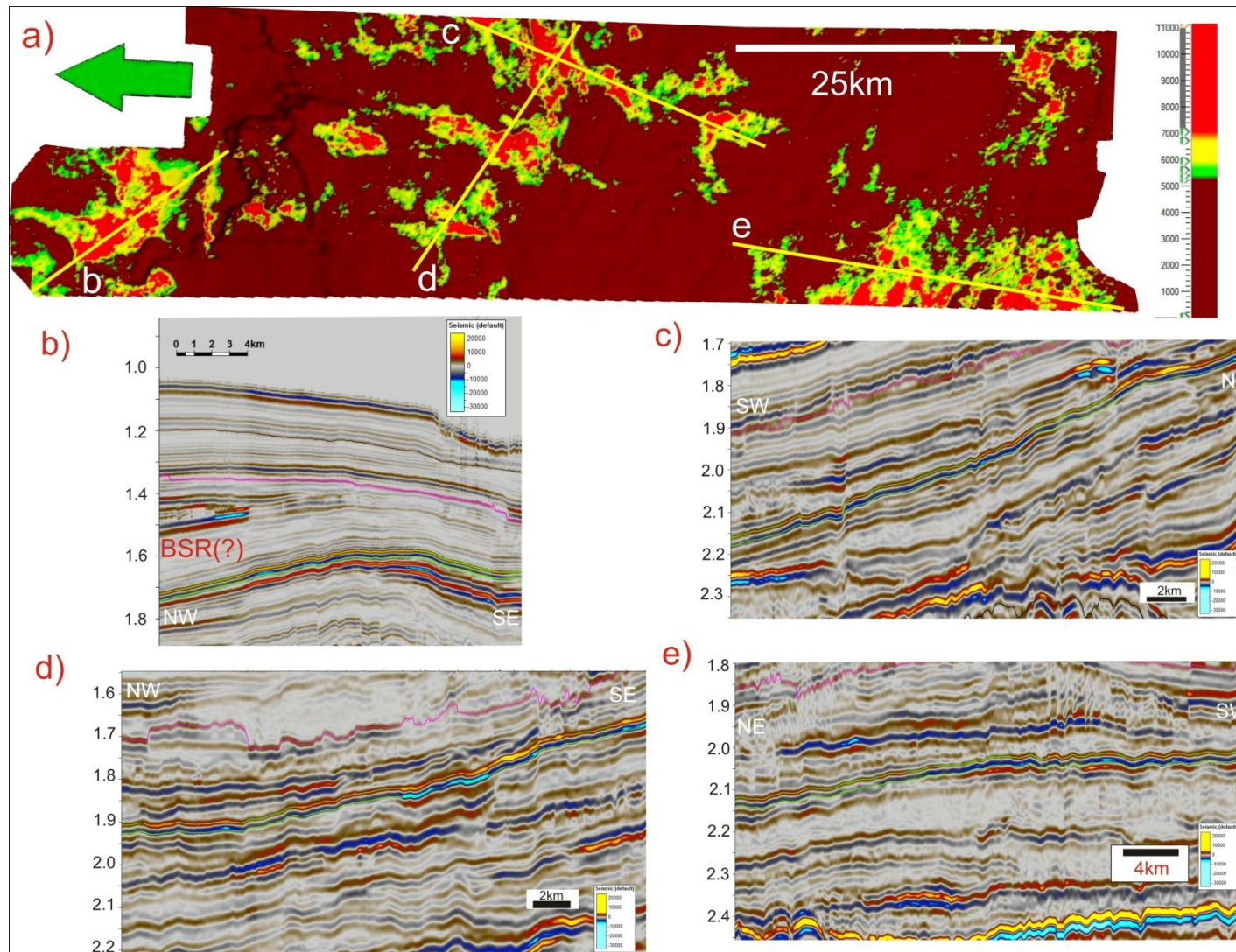
Figure 31. a) RMS amplitude map for Naust A with corresponding seismic sections (b-e).b-e) Seismic sections indicated high amplitude anomalies and phase reversals.
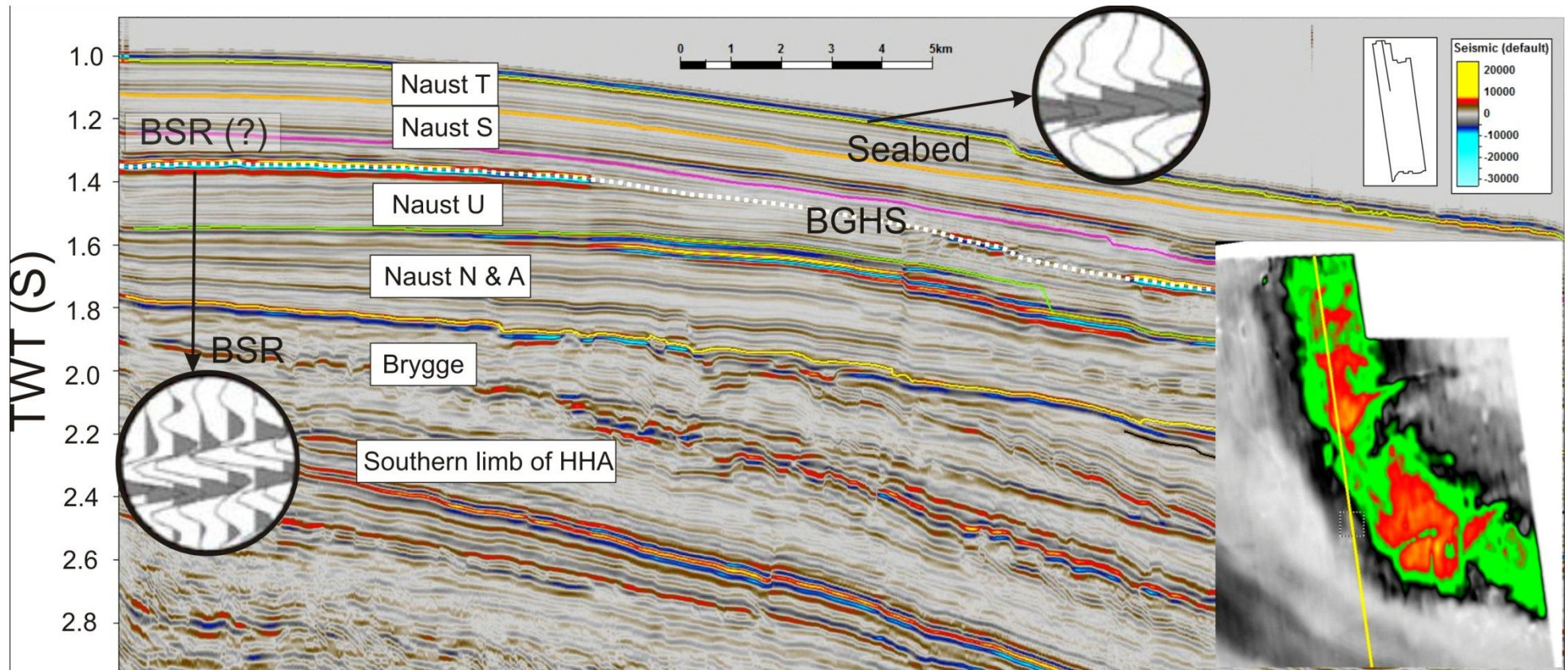
Figure 32. Seismic section of inline 2640 showing BSR at the upper part of Naust U unit. The small insets within circles show corresponding wiggle trace as indicated by arrowline. The inset on the right bottom corner shows the time slice RMS amplitude map at 1348ms pasing through the BSR. White dotted line indicates the base of gas hydrate stability zone (BGHS).
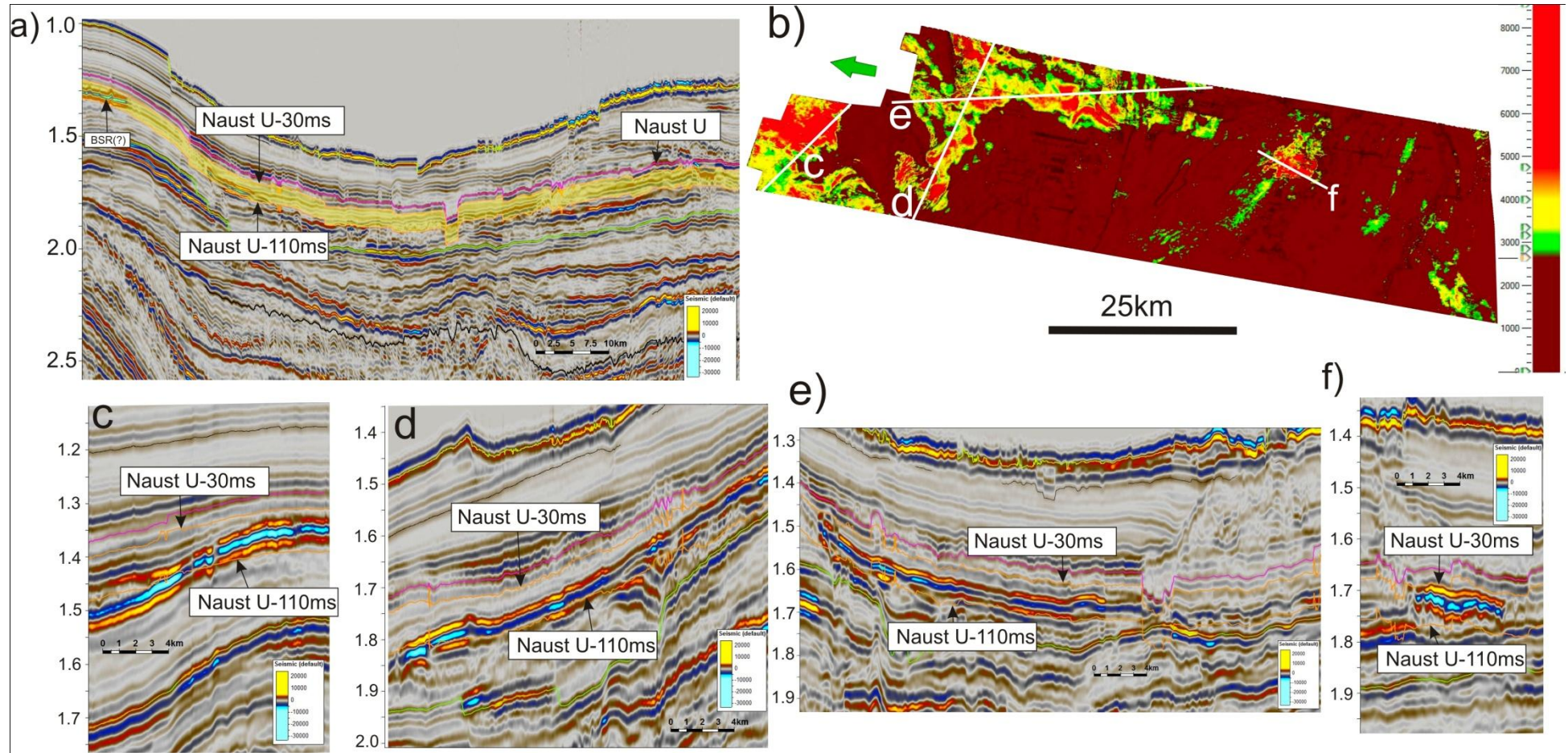
Figure 33. a) Seismic inline 2596 showing a shaded window for 80ms (from top of Naust U and 30-110 ms downward) b) RMS amplitude map for shaded volume shows the inferred distribution of gas accumulation at the northern and central part of the study area. c-f) Seismic sections as indicated in b showing acoustic anomalies.
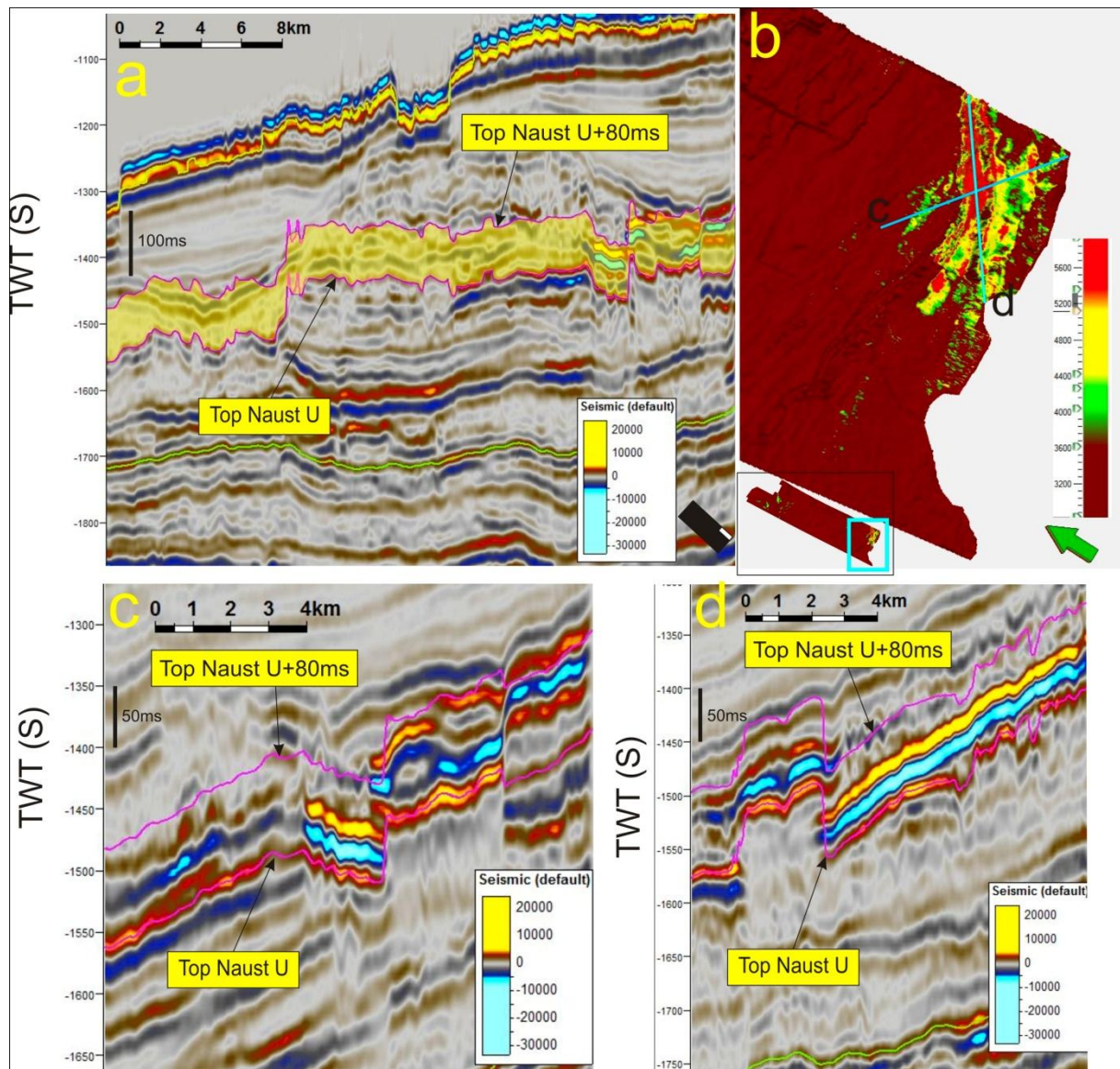
Figure 34. Southernmost part of seismic inline 3944 showing a shaded window (80ms of pale yellow) above top Naust U. Acoustic anomalies are within the window and are located at the southeastern part of the study area as shown in figure b. b) RMS amplitude map for the shaded volume showing the prominent high amplitudes at the southeastern part of the study area. c-d) Seismic sections as indicated in (b) showing acoustic anomalies.

4.3. Storegga Slide region

4.3.1 Seismic Stratigraphy

The nomenclature for the stratigraphy of the study area is based on the work by Rise et al. (2006).

The study area covers the southern part of Helland Hansen Arch (HHA) (Fig 35). The representative seismic units for this region are presented from the southern part of HHA in a 3D seismic view (Fig 35). It shows the Brygge, Kai and Naust formations. The Neogene succession of the Naust Formation has been subdivided into five sub-units as Naust N (oldest), A, U, S and T. These units are identified on the basis of seismic facies parameters and provided isochron surfaces from the northern part of the survey area. They are correlated based on the seismic data to the whole survey area.
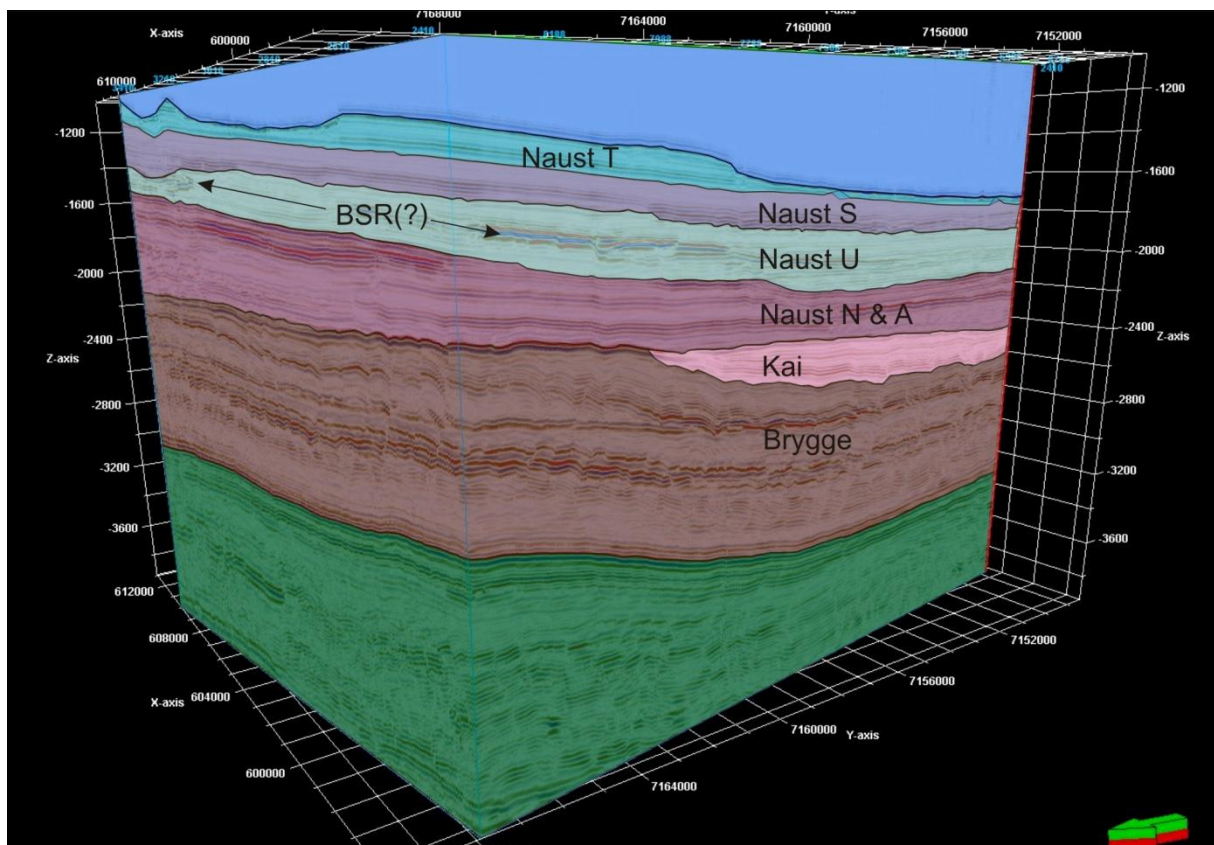
Figure 35. Representative 3D view of south part of HHA showing all stratigraphic units used in this study.
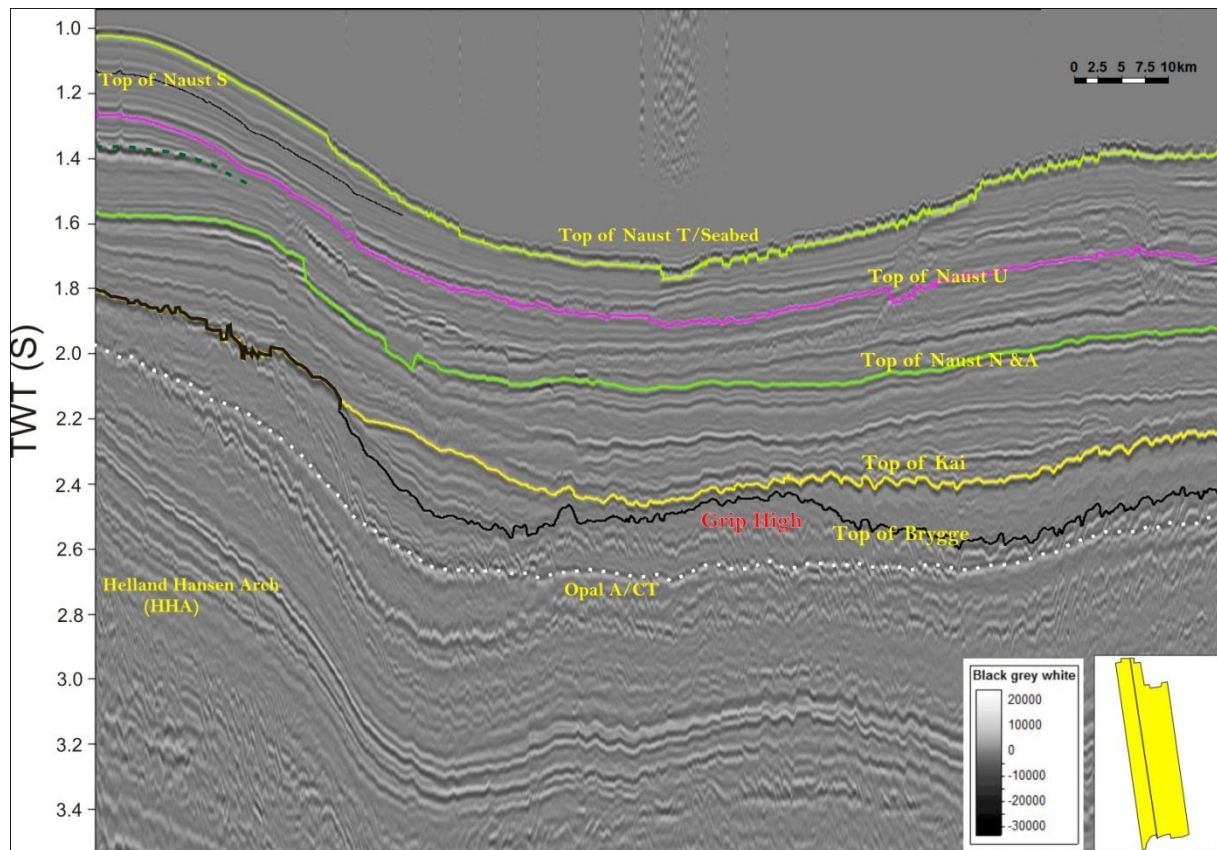
Figure 36. Seismic inline 2596 showing all stratigraphic units. Helland Hansen Arch (HHA) and Grip High are also shown within this seismic section. Opal A/CT boundary marked by positive reflection is present at about 2.4 S TWT is indicated by a dotted white line. Green Dash line at 1400ms indicated high amplitude negative reflection is BSR.

The strong positive reflection at 1.8s TWT (Fig 36) marks the top of the Brygge formation which dates back to Eocene and Oligocene times (Eidvin et al., 2007). This formation exists throughout the whole survey area from N to S. The northern limit covers the southern part of HHA which is obvious in the seismic strata as a regional high (fig 36). Within the Brygge formation, the Opal A/CT boundary occurs at 2.4s TWT indicated by white dotted line. The Kai formation overlies the Brygge formation which shows significant thickness variations throughout the survey area. This formation is thin and becomes partly absent over the HHA. The HHA has acted as a barrier for the sediments preventing them to be transported towards the west.

The uppermost 800ms TWT represents the Neogene succession of the Naust formation. The significant thickness over the Brygge and Kai formation is mainly due to the high sediment deposition rates during the last 2.8 Ma in this area (Rise et al., 2006).

4.3.2 Identification of Submarine Slides at the northern escarpment of the Storegga slide

Potential submarine slide areas within the Naust sediment formation exists at the northern escarpment of the Storegga slide. One of the best seismic section showing step-back paleoslides within Naust U unit and a recent slide at Naust T unit is presented in Fig. 37 along with their features. These slides are characterized by chaotic internal seismic reflection patterns with a laterally continuous reflector at the base of the slides, which marks the glide plane of the downward moving material (Fig 37). The chaotic masses terminate upslope at a headwall at which the sliding ends. Rotated blocks lie near to the headwall where listric faults are seen as well (Fig.37). The blocks collapsed at the time of the initiation of the slide and converted into chaotic masses after detachment from the headwall moving to a greater downslope distance. The topmost sequence of submarine slides occurs at the seafloor (Fig. 37).

The mass movement material gives rise to chaotic reflections above a continuous glide plane at the base (Fig. 37). The characteristic of such slides have been identified beneath the northern escarpment of the Storegga slide (Haflidason et al., 2004). The glide planes are normally identified by a continuous, parallel and undeformed reflector which is in contrast to the defomed material above it. The escarpments correspond to extensional failure surfaces and are similar to extensional faults. The three slides within the Naust formation at the northern escarpment of the Storregga slide show all very clearly a headwall, block faulting, chaotic material and relatively short run out distances of approx < 5 km (Fig. 37).
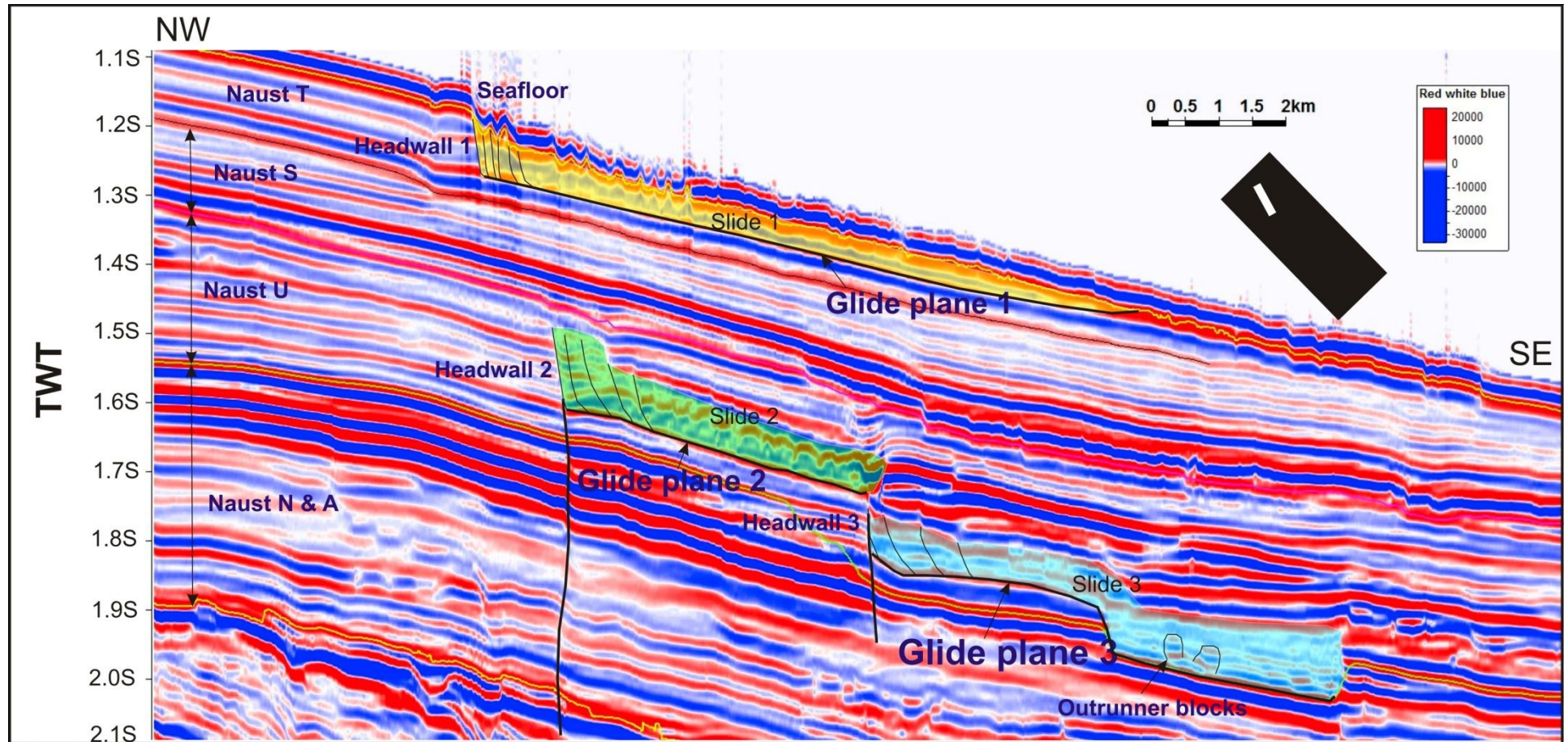
Figure 37. An interpreted seismic section (line) across the northern escarpment of the Storegga slide showing several slides within the NAUST formation with their corresponding glide planes and headwalls.

4.3.3 Sediment Architecture of slides at the northern escarpment of the Storegga slide

Sediment architecture describes the internal details of the seismic strata within the Storegga slide to infer possible slide mechanisms and processes. A seismic profile perpendicular to the major headwall shows the important morphology of the sediments showing troughs and ridges (Fig 38). The troughs and ridges represent the blocky and irregular nature of the slide material.
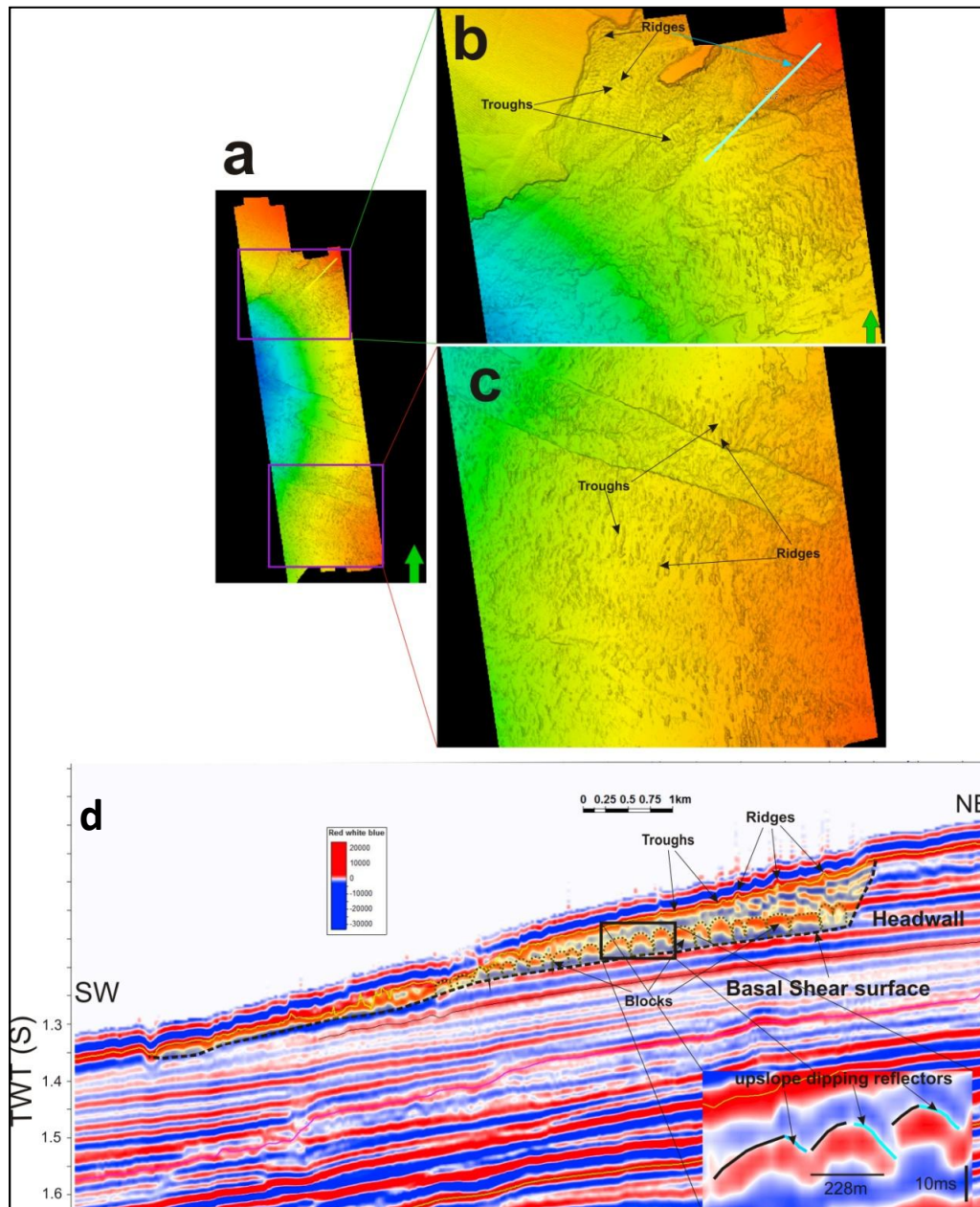
Figure 38. a) Seabed morphology of the study area. b) The northeastern part of the study area showing distinctive ridges and troughs on the seafloor. c) The southern part of the study area with widespread ridges and troughs. d) Seismic section (indicated in b by sky blue line) through the headwall and blocky material. The failed material is indicated in pale yellow. Inset figure in (d) is the enlarged portion of slide mass as indicated by a rectangle.

The groups of subseabed reflections interpreted as blocks are separated from (Sky blue color on inset Fig. 38d). Considering average P wave velocity as 1700m/s (Micaleff et al., 2007), the dip of these reflectors on average is 25°. The blocks are rhomboid or trapezoid in shape with top or base of approx. 220m long. The mean thickness of the block is around 30 ms TWT (i.e. ~25m considering Vp = 1700m/s). The blocks morphology is best observed near the headwall while it becomes obscured because of the reorientation and further disintegration of material at a greater distance. They become also more widely spaced and more tilted with greater distance from the headwall. The upslope dipping reflectors for the blocks are interpreted as shear planes developed as a result of extension by virtue of its dip angle as expected for Mohr Coulomb Failure for these kinds of sediments (Kvalstad et al., 2005b). In order to accommodate the material extension, the blocks translated downslope so that their surface is steeper than the basal shear surface indicating that the blocks have tilted downslope. The observed ridges and troughs are the results of this tilting mechanism of the blocks where only their top parts are exposed in stair-case pattern in the form of ridges. The greater the distance of movement the greater the extension in the blocks. Eventually, spreading of sediments within the northern escarpment of the Storegga slide has created ridge and trough morphologies which are discussed in chapter 5.

5. DISCUSSION

5.1 Fluid Migration

The discussion is based on 3D seismic interpretations to document potential relationships between fluid migration, gas accumulation and areas of slope instability. The migration of fluid has taken place through polygonal faults pervasive on the top of Brygge and Kai formation. Some of these faults have been extended to the base of Naust formation too. Some other faults reported within the study area acted as pathways for fluid migration.

5.1.1 Polygonal faults within the study area.

The uppermost Brygge and Kai formation in seismic profile show small offset, steeply dipping (50-85°) normal extensional faults. Time slice reveals these small offset faults a polygonal shape in plan view (Fig. 23b, 23c, 24b and 24c) so why are termed as polygonal faults. These polygonal faults have different orientation within a seismic profile thereby lacking a dominant strike direction (Berndt et al., 2003). Within the study area, these polygonal faults occur into two tiers in the uppermost Brygge and in the Kai formations (Fig. 39). In general, these faults are found to be bounded within a certain layer suggesting typical properties of the material within the sediment formation. Similar layer bound, steeply dipping and closely spaced, planar normal faults have been identified by Berndt et al., 2003 at the top of Kai formation in most part of the Vøring basin. These layer bound polygonal faults have variable extent showing their upper and lower terminations at different stratigraphic level (Fig. 40) (Berndt et al., 2003). This variable extension suggests their vertical extent not exclusively controlled by the stratigraphy.

In a seismic profile (Fig. 40), the fault frequency is much higher in the lower part than in the upper part of the successions as found by the Berndt et al., 2003 on mid-Norwegian margin. Some major faults have cut the whole tier whereas many smaller faults have confined to the lower part of the tier and have terminated to a major fault (Fig.39).

The uppermost Brygge and Kai formation comprise fine grained hemipelagic oozes. The two formations are overlain by Plio-Pleistocene glacially derived debris flows of the Naust formation and interglacial sediments consisting of contourites (Blystad et al., 1995; Rokoengen et al., 1995). Even though the lower Naust formation has different sediment

composition than that of Brygge and Kai formation, some polygonal faults have extended to lower sequence of Naust formation (Fig. 39 and 40). This kind of extension of polygonal faults may be due to the instantaneous compaction caused by the rapid loading of debris flow deposits during submarine sliding. This loading might have reactivated the polygonal faults within the underlying Brygge and Kai formation and have caused their propagation within the base of the Naust formation (Gay and Berndt, 2007).
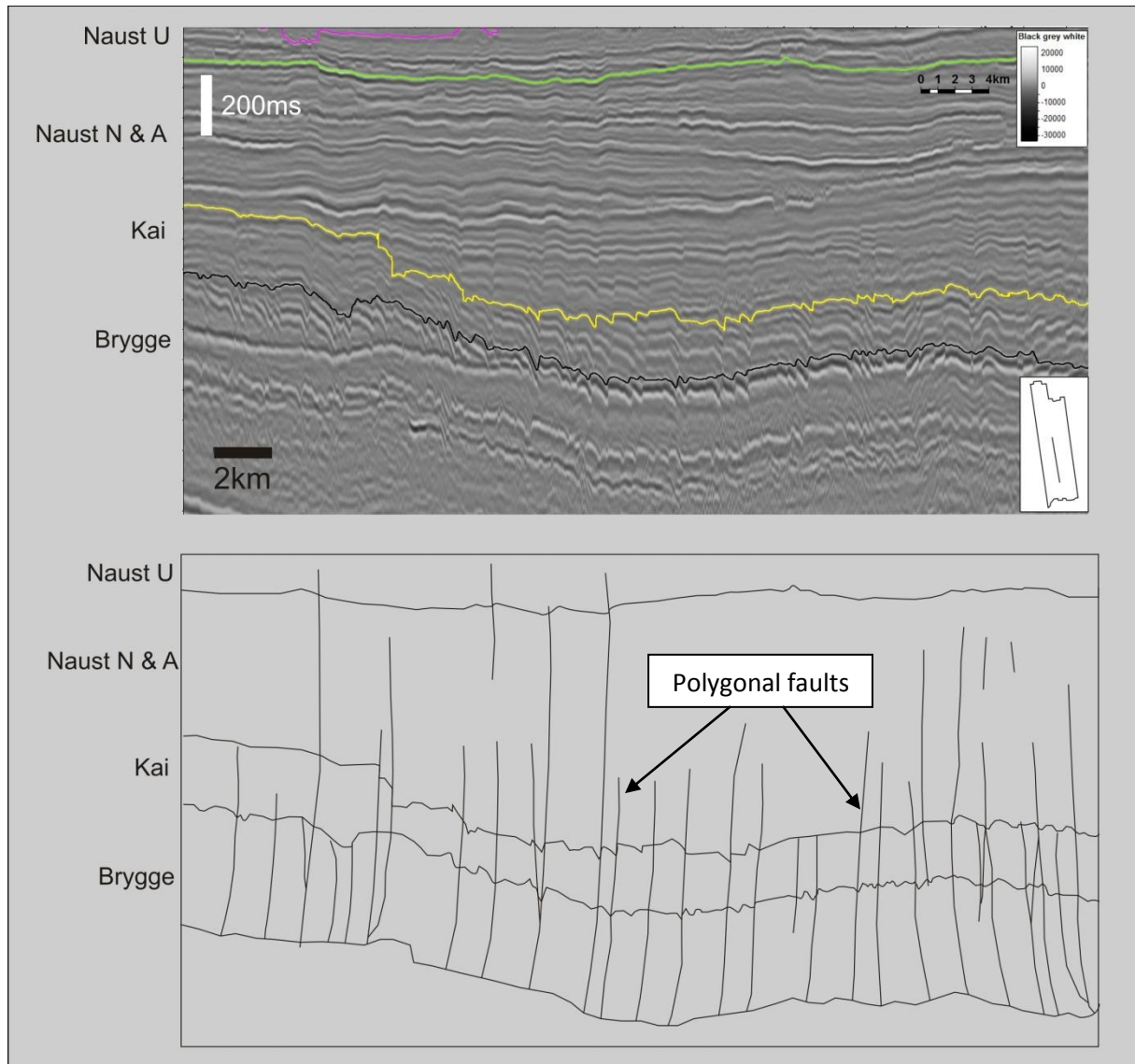
Figure 39. Seismic section on the middle part of the Storegga slide showing the upper Brygge and Kai formations are characterized by numerous polygonal faults terminating at different stratigraphic levels and sometimes to major faults at deeper part.

It is noteworthy to explain here about the origin of polygonal faults within the ooze sediments of Brygge and Kai formation. Polygonal faults systems occur frequently in fine

grained fill of sedimentary basins (Cartwright and Dewhurst, 1998). Cartwright and Lonergan (1996) have suggested that the formation of polygonal fault systems is related to sediment contraction and fluid expulsion. The three possible processes involved in polygonal fault development are;

- Syneresis of colloidal sediments (Dewhurst et al, 1999)
- Rayleigh-Taylor instabilities caused by density inversions and gravity collapse (Watterson et al, 2000)
- Faulting controlled by residual shear strength and low coefficients of friction (Goulty, 2001)

During the syneresis process, spontaneous volumetric contraction and fluid expulsion takes place (Scherer, 1986; Van Vliet et al, 1991), which causes the mud dominated sediment sequence to shrink more (Cartwright and Lonergan, 1996; Dewhurst et al, 1999). The amount of shrinkage of a layer of fine grained sediment increases with an increase amount of smectite content (Dewhurst et al, 1999). The clayey ooze dominated Kai formation in the Vøring basin with high smectite content exhibits a typical shrinkage upon freeze-drying thereby creating voids in weak zones (Forsberg and Locat, 2005). Though this process initiates at a microscale it may explain the contraction of the mud-dominated Kai formation, which caused the formation of normal faults at a large scale. According to Gay et al, (2004), polygonal faults are the result of vertical loading.

5.1.2 Fluid flow through polygonal faults

Polygonal fault system is widespread within 2400-2900ms TWT down specially including upper part of Brygge and Kai formation within the study area (Fig 23a and 40). Polygonal fault system within the Kai and Brygge formation sediment itself acts as a source for fluids (Berndt et al, 2003). The faults act as fluid migration pathways for pore fluids and fluids migrating from deeper parts (Gay et al, 2004). However, the fluid flow indicators are not as strong as for other fault systems. A diffusive fluid flow from the polygonal fault system is not observable unless fluids get trapped either by less permeable and hydrate cemented sediments or by less permeable debris flows (Berndt et al, 2003). Pockets of gas may develop with elevated pore pressure and eventually fluids may be expelled episodically, after these

pockets exceed the yield strength of the trap. This expulsion causes to form acoustic pipes within the seismic section (Fig 25a).

North of the northern escarpment of the Storegga slide fluid-escape features exists. Polygonal faults terminate at an area of increased reflectivity layer shown in the seismic sections (Fig 40). These layers suggest the accumulation of gas within the pore space of sediments. This spatial relationship between faults that cut the fluid/gas rich Brygge and Kai formation and local high reflection amplitudes within the Naust unit (Fig. 40) indicates the gas escapes from lower units (Brygge and Kai or further deep sources) and migrate upwards. Seismic facies with high amplitude anomalies (Fig. 40) has succeeded vertically across the debris flow deposits from deeper strata at 2150ms on part A and B to shallower strata at 1600ms (for part A) and at 1800ms (for part B) in figure 40 suggesting the lateral fluid migration within the marine clays until they find a faulted or fractured weak zone. The faulted and fractured zone at both part (part A and part B in Fig.40) provide the conduits for further upward migration of gas.
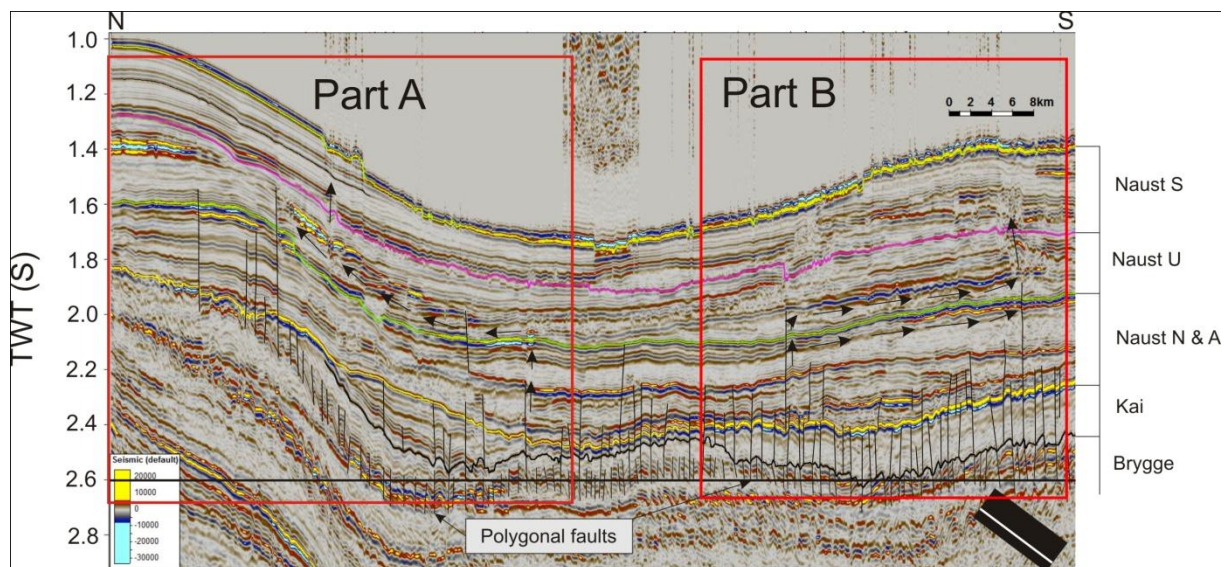

Figure 40. Lateral fluid migration within the marine clays in a seismic section of 2596 inline into two parts (A and B). The extension of polygonal faults has provided the vertical conduits for gas migration from deeper source. Faulted and fractured zone on the upper part of the Naust unit forms a fluid escaping pathways to the seafloor.

Two prominent pipes (Figs. 25a) at the northernmost part of the study area initiate at the upper termination of polygonal faults suggesting preferential pathways for fluid migration. Buenz et al (2003) considered thermogenic hydrocarbon leakage from deep reservoirs into overlying gas-hydrate systems in the uppermost Naust formation through the polygonal fault systems (Fig. 41). Deeper fluids are preferentially driven up through the triple junction of three contiguous polygonal faults (Gay et al, 2004; Hansen et al, 2005). This interconnected network of polygonal faults at the top of Brygge, Kai and Lower units of Naust formation allow deeper fluids to migrate upwards reaching to the base of the debris flow deposit in the upper Naust formation (Gay and Berndt, 2007) (Fig. 42).

5.2 Acoustic pipes:

Acoustic pipe structures are commonly associated with focused migration of fluids (Hustoft et al., 2007). Acoustic pipes at the north of the northern escarpment show pull up effects (Fig 25a). They may be associated with locally high velocity zones caused by gas hydrate plugs (e.g. Hustoft et al., 2007; Westbrook et al., 2008; Plaza-Faverola et al., 2010 and Rajan et al., 2012). The termination of some pipe structures beneath the seafloor suggests that they are either a paleostructure or they do not possess enough overpressure to reach the seafloor (Rajan et al., 2012). As mentioned by Berndt et al., 2003, these pipes have their origin above the Kai formation. At the study area the pipes originate from the suggested free gas zone within the Naust U unit beneath the gas hydrate zone (Fig 25a and 32).

5.3 High amplitude anomalies

High amplitude anomalies are widely distributed at the top of the Brygge formation within the study area (Figs.28, 41), which shows reverse polarity (onset figure in fig 41) if compared to the seabed. The Kai formation provides a seal for vertical migrating fluids and forms a structural trap (Rokoengen et al., 1995; Stuevold et al., 2003; Hustoft et al., 2010). The polygonal faults developed in this area provide conduits for the deeper fluids (thermogenic gas) migrating upwards to the top of the Brygge formation and accumulated there in the form of traps. The transparent zone 300ms below the Brygge top could be caused by homogenous sediments and/or by gas, because of frequency decreases due to the presence of gas (Fig 41).
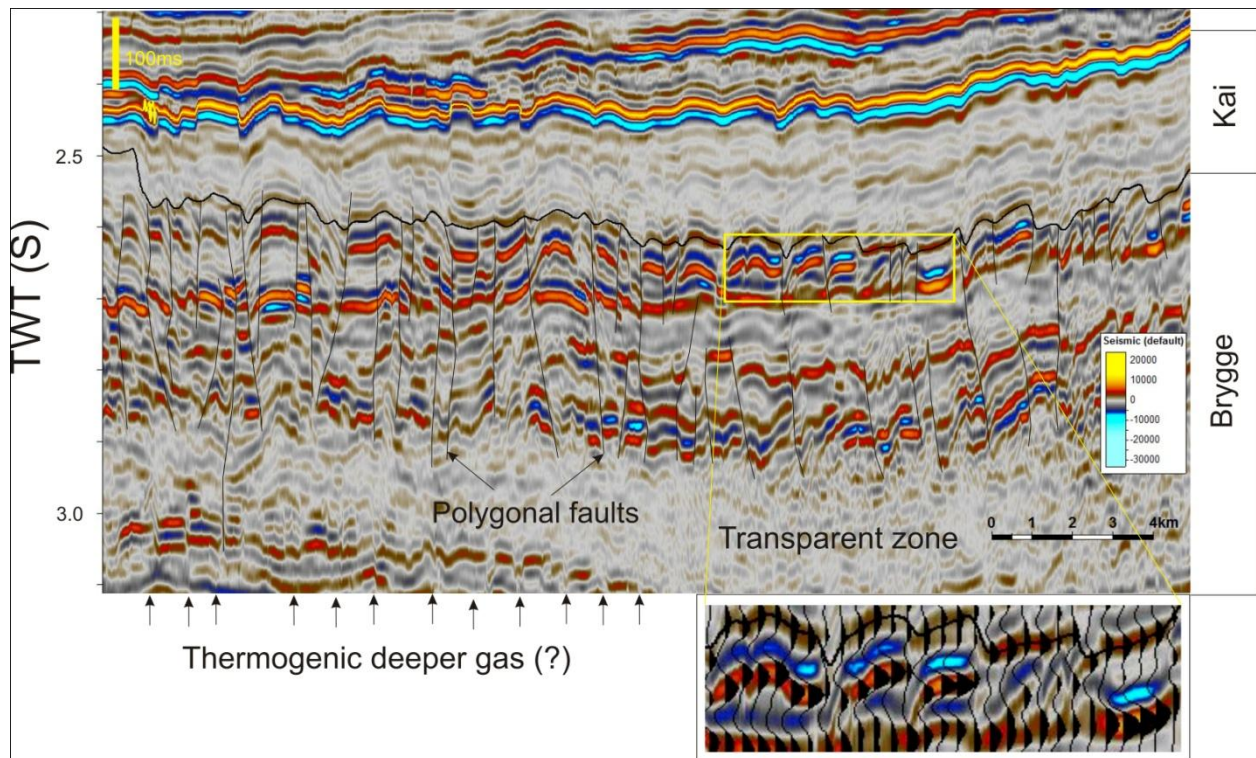
Figure 41. Accumulation of gas at the top of the Brygge formation (southern part of inline 2400) due to the sealing properties of Kai oozes at its top. Polygonal faults throughout this region provide conduits for fluid migrating upwards from the deeper thermogenic sources (?). The inset figure shows the reverse polarity as compared to the seabed. Transparent zone at the bottom of the figure shows gassy sediment.

The high amplitude anomalies at the crest of the HHA within the study area (Fig 42) may represent zones of gas accumulations. These zones occur with polygonal faults below the acoustic transparent zones (fig 52)
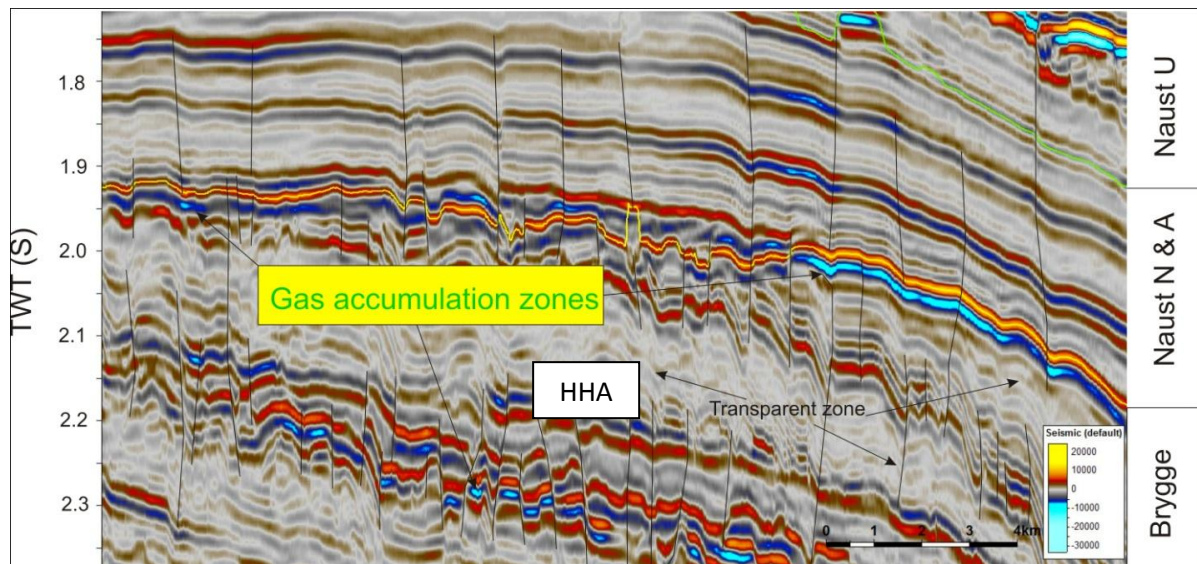
Figure 42. Accumulation of gas at the southernmost limb of the Helland Hansen Arch (HHA). The gases are accumulated at the top of the Bryge formation below which transparent zone is distinct. The gas accumulating zones are feeding with polygonal faults. Some polygonal faults have been extended to upper Naust unit.

A continuous high amplitude negative anomaly is obvious at the top of the Kai formation throughout the study area (Figs. 30a, 30c, 41). The Kai formation is composed of ooze-dominated fine sediments (Eidvein et al., 2007) overlain by Naust formation of highly compacted glacigenic debris-flow and slide deposits. Because of this difference in sediment properties, acoustic impedance difference at their interface gives rise to high amplitude anomalies. Since the acoustic impedance decreases at the interface from Naust to Kai formations, negative amplitude anomalies are produced.

Debris flow deposits contain large blocks or slabs of nearly compact sediments (Gay and Berndt et al., 2007). The slide deposits and glacigenic debris flow (GDF) deposits consist of stiff material (Dimakis et al., 2000; De Blasio et al., 2004a). GDF deposits are composed of unsorted grain-size material distribution and have a higher plasticity index with lower water content (Mitchel, 1993) than its surrounding sediments (Gay and Berndt et al., 2007). Because of these properties, the glacigenic debris flow deposits act as a seal for trapping the upward migrating fluid from deeper levels. The high amplitude anomalies at different sections within the Naust sequence (specially within Naust N & A, Naust U and at the base of the Naust S unit) can be explained by the impedance contrast between an overconsolidated and impermeable thick debris-flow deposit and a gas charged layer beneath it (Fig.32, 33, 43).
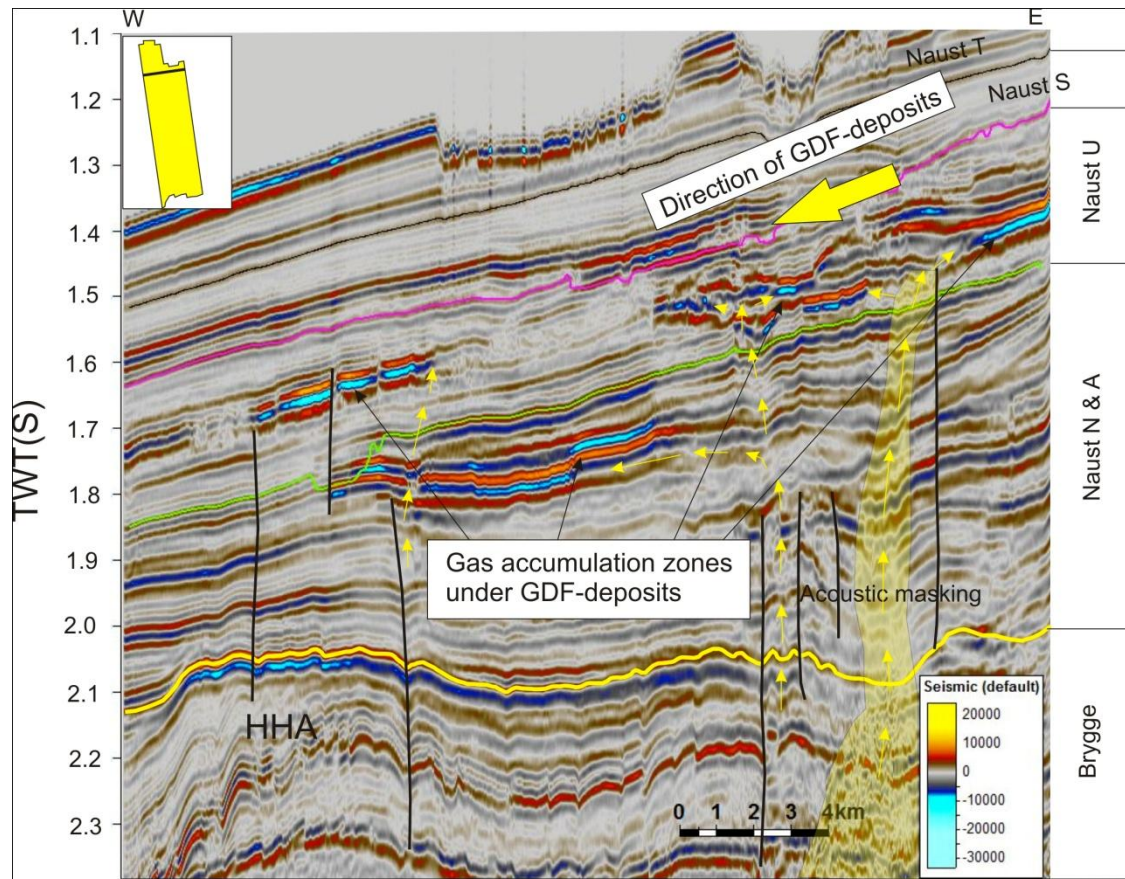
Figure 43. Seismic section of crossline 8284 nearby the northern headwall showing accumulations of gas within different units of Naust sequence. Gas accumulation at the crest of the HHA that liesjust beneath the top of the Bryge formation. Gas accumulations within different sections of the Naust unit occur beneath the glacigenic debris flow (GDF) deposits. Faults and Acoustic masking zones are the conduits for deeper fluids migrating upwards. Yellow arrowlines indicate the direction of fluid migrating upwards into different sections within the Naust formation. Large yellow arrow indicates the direction of glacigenic debris flow (from east to west).

BSR and Gas Hydrate

BSR is located around 180m below the seafloor by considering the average P wave velocity as 1800m/s as suggested by Plaza Faverolla et al., 2010 on the northern flank of the Storegga slide. This depth is nearly equivalent to depth (180m) suggested by Andreasson et al., 1990 and Mienert and Posewang, 1998. A layer of approx. 50-100m (100m suggested by Plaza Faverola et al., 2010 and 50-80 m by Buenz et al., 2004 are correlable to this present study too) above the BSR shows a slightly higher than normal velocity (1880m/s) refers to the gas hydrate. Velocity inversion of approx. 500m/s just below the BSR, as defined by the Low Velocity zone (LVZ1), Plaza Faverolla et al., 2010, is attributed to free gas zone which is supported by previous work based on shear wave analysis (e.g. Buenz et al., 2004;

Westbrook et al., 2008a). BSR and the LVZ1 with free gas lie within the Naust U unit (Fig. 32). The BSR lies at the upper part of the Naust U unit within the contouritic drift deposits at the northern part of the study area which provides a favorable environment for the formation of gas hydrate. The northern flank of the Storegga slide is the only place on the margin where continuous contourite sediments have been built up (Buenz et al., 2003) by S-N oriented warm North Atlantic Current (NAC) during interglacial time period. The BSR is quite observable for 10km length within the seismic profile where the area is unaffected by glacigenic debris flow (Fig 32). This infers that it is not observed other elsewhere in the disturbed part of study area. The existence of a BSR north of the Storegga escarpment and its extension is geologically controlled by the termination of debris flow deposits (Buenz et al., 2003). The presence of debris flow on the margin of south Vøring may hinder gas hydrate build-up on south of northern escarpment of the Storegga slide.

The exact origin of free gas below the BGHS (Fig 32) isn't well understood but it might have resulted either from methanogenesis within Naust formation sediments, or from hydrate recycling (Paull et al., 1994) or from advection from deeper strata or sometimes combinations of all these three processes. Buenz et al., 2003 have suggested that hydrate recycling and methanogenesis within Naust formation sediments haven't contributed significantly because of its average organic carbon content. Polygonal fault system within Kai formation and some of their extension to Naust formation supports the origin of gas at deep-seated hydrocarbon reservoir as hypothesized by Buenz et al., 2003. The content of water molecule needed for the development of hydrate might have been supplied from the expulsion of water during the formation of polygonal faults.

5.4 Fluid flow impact on Slope failure:

The distribution of BSR and gas hydrate within the study area has been found north of northern escarpment of the Storegga slide and is not found elsewhere down in the disturbed area (Fig. 32). This occurrence of BSR and gas hydrate has left a space for discussion to relate the gas hydrate and slope failure. Gas hydrate are sensitive to temperature and pressure (Mienert et al., 1998; Mienert and Posewang, 1998; Buenz et al., 2003). As a consequence of increase in temperature just before the occurrence of Storegga slide, gas released due to decomposition of gas hydrate increased the internal pressure and contributed to cause the

slope failure (Mienert et al., 1998) along a glide plane on marine clay. The glide plane for Storegga slide is ~50ms TWT i.e.18.75m by considering the average velocity 1500m/s within the sediment. This depth is equivalent to the depth of weak layer at 19m as described by Haflidason et al., 2003 and sultan et al., 2004. The composition of sediments from the geotechnical study (liquid limit 35 and clay content 26%) (Sultan et al., 2004) has also supported the weak layer sensitive to liquefaction (Andrews and Martin, 2000).

According to Sultan et al., 2004b the failure interface is initiated at the top of the hydrate layer and not at the bottom of hydrate stable zone (HSZ). The glide plane under the headwall of the Storegga slide is ~100m (assuming Vp = 1800m/s for 110ms TWT hydrate bearing sediment, Plaza Faverola et al., 2010) high above the present BSR (Fig. 32) which is supposed to be the top of hadrate bearing sediment (Plaza Faverola et al., 2010). This has supported the formation of glide plane at the top of the hydrate layer. In addition to this, the melting of gas hydrate induces a decrease of hydrate fraction within sediment and generates excess pore pressure at the top of the hydrate layer (Sultan et al., 2004b). This excess pressure decreases the soil resistance and makes sediments more susceptible to cause failure.

From the observations made at submarine slides, sediment blocks and elongated ridges are indicators of down-slope flow of sediments as observed in many geological settings (Urgeles et al., 1997; Laberg and Vorren, 2000; Lastras et al., 2002; Buenz et al., 2005). Potential gas accumulations in the area suggest a possible relationship between fluids that leak from the reservoir and slope instabilities in the sediment above the reservoir (Buenz et al., 2005).

The retrogressive nature of the Storegga slide may be a result of excess pore pressure within the marine clay (Bryn et al., 2005). Solheim et al., 2005 have outlined the variation of sediments, till and glacial debris flows overlying fine grained drift deposits. It is the most important prerequisite for the slide development as rapid loading causes excess pore pressure in marine deposits thereby reducing effective strength with potential instability as a result. Solheim et al., 2005 consider pore pressure build-up and a strong earthquake as a possibly process for triggering the slides in the Storegga region. The intensive polygonal faults under the slides are considered as indicators to support the developed instability in this area.
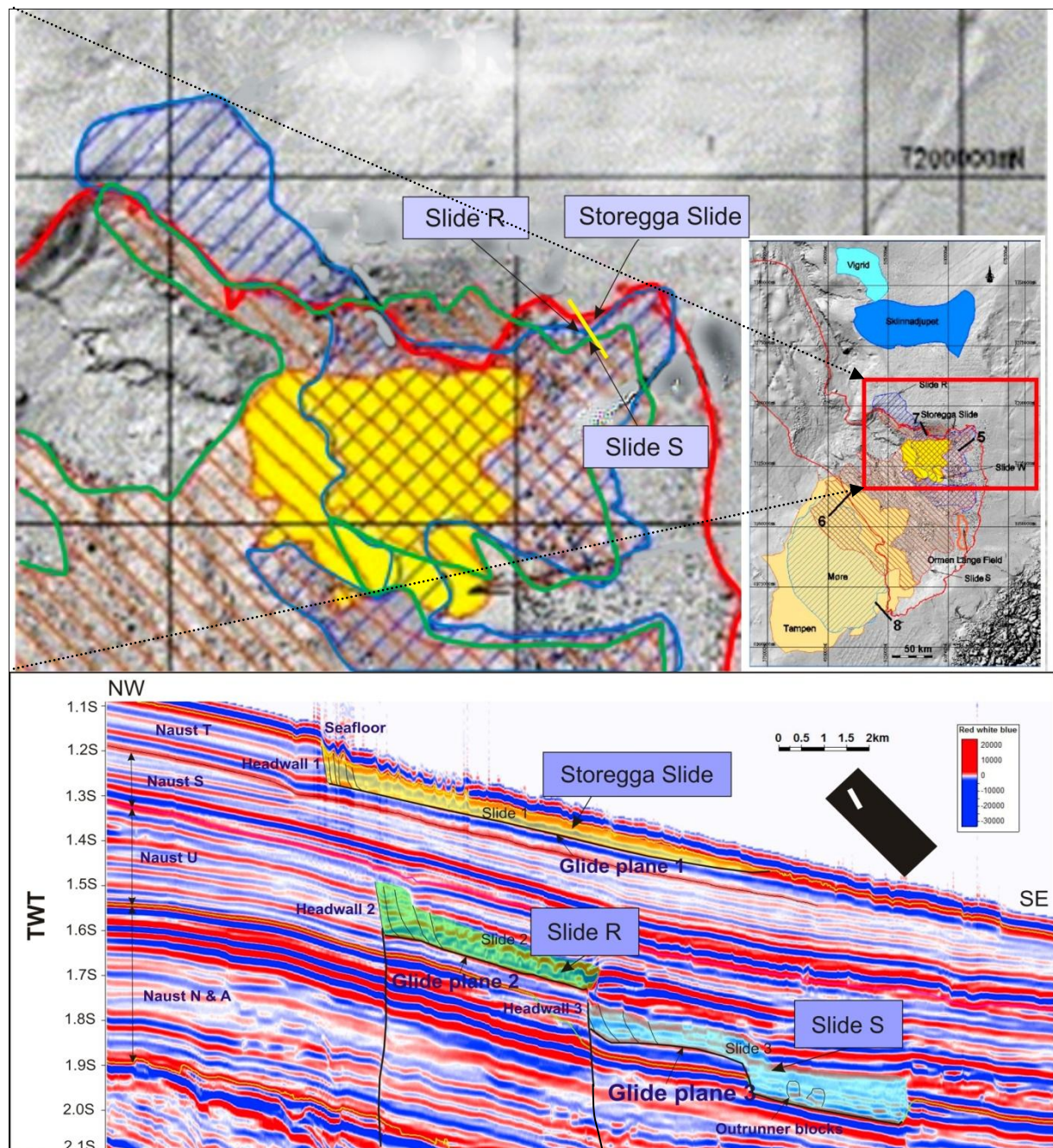
Figure 44. a) 3 slides (Slide S, Slide R and Storegga slide) within the study area are shown in a map of 7 pre-Holocene slides in the Norwegian continental margin (inset figure). The Storegga slide, Slide R and Slide S are marked by red, blue and green lines respectively. Yellow line on the northern sidewall of the Storegga slide represents a seismic section shown in Fig b with corresponding three slides. (Figure from Solheim et al., 2005). b) Seismic section on the northern sidewall of the Storegga slide showing three slides corresponding to the slides in figure (a) within Naust units.

The seafloor morphology from the Ormen Lange area is characterized by three prominent headwalls which are associated with three slide stages identified by Bugge et al., 1998. Similar to this observation, three headwalls (fig 37, 44b) are clearly visible in a seismic

section near the northern sidewall of Storegga slide. The basal shear surface (glide plane) of each slide occurs in the fine grained marine clay of contourite currents (Fig 37 and 44) (Bryn et al., 2003). Bryn et al, 2003 have considered excess pore pressure development in the marine clays, which is enhanced by the rapid deposition of the glacigenic debris flow units over the contourite deposits. In fig 37 and 44b, a sub-vertical fault is present just below the headwall 2 and 3 which may supply fluid from deeper reservoirs. Small offset of sedimentary strata is documented nearby the headwall 3. Some extensional polygonal faults beyond the lower Naust sequence (Fig 39) are responsible for driving the fluids into the slide rich Naust U unit, which enhances the pore pressure build-up within the sediment and make it more susceptible to failure.

The three slides are clearly visible with characteristic features of submarine slides in a seismic section on the northern sidewall of the Storegga slide (Fig. 44b). These slides are well correlable to three slides (Slide S, R and Storegga slide) provided by Solheim et al., 2005 on the mid-Norwegian margin (Fig. 44a). The older slide (Slide 3) is correlable to slide S, slide 2 to slide R and slide 1 to recent Storegga slide (Fig 44a and 44b).

Kvalstad et al., 2005 have presented some simulation results of excess pore pressure caused by the rapid deposition during glacial times. Rapid deposition of glacigenic debris flow is a potential mechanism that could have driven fluid expulsion from previously overpressured shallow gas reservoirs in Nyegga (Hustoft et al., 2010). This upward moving fluid enhances the pore pressure within the sediment formation, which makes the sediment sequence (within an influenced region) viable to cause slope failure on any sort of strong likely trigger.

5.5 Spatial Distribution of Spreading

Ridge and trough morphology found within the Storegga slide are indicative of material movements, which can be identified by a repeated extensional pattern orientated perpendicular to the direction of mass movement (e.g. Micaleff et al., 2007). 3D seismic data GH01 has been analyzed along with published geological information to determine the spatial distribution of material spreading within the Storegga slide (fig 45). Mass movements are analyzed on the basis of morphology and their internal structure. Within the study area,

we can see spreads and translational slide (Fig 45) along with rotational slides and debris flow. Turbidity currents lie towards the west of the study area. Spreads can easily be seen in the vicinity of headwalls and further downslope to the central part of the study area (Fig. 45).
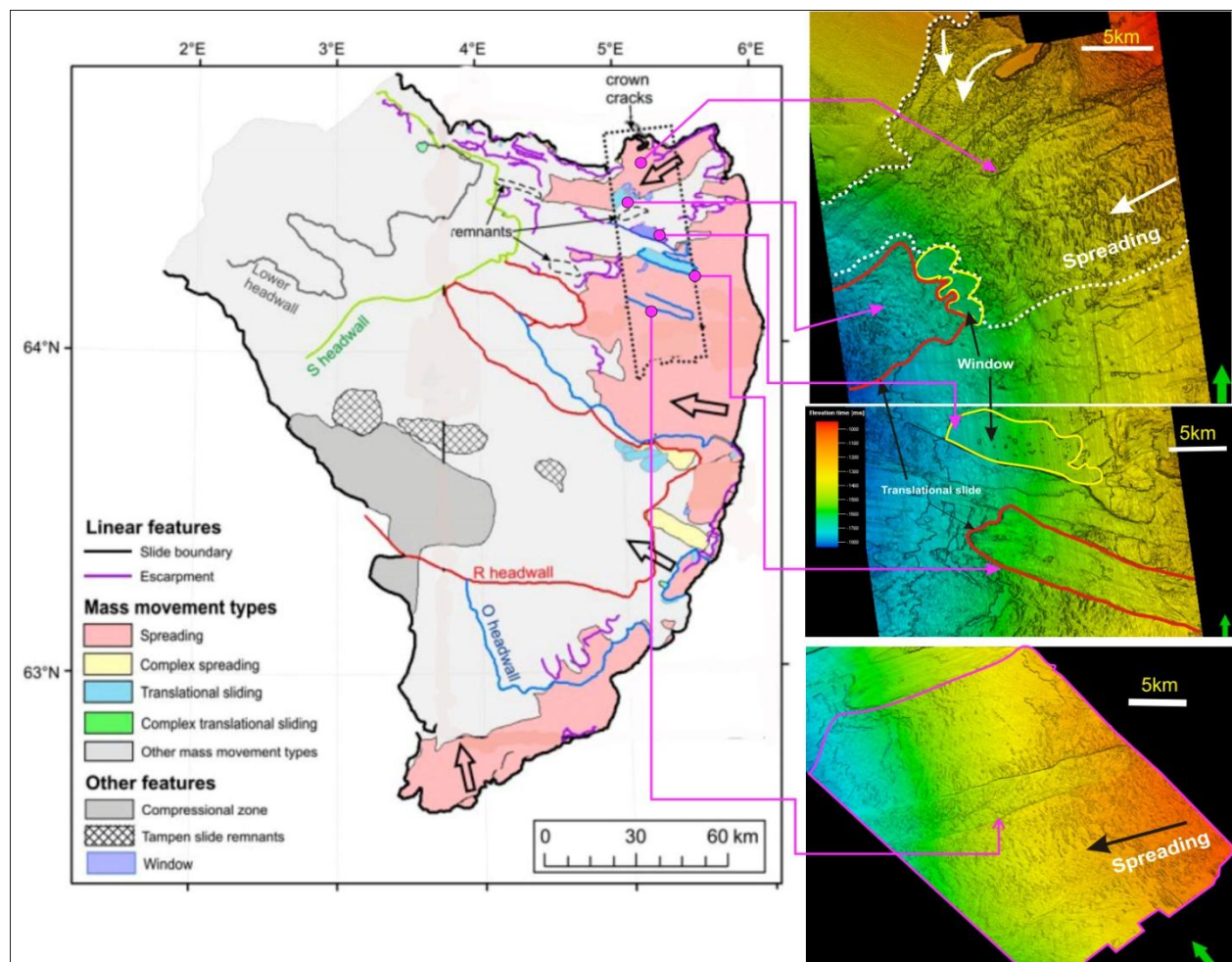
Figure 45. Distribution map of various types of mass movements within the Storegga Slide. Study area is indicated by dotted polygon. Pink arrows indicate the corresponding points on the seabed. The area bounded within white dotted line is spreading, area within yellow line is window, area within red are translational slide and are within pink polygon is spreading (Figure modified from Micallef et al., 2007).

Sediment mobilizations are concentrated along the main headwall. The spreading occurs at the northern and southern part of the study area (Fig. 45). Translational slide of ~80km^2 is observed at the central part of the study area which has side wall of 48 m high. The upslope extent of this translational slide is beyond the study area. Some windows of irregular shape are present at the north of the translational slides that expose the underlying basal shear

surface. Spreading is mainly caused by extensional processes but some of the ridges and troughs are formed by local events of compression. Windows are located downslope of such compressional ridges and troughs.

5.6 Ridge and Trough Morphology

The spreading of sediment material has created ridge and trough morphology in the vicinity of the headwall (Fig. 46a). They are repetitive and parallel to sub parallel to headwall. In proximity to the headwall, the ridges are quite continuous and linear and that possesses concave downslope structure as found by Micallef et al., 2007 near the eastern headwall around the Orman Lange (Fig. 46b). Downslope they are discontinuous and less distinctive. While spreading downslope, blocks disintegrate into smaller non-linear discontinuous ridges. In some places, they might have been aligned into a convex-downslope pattern similar to the pattern found by Micallef et al., 2007 at approx 10km west from the headwall (Fig. 46b). Ridges and troughs can be observed within the study area especially on the northern and southern part. Some are seen on the central part of the study area too but they are short discontinuous and sparse. Ridges and troughs can be observed in water depth down to 1500m. Just below the northern headwall within the study area the ridge length and spacing are around 1300m and 243m respectively and the trough depth is around 10m. Ridges upto 4 km long are found on the northeastern part of the study area. Ridges on the southern part of the study area (Fig. 46c) are widely distributed and some of them are up to 2.5 km long. Ridge spacing and trough depth increase with distance from the headwall. The morphological change demonstrates that the spreading of blocks undergo increasing displacement, deformation, defragmentation and tilting with distance downslope.
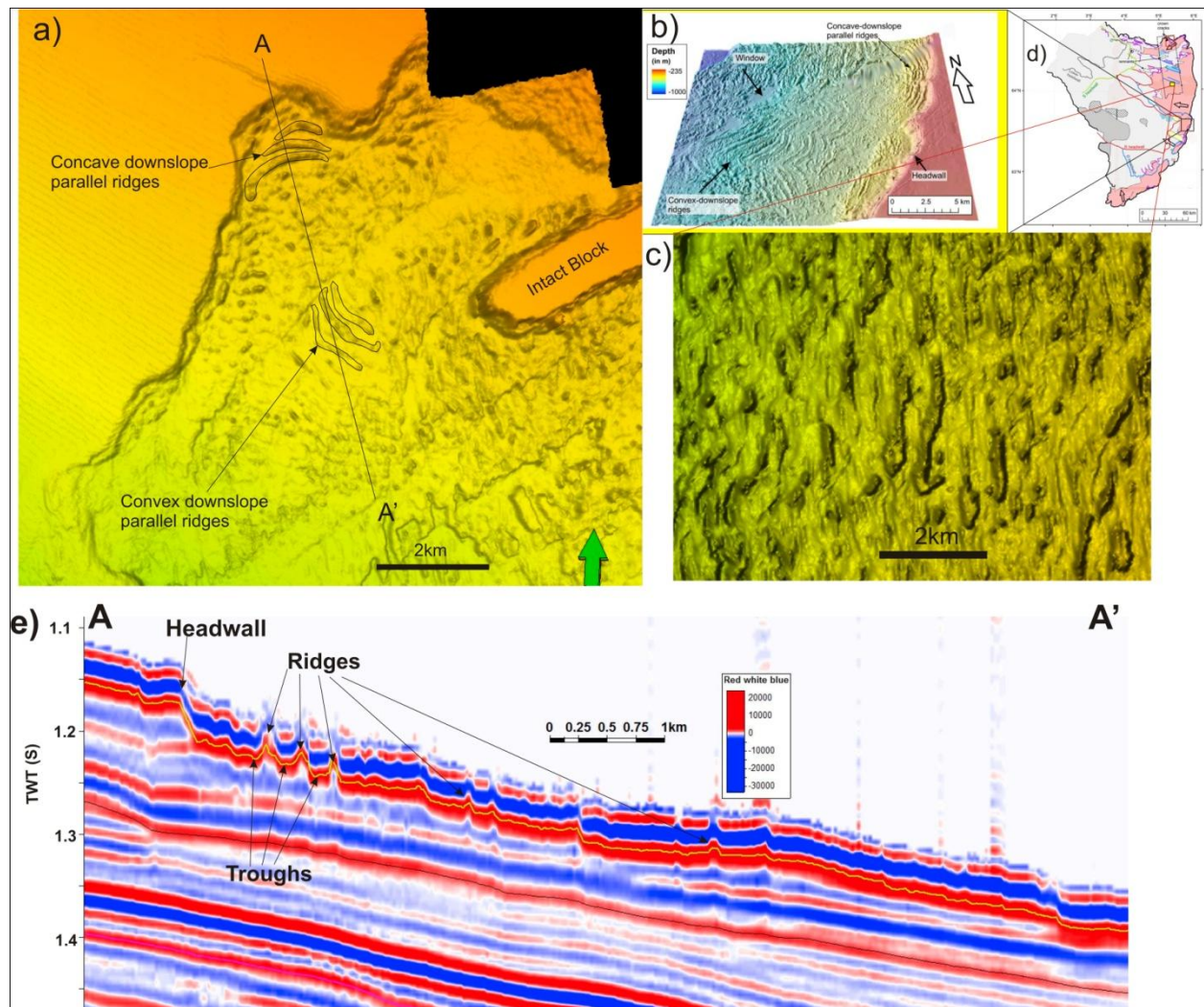
Figure 46. a) 3D shaded relief map map of seabed showing the ridge and trough morphology near the proximity to northern headwall of Storegga slide. Concave-downslope and convex-downslope ridges are noted. Red square in fig d represents the fig a. b) Different kinds of ridge system in Ormen Lange area whose location is shown in black square in fig d. c) Seabed images showing straight N-S oriented ridges on the southern part of the study area whose location is indicated by yellow square in fig d. d) The eastern part of the Storegga slide showing the respective location of a, b and c. e) Seismic section as indicated in fig a showing the ridge and trough morphology near the northern headwall of the Storegga slide. (Figure b and d from Micallef et al., 2007).

5.7 Present Day Seabed Morphology

The overall outline of the Storegga slide scar corresponds to a basin-like geometry with a 320km long headwall along the present day continental shelf break (Haflidason et al., 2005). Haflidason et al., 2005 have determined the slope gradients along the failure planes are on average only 1.1°-1.4°. The slope gradients closest to the shelf area are found to be around 20°, in some cases it is up to 45°. The area immediately below the slide scar is commonly approx. 4° steep. The central slide scar of the Storegga Slide is dominated by blocky debris flows and the upper headwall with lateral spreads (Bryn et al., 2005).

The slide scar within the study area occupies approximately 70 km^2. The seabed just above the slide escarpment is smooth while below the escarpment it is rough because of the presence of blocks and slided debris. The seafloor depth changes by 50-150m down from the undisturbed northern part of the slide scar (Fig. 47A and 48A). Several sediment blocks have been identified on the seafloor within the Storegga slide (fig 48 A). The variance map for the seafloor (Fig. 48A) has clearly shown several seemingly rectangular blocks and more continuous ridge like features. Down the escarpment, these blocks and ridges show a staircase-like pattern that is especially visible in the eastern and northwestern sidewall of the intact blocks (Fig. 47A). The ridges near the headwalls show less deformation, while they got deformed more at greater distances from the headwall. The blocks near the escarpment have almost the same orientation and are massive but they are becoming increasingly disoriented and decrease in size with an increase in distance from the sidewall. The orientation of the blocks and ridges on either side of the intact blocks are different. The blocks or ridges nearby the headwall have an orientation along their long axis E-W but on the southern part of the study area they have oriented their long axis almost N-S (Fig. 46C). The identified blocks have dimensions up to 50m high and 100m long. The ridges nearby the headwall are up to 4 km long and 243m wide while in the southern part of the survey, they are 2.5km long. As shown in fig 38, the translational slide on the middle part of the study area has formed a channel like feature that is 3840m wide with 48m high sidewall on both (N and S) directions. Within the study area two windows exist north of the translational slide that clearly show the basal shear surface of the slide. At the lower window, one can notice some irregular shaped sized blocks.

The southern seafloor within the study area is very rough because of the sediment spreading from the eastern headwall of the Storegga slide. Sediments seem to have been moved and trends along N-S at present. The direction of movement is E-W. The orientation of ridges or blocks is perpendicular to the direction of movement (Fig. 38).
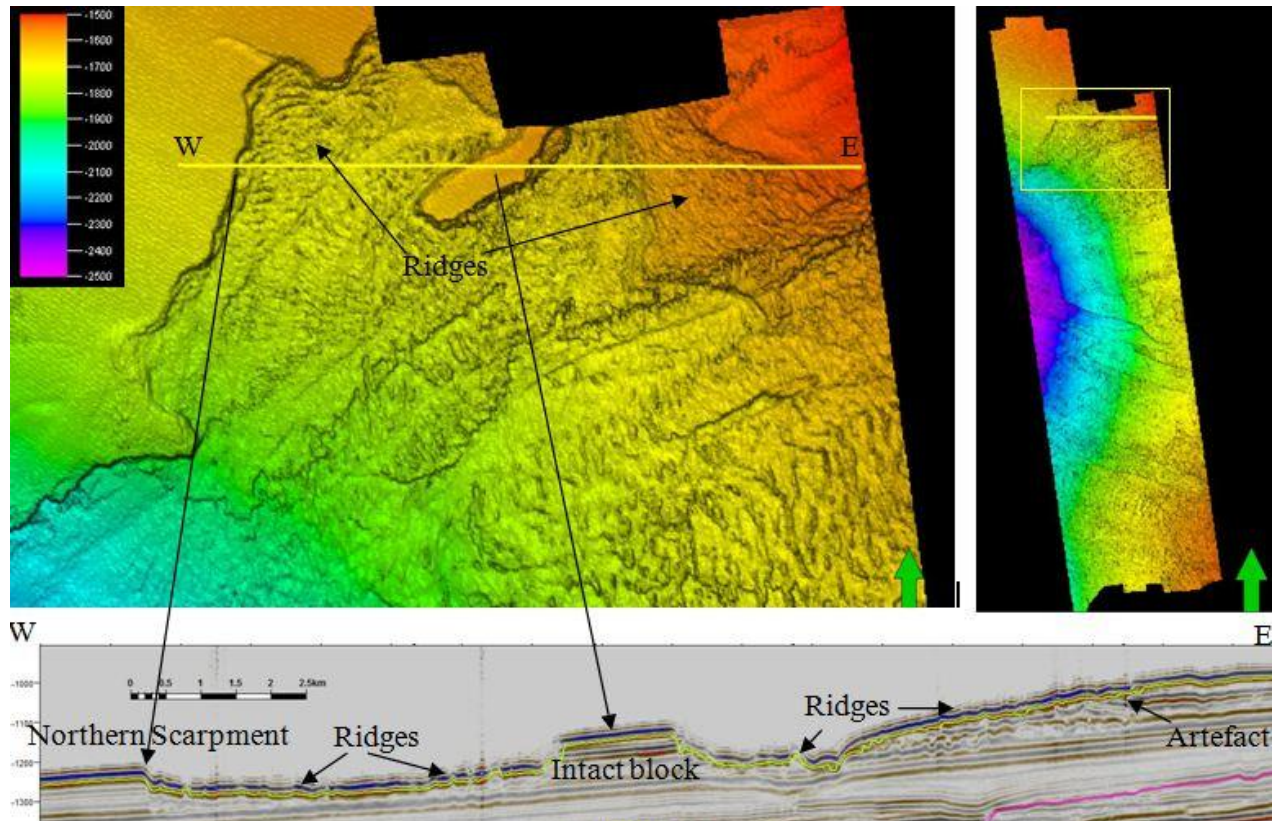
Figure 47. A display a depth-map of the northern part of seafloor of survey GH01 with prominent morphologies. B display a seismic section as indicated in A showing northern escarpment, intact blocks and ridges.
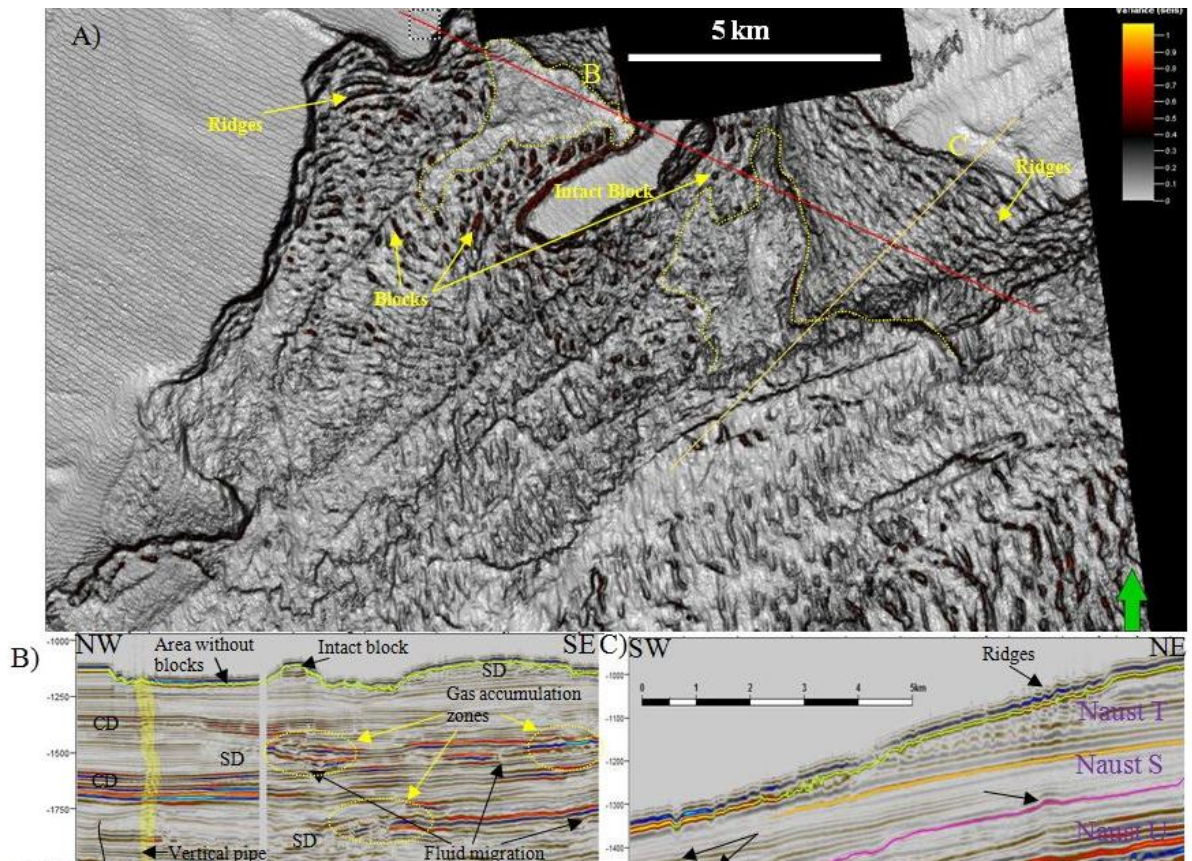
Figure 48. A) Display a variance map of seafloor showing northern part of the survey GH01 with clear indications of ridges and blocks beneath the northern escarpment. B and C display the seismic sections as indicated in A showing morphology and features underneath.

6. CONCLUSIONS

- 3D seismic data and the use of petrel software allowed visualizing and mapping fluid migration pathways, gas accumulation zones and the impact of fluid flow on slope failure on the northern flank of the giant Storegga slide.

- Potential fluid migration has taken place vertically through polygonal faults and acoustic pipes and laterally along permeable strata.

- A high density of layer bound polygonal faults exists within 2400-2900ms TWT (within Brygge and Kai formations) with small fault offsets of ~20 ms TWT, steep slopes of 50-85° and an average spacing of 1km.

- Laterally narrow (20-200m wide), elliptical to circular (in plan view) acoustic pipes are found north of northern flank of the Storegga slide that provide conduits for vertical fluid migration. Roots occur between 1600-1700ms TWT and the upper terminations at various stratigraphic levels but within Naust formations or at the seabed resulting in pockmarks.

- The accumulation of fluids in different units of the Naust formation are inferred to be the result of trapping of upward migrating fluid beneath impermeable glacigenic debris flow deposits.

- The continuous high amplitude anomaly at the top of the Kai formation is the result of an acoustic impedance difference at the interface between sediments of different physical properties.

- The three identified slides (two consecutive slides in Naust U units and one slide in Naust T unit) at the northern flank of the Storegga slide have their basal surface in marine sediments suggesting excess pore pressure built up during rapid sediment loading by glacigenic sediments on top.

- The three slides show all a very clearly Common features of the three mapped slides are a headwall, block faulting and chaotic material with relatively short run out distances of < 5km.

- Based on the investigations fluid flow appears to be not solely responsible for the slope failures but the presence of faults down the headwall of each slide may indicate the role of fluid migration on cracking slope failure.

REFERENCES

Alsop, G., N. G. Evans, and M. Safaricz, 2000, Observations on deformation pattern and mechanics of salt diapir penetration in the central North Sea: Marine and Petroleum Geology, v. 17, p. 601 – 618.

Andreassen, K., Hogstad, K., Berteussen, K.A., 1990, Gas hydrate inthe southern Barents Sea, indicated by a shallow seismic anomaly: First Break 8(6), pp.235-245.

Andreassen, K., 2009, Marine Geophysics. Lecture notes for GEO-3123. University of Tromsø., p. 106.

Andrews, D.C.A. and Martin, G.R. (2000) "Criteria for Liquefaction of Silty Soils." Proc.12th World Conf. Earthquake Engineering, Auckland, NZ, Paper 0312.

Badley, M. E., 1985, Practical Seismic Interpretation, International Human Resources Development Corporation: Boston.

Berg, K., Solheim, A., Bryn, P., 2005. The Pleistocene to recent geological development of the Ormen Lange area. Marine and Petroleum Geology, this issue, doi:10.1016/j.marpetgeo.2004.10.009

Berndt, C., Bunz, S. & Mienert, J. 2003. Polygonal fault systems on the midNorwegian margin: a long-term source for fluid flow. In: Van Rensbergen, P., Hillis, R.R., Maltman, A.J. & Morley, C.K. (eds) Subsurface Sediment Mobilization. Geological Society, London, Special Publications, 216, 283–290.

Bertoni, C., and J. A. Cartwright, 2005, Submarine dissolution of buried evaporites in the Levant margin (eastern Mediterranean): Journal of the Geological Society (London), v. 158, p. 765 – 786.

Blystad, P., Brekke, H., Færseth, R.B., Larsen, B.T., Skogseid, J. & Tørudbakken, B. I.1995: Structural elements of the Norwegian continental shelf, Part 2. The Norwegian Sea Region. Norwegian Petroleum Directorate Bulletin 8, 45pp.

Bondevik, S., Mangerud, J., Dawson, S., Dawson, A., Lohne, Ø., 2003. Record-breaking height for 8000-year old tsunami in the North Atlantic. EOS 84, 289–293.

Boswell, R. & Collett, T.S. 2011, "Current perspectives on gas hydrate resources", Energy and Environmental Science, vol. 4, no. 4, pp. 1206-1215.

Bouriak, S., Vanneste, M. and Soutkine, A., 2000. Inferred gas hydrates and clay diapirs near the Storegga Slide on the southern edge of the Vøring Plateau, offshore Norway. Marine Geology, 163 125-148.

Branney, M. J., 1995, Downsag and extension at calderas: Bulletin of Volcanology, v. 57, p. 303 – 318.

Brekke, H., 2000. The tectonic evolution of the Norwegian Sea Continental Margin with emphasis on the Vøring and Møre Basins. In: A. Nøttvedt (Editor), Dynamics of the Norwegian Margin. Geological Society, London, pp. 327-378.

Brown, A., 1999. Interpretation of Three-Dimensional Seismic Data, Fifth Edition. AAPG Memoir 42 SEG Investigations in Geophysics, No. 9.

Brown, H. E., W. S. Holbrook, M. J. Hornbach and J. Nealon (2006), Slide structure and role of gas hydrate at the northern boundary of the Storegga Slide, offshore Norway, Marine Geology, 229, 179-186.

Bryn, P., Solheim, A., Berg, K., Lien, R., Forsberg, C. F., Haflidason, H., Ottensen, D., and Rise, L., 2003, The Storegga Slide Complex: Repeated Large Scale Sliding in Response to Climatic Cyclicity, in Mienert, J., ed., Submarine Mass Movements and their Consequences, Kluwer Academic Publishers, p. 215-222.

Bryn, P., Berg, K., Forsberg, C., F., Solheim, A. and Kvalstad, T., J., 2005b. Explaining the Storegga Slide, Marine and Petroleum Geology 22 (2005) 11-19.

Bryner, L., 1961, Breccia columns associated with epigenetic ore deposits: Economic Geology, v. 56, p. 488 – 508.

Bukovics, C., & Ziegler, P. A. (1985). Tectonic development of the Mid-Norway continental margin. Marine and Petroleum Geology, 2, 2–22.

Bugge T (1983) Submarine slides on the Norwegian continental margin, with special emphasis on the Storegga area. Continental Shelf Institute, Norway. IKU Publication 110, Section 5.7.3, 152 pp.

Bulat, J., 2005, Some considerations on the interpretation of seabed images based on commercial 3D seismic in the Faroe-Shetland Channel: Basin Research, v. 17, no. 17, p. 21.

Bull, S., Cartwright, J. and Huuse, M., 2009a. A review of kinematic indicators from mass-transport complexes using 3D seismic data. Marine and Petroleum Geology 26: 1132-1151.

Bungum, H., Lindholm, C. and Faleide, J., J., 2005. Postglacial seismicity offshore mid-Norway with emphasis on spatio-temporal-magnitudal variations. Marine and Petroleum Geology 22 (2005) 137-148.s

Buenz S, Mienert J (2004) Acoustic imaging of gas hydrate and free gas at the Storegga Slide. J Geophys Res 109:B04102. doi: 10.1029/2003JB002863

Buenz S, Mienert J, Berndt C (2003) Geological controls on theStoregga gas-hydrate system of the mid-Norwegian margin. Earth Planet Sci Lett 209(3–4):291–307

Buenz, S., Mienert, J., Vanneste, M. and Andreassen, K., 2004. Gas hydrates at the Storegga Slide: Constraints from an analysis of multicomponent, wide-angle seismic data. In: Geophysics vol 70. No. 5.

Canals, M., Lastras, G., Urgeles, R., Casamor, J. L., Mienert, J., Cattaneo, A., De Batist, M., Haflidason, H., Imbo, Y., and Laberg, J. S., 2004, Slope failure dynamics and impacts from seafloor and shallow sub-seafloor geophysical data: case studies from the COSTA project: Marine Geology, v. 213, no. 1-4, p. 9-72.

Cartwright, J., Huuse, M., and Aplin, A., 2007, Seal bypass systems: AAPG Bulletin, v. 91, no. 8, p. 1141-1166.

Cartwright, J.A., Lonergan, L., 1996. Volumetric contraction during the compaction of mud rocks: a mechanism for the development of regional-scale polygonal fault system. Basin Res. 8, 183–193.

Cartwright, J.A., Dewhurst, D.N., 1998. Layer-bound compaction faults in fine-grained sediments. Geol. Soc. Amer. Bull. 110 (10), 1242–1257.

Chand, S., and Minshull, T. A., 2003, Seismic constraints on the effect of gas hydrate on sediment physical properties and fluid flow: a review: Geofluids, v. 3, no. 4, p. 275-289.

Collett, T.S., Boswell, R., Lee, M.W., Anderson, B.J., Rose, K. & Lewis, K.A. 2011, "Evaluation of long-term gas hydrate production testing locations on the Alaska north slope", Society of Petroleum Engineers - Arctic Technology Conference 2011, pp. 955.

Cooper, A. H., 1986, Subsidence and foundering of strata caused by dissolution of Permian gypsum, North Yorkshire, in G. M. Harwood and D. B. Smith, eds., The English Zechstein and related topics: Geological Society (London) Special Publication 22, p. 127 – 139.

Dalland, A., Worsley, D. and Ofstad, K. (1988) A lithostratigraphic scheme for the Mesozoic and Cenozoic succession offshore mid-and northern Norway. *Norwegian Petroleum Directorate Bulletin*, 4, 65 pp.

Davies, R. J., and S. A. Stewart, 2005, Emplacement of giant mud volcanoes in the South Caspian Basin: 3D seismic reflection imaging of their root zones: Journal of the Geological Society (London), v. 162, p. 1 – 4.

Davison, I., G. I. Alsop, N. G. Evans, and M. Safaricz, 2000, Overburden deformation patterns and penetration mechanisms of salt diapirs in the Central Graben, North Sea: Marine and Petroleum Geology, v. 17, p. 601 – 618.

De Blasio, F. V., Elverhoi, A., Issler, D., Harbitz, C. B., Bryn, P., and Lien, R., 2004a, Flow models of natural debris flows originating from overconsolidated clay materials: Marine Geology, v. 213, no. 1-4, p. 439-455.

Dewhurst, D.N., Cartwright, J.A. & Lonergan, L. 1999. The development of polygonal fault systems by syneresis of colloidal sediments. Marine and Petroleum Geology, 16, 793-810.

Dickens, G. R., 2001b, The potential volume of oceanic methane hydrates with variable external conditions, Org. Geochem., 32, 1179–1193,.

Dimakis, P., Elverhoi, A., Hoeg, K., Solheim, A., Harbitz, C., Laberg, J. S., Vorren, T.O., & Marr, J., 2000. Submarine slope stability on high latitude glaciated Svalbard-Barents Sea margin. *Marine Geology*, 143, 207-221.

Eidvin, T., Bugge, T. and Smelror. M., 2007. The Molo Formation, deposited by coastal progradation on the inner Mid-Norwegian continental shelf, coeval with the Kai Formation to the west and the Utsira Formation in the North Sea. In: Norwegian Journal of Geology, Vol. 87, pp. 75-142

Einsele, G., J. M. Gieskes, J. Curray, and D. M. Moore, 1980, Intrusion of basaltic sills into highly porous sediments, and resulting hydrothermal activity: Nature, v. 283, p. 441 – 445.

England, W.A. (1994). Secondary migration and accumulation of hydrocarbons. AAPG Mem. 60, 211-217.

Evans, D.J., Walker, A.S.D. & Chadwick, R.A. 2002, "The Pennine Anticline, northern England - A continuing enigma?", Proceedings of the Yorkshire Geological Society, vol. 54, no. 1, pp. 17-34.

Evans, D., Graham, C., Armour, A. and Bathurst, P. (2003) *The Millenium atlas: Petroleum geology of the Central and Northern North Sea*, Geological Society of London, 990 pp.

Evans, D., King, E. L., Kenyon, N. H., Brett, C., and Wallis, D., 1996, Evidence for long-term instability in the Storegga Slide region off western Norway: Marine Geology, v. 130, no. 3-4, p. 281-292.

Evans, D. G., J. A. Nunn, and J. S. Hanor, 1991, Mechanisms driving groundwater flow near salt domes: Geophysical Research Letters, v. 18, p. 927 – 930.

Fjellanger, E., Surlyk, F., Wamsteeker, L.C. and Midtun, T., 2004, Upper Cretaceous basin-floor fans in the Vøring Basin, Mid Norway shelf, in Wandås, B.T.G., Nystuen, J.P., Eide, E.A. and Gradstein, F.M., eds. Onshore-Offshore Relationship on the North Atlantic Margin: Norwegian Petroleum Society, Special Publication, no.12, Elsevier, pp. 135-164.

Forsberg, C. F. and Locat, J., 2005. Mineralogical and microstructural development of the sediments on the Mid-Norwegian margin. Marine and Petroleum Geology 22 (2005) 109-122.

Gaarenstroom, M., R. A. J. Tromp, M. J. de Jong, and A. M. Brandenburg, 1993, Overpressures in the central North Sea: Implications for trap integrity and drilling safety, in J. R. Parker, ed., Petroleum geology of northwest Europe: Proceedings of the 4th Conference, London, Geological Society, p. 1305 – 1313.

Gassman, F., 1951, Elasticity of porous media: Ubre die elastizitat poroser medien: Vierteljahrsschrift der Naturforschenden Gesselschaft, v. 96, p. 1-12.

Gauer, P., Kvalstad, T.J., Forsberg, C.F., Bryn, P., Berg, K., 2005. The last phase of the Storegga Slide: simulation of retrogressive slide dynamics and comparison with slide-scar morphology. Marine and Petroleum Geology 22, 171–178.

Gay, A., Berndt, C., 2007. Cessation/reactivation of polygonal faulting and effects on fluid flow in the Vøring Basin, Norwegian Margin. J. Geol. Soc. 164 (1), 129–141.

Gay, A., Lopez, M., Cochonat, P. & Sermondadaz, G. 2004. Polygonal faults– furrows system related to early stages of compaction—Upper Miocene to present sediments of the Lower Congo Basin. Basin Research, 16, 101–116.

Ginsburg, G. D., and Soloviev, V. A., 1997, Methane migration within the submarine gas-hydrate stability zone under deep-water conditions: Marine Geology, v. 137, no. 1-2, p. 49-57.

Gluyas, J., and Swarbrick, R., 2004, Petroleum Geoscience, p. 147-148.

Goulty, N.R. 2001. Polygonal fault networks in fine-grained sediments—an alternative to the syneresis mechanism. First Break, 19, 69–73.

Grauls, D., and C. Cassignol, 1992, Fluid pressure-induced open fracture anomaly-characterization from well data and seismic velocities — Mechanisms and major implications: Bulletin des Centres de Recherches Exploration-Production Elf Aquitaine, v. 16, p. 275 – 284.

Haflidason, H., Gravdal, A. and Sejrup, H.P., 2003. Northern Storegga Slide escarpment Morphology and Features. In: Mienert, J. and Weaver, P. (Eds): European Margin Sediment Dynamics: Side-scan sonar and seismic images – Springer-Verlag Berlin 45-54

Haflidason, H. Sejrup, H.P. Berstad, I.M., Nygård, A., Richter, T., Bryn, P., Lien, R. and Berg, K., 2003. Weak layer features on the northern Storegga Slide escarpment. In: Mienert, J. and Weaver, P. (Eds). European Margin Sediment Dynamics: Side-scan sonar and seismic images – Springer-Verlag Berlin 55-62.

Haflidason, H., Sejrup, H. P., Nygård, A., Mienert, J., Bryn, P., Lien, R., Forsberg, C. F., Berg, K. and Masson, D., 2004. The Storegga Slide: architecture, geometry and slide development. Marine Geology 213, 201-234.

Hampton, M. A., 1972. The role of subaqueous debris flow in generating turbidity currents. Journal of Sedimentary Petrology, 42, 775-793.

Hansen, J.P.V., Cartwright, J.A., Huuse, M. & Clausen, O.R. 2005. 3D seismic expression of fluid migration and mud remobilization on the Gjallar Ridge, offshore mid-Norway. Basin Research, 17, 123–139.

He, C., Tang, L., Huang, D. and Shi, S., 2010. Polygonal faults in the Sanzhao sag of the Songliao basin: their significance in hydrocarbon accumulation. *Mining Science and Technology (China),* **20**(2), pp. 300-305.

Heggland R (1997) Detection of gas migration from a deep source by the use of exploration 3D seismic data. Mar Geol 137:41–47

Heggland R (1998) Gas seepage as an indicator of deeper prospective reservoirs. A study based on exploration 3D seismic data. Mar Pet Geol 15:1–9.

Henriksen, S. & Vorren, T.O. 1996. Late Cenozoic sedimentation and uplift history on the mid Norwegian continental shelf. *Global and Planetary Change 12*, 171-199.

Hjelstuen, B. O., Eldholm, O. and Skogseid, J., 1997. Vøring Plateau diapir fields and their structural and depositional settings. Marine Geology, 144 (1-3), 33-57

Hjelstuen, B. O., Eldholm, O. and Skogseid, J., 1999. Cenozoic evolution of the northern Vøring margin. Geological Society of America Bulletin, 111: 1792-1807.

Hovland, M., and Judd, A., 1988a, Seabed pockmarks and seepages : impact on geology, biology and the marine environment.

Hunt, J. M., 1996, Petroleum geochemistry and geology.

Hurst, A., J. A. Cartwright, M. Huuse, R. Jonk, A. Schwab, D. Duranti, and B. Cronin, 2003, Significance of large scale sand injectites as long-term fluid conduits: Evidence from seismic data: Geofluids, v. 3, p. 263 – 274.

Hustoft, S., Bünz, S., Mienert, J. 2010, "Three-dimensional seismic analysis of the morphology and spatial distribution of chimneys beneath the Nyegga pockmark field, offshore mid-Norway. Basin Research Vol.22, p. 465-

Hustoft, S., Mienert, J., Bünz, S., Nouzé, H., 2007. High-resolution 3D-seismic data indicate focussed fluid migration pathways above polygonal fault systems of the mid-Norwegian margin. Marine Geology 245 (1–4), 89–106.

Huuse, M., and M. Mickelson, 2004, Eocene sandstone intrusions in the Tampen Spur area imaged by 3D seismic data: Marine and Petroleum Geology, v. 21, p. 141 – 155.

Jonk, R., J. Parnell, and A. Hurst, 2005, Aqueous and petroleum flow associated with sand injectites: Basin Research, v. 17, p. 241 – 257.

Kopf, A., 2002, Significance of mud volcanism: Reviews of Geophysics, v. 40, p. 1005, doi:10.1029/2000RG000093.

Kvalstad, T.J., Andresen, L., Forsberg, C.F., Berg, K., Bryn, P., Wangen, M., 2005. The Storegga Slide: evaluation of triggering sources and slide mechanics. Marine and Petroleum Geology, this issue, doi:10.1016/j.marpetgeo.2004.10.019

Kvalstad, T.J., Nadin, F., Kaynia, A.M., Mokkelbost, K.H., Bryn, P., 2005b. Soil conditions and slope stability in Ormen Lange area. Mar Petrol Geol 22:299-301. doi: 10.1016/j.marpetgeo.2004.10.021.

Kvenvolden, K.A. 1993, "Gas hydrates-geological perspective and global change", Reviews of Geophysics, vol. 31, no. 2, pp. 173-187.

Laberg, J.S. & Vorren, T.O. 2000, "The Trænadjupet Slide, offshore Norway - Morphology, evacuation and triggering mechanisms", Marine Geology, vol. 171, no. 1-4, pp. 95-114.

Laberg, J.S., Dahlgren, K.I.T., Vorren, T.O., Haflidason, H., Bryn, P., 2001. *Seismic analyses of Cenozoic contourite drift development in the Northern Norwegian Sea.* Marine Geophysical Researches 22, 401-416.

Lastras,G., Canal s,M., Hughes-Clarke, J.E., Moreno,A., Batist, M.D., Masson, D.G. & Cochonat, P. (2002) Seafoor imagery from the BIG'95 debris fow, western Mediterranean. Geology, 30, 871-874.

Leeder, M., 2006. Sedimentology and Sedimentary Basins, from turbulence to tectonics. Blackwell Publishing.

Levorsen, A.I., 1967, Geology of Petroleum: Second edition, W.H. Freeman Company, San Francisco. 724 pages.

Lien, T., 2005, From rifting to drifting: effects on the development of deep-water hydrocarbon reservoirs in a passive margin setting, Norwegian Sea: Norwegian Journal of Geology, v. 85, pp. 319-332.

Locat, J. & Lee, H. 2002: Submarine landslides: advances and challenges Canadian Geotechnical Journal 39, 193–212.

Løseth, H., Gading, M., and Wensaas, L., 2009, Hydrocarbon leakage interpreted on seismic data: Marine and Petroleum Geology, v. 26, no. 7, p. 1304-1319.

Løseth H, Wensaas L, Arntsen B, Hanken N, Basire C, Graue K (2001) 1000 m long gas blow-out pipes. In: Extended Abstr Vol 63rd EAGE Conference & Exhibition, Amsterdam, p 524.

Magoon, E. A. B. a. L. B., 2003, Petroleum systems Exploring for oil and gas traps, v. Chapter 3.

Micallef, A., Masson, D.G., Berndt, C., Stow, D.A.V., 2007c. Morphology and mechanics of submarine spreading: A case study from the Storegga Slide. Journal of Geophysical Research 112, F03023.

Mienert, J. & Posewang, J. 1999, "Evidence of shallow- and deep-water gas hydrate destabilizations in North Atlantic polar continental margin sediments", Geo-Marine Letters, vol. 19, no. 1-2, pp. 143-149.

Mienert, J., J. Posewang, and M. Baumann, 1998. Gas hydrates along the northeastern Atlantic margin: possible hydrate-bound margin instabilities and possible release of methane, in Gas Hydrates: Relevance to World Margin Stability and Climate Change, edited by J.-P. Henriet, and J. Mienert, vol. 137 of Spec. Publ., pp. 275-291, Geol. Soc. London.

Mienert, J., Vanneste, M., Bünz, S., Andreassen, K., Haflidason, H., and Sejrup, H.P., 2005b, Ocean warming and gas hydrate stability on the mid-Norwegian margin at the Storegga Slide: Marine and Petroleum Geology, v. 22, p. 233-244.

Mienert, J., 2004, COSTA - Continental Slope Stability, Marine Geology special issue. Vol. 213, No. 1- 4. p. 1-504., p. 1-504.

Minescu, F., Popa, C. & Grecu, D. 2010, "Theoretical and practical aspects of tertiary hydrocarbon migration", Petroleum Science and Technology, vol. 28, no. 6, pp. 555-572.

Mitchell, J. K. (1993). Fundamentals of soil behaviour (2nd ed.). New York: Wiley (p. 437).

Morley, C. K., 2003, Outcrop examples of mudstone intrusions from the Jerudong anticline, Brunei, and inferences for hydrocarbon reservoirs, in P. van Rensbergen, R. Hillis, A. Maltman, and C. Morley, eds., Subsurface sediment mobilisation: Geological Society (London) Special Publication 216, p. 381 –394.

Orton, E. (1889), The Trenton limestone as a source of pertroleum and inflammable gas in Ohio and Indiana. Washington DC: Government Printing Office, 8th Annual Report of the Director of the U.S. Geological Survey, 1886-87, pt. II, 475-662.p

Paull, C.K., Buelow, W.J., Ussler, W., III, and Borowski, W.S., 1996a, Increased continental-margin slumping frequency during sea-level lowstands above gas hydrate- bearing sediments: Geology, v. 24, p. 143–146.

Plaza-Faverola, A., S. Bünz, and J. Mienert (2010), Fluid distributions inferred from P wave velocity and reflection seismic amplitude anomalies beneath the Nyegga pockmark field of the mid-Norwegian margin, Mar. Pet. Geol., 27(1), 46–60, doi:10.1016/j.marpetgeo.2009.07.007.

Plaza-Faverola, A., Bünz, S., Mienert, J., 2012. The free gas zone beneath gas hydrate bearing sediments and its link to fluid flow: 3-D seismic imaging offshore midNorway. Marine Geology. doi:10.1016/j.margeo.2011.07.002 (available online).

Rajan, A., Mienert, J., Buenz, S., 2012, Acoustic evidence for a gas migration and release system in Arctic glaciated continental margins offshore NW-Svalbard: Marine and Petroleum Geology. doi:10.1016/jmarpetgeo.2011.12.008.

Rice, D. D., and G. E. Claypool, 1981, Generation, accumulation, and resource potential of biogenic gas: AAPG Bulletin, v. 65, p. 5–25.

Riis, F. 1996: Quantification of Cenozoic vertical movements of Scandinavia by correlation of morphological surfaces with offshore data. *Global and Planetary Change 12*, 331-357.

Rise, L., Ottesen, D., Berg, K., Lundin, E., 2005. Large-scale development of the mid-Norwegian shelf and margin with emphasis on the last 3 million years. Marine and Petroleum Geology, 22, 33-44.

Rise, L., Ottesen, D., Longva, O., Solheim, A., Andersen, E. S., Ayers, S, 2006. The Sklinnadjupet slide and its relation to the Elsterian glaciation on the mid-Norwegian margin. Marine and Petroleum Geology 23 (2006) 569-583.

Rokoengen, K., Rise, L., Bryn, P., Fregstad, B., Gustavsen, B., Nyggard, E. and Sættem, J., 1995. Upper Cenozoic stratigraphy on the Mid-Norwegian continental shelf. Nor. Geol. Tidsskr., 75: 88-104.

Scherer, G. W. (1986). Drying gels: I. General theory. Journal of Non-Crystalline Solids, 87, 199±225.

Schlumberger, 2011, Seismic interpretation and visualization, Petrel 2011.

Sejrup, H. P., Haflidason, H., Hjelstuen, B. O., Nygard, A., Bryn, P., and Lien, R., 2004, Pleistocene development of the SE Nordic Seas margin: Marine Geology, v. 213, no. 1-4, p. 169-200.

Selley, R. C., 1998, Elements of Petroleum Geology (2.ed.), no. 2. ed.

Shoulders, S., 2005, Mechanics of sandstone intrusions: Ph.D. thesis, Cardiff University, Cardiff, United Kingdom, 287 p.

Showalter, T.T. (1979). Mechanics of secondary hydrocarbon migration and entrapment. AAPG Bull. 63, 723-760.

Sheriff, R. E., 2006, Encyclopedic Dictionary of Applied Geophysics, Society of Exploration Geophysicists, 429 p.

Shipley, T. H., Houston, M. K., Buffler, R. T., Shaub, F. J., McMillan, K. J., Ladd, J. W., and Worzel, J. L., 1979, Seismic reflection evidence for the widespread occurrence of possible gas hydrate horizons on continental slopes and rises: American Association of Petroleum Geologists, Bulletin, v. 63, p. 2201-2213.

Sloan, E.D., Subramanian, S., Matthews, P.N., Lederhos, J.P. & Khokhar, A.A. 1998, "Quantifying hydrate formation and kinetic inhibition", Industrial and Engineering Chemistry Research, vol. 37, no. 8, pp. 3124-3132.

Sloan, E. D., Jr.; Koh, C. A. *Clathrate Hydrates of Natural Gases*, 3rd ed.; Taylor & Francis-CRC Press: Boca Raton, FL, 2007.

Solheim, A., Berg, K., Forsberg, C.F. & Bryn, P. 2005: The Storegga Slide Complex: repetitive large scale sliding with similar cause and development. Marine and Petroleum Geology 22, 97-107

Stanton, R.J. (1966) The solution-brecciation process. AAPG Bull., 77, 843–848.

Stuevold, L. M., and Eldholm, O., 1996, Cenozoic uplift of Fennoscandia inferred from a study of the mid-Norwegian margin: Global and Planetary Change, v. 12, p. 359–386.

Sultan, N., Cochonat, P., Canals, M., Cattaneo, A., Dennielou, B., Haflidason, H., Laberg, J. S., Long, D., Mienert, J., and Trincardi, F., 2004a, Triggering mechanisms of slope instability processes and sediment failures on continental margins: a geotechnical approach: Marine Geology, v. 213, no. 1-4, p. 291-321.

Sultan, N., Cochonat P., Foucher, J. P., and Mienert, J. (2004b), Effect of gas hydrates melting on seafloor slope instability, Mar. Geol., 213, 379 – 401.

Swiecicki, T., Gibbs, P. G., Farrow, G. E., and Coward, M. P., 1998. A tectonostratigraphic framework for the Mid-Norway region. Marine and Petroleum Geology, 15, 245-276.

Tissot, B. P., and Welte, D. H., 1984, Petroleum Formation and Occurrence, Springer Verlag.

Urgeles, R., Ca na l s, M., Baraza, J., Alonso, B. & Massonn, D. (1997). The most recent megalandslides of the Canary Islands: El Golfo debris avalanche and Canary debris fow, west El Hierro island. J. Geophys. Res., 102, 20305-20323.

Vanneste, M., Mienert, J. and Bünz. S., 2006. The Hinlopen Slide: A giant, submarine slope failure on the northern Svalbard margin, Arctic Ocean. Earth and Planetary Science Letters 245, 373-388.

Van Vliet, T., van Dijk, H. J. M., Zoon, P., & Walstra, P. (1991). Relation between syneresis and rheological properties of particle gels. Colloid and Polymer Science, 269, 620±627.

Vorren, T.O., Laberg, J.S., Blaume, E Dowdeswell, J.A., Kenyon, N.H. Mienert, J., Rumohr, J. & Werner , F. 1998. The Norwegian - Greenland Sea continental margins: Morphology and late Quaternary sedimentary processes and environment. Quaternary Science Reviews, 17, 273-302.

Watterson, J, Walsh, J., Nicol, A., Nell, PA.R. & Bretan, P.G. 2000. Geometry and origin of a polygonal fault system. Journal of the Geological Society, 157, 151-162.

Westbrook, G. K., et al. (2008), Estimation of gas hydrate concentration from multi-component seismic data at sites on the continental margins of NW Svalbard and the Storegga region of Norway, Mar. Pet. Geol., 25(8), 744–758, doi:10.1016/j.marpetgeo.2008.02.003.

Yilmaz, O., 2001, Seismic data analysis: Processing, inversion and interpretation of seismic data. Investigations in Geophysics, v.2.